PhD Dissertation

Advanced signal processing techniques for sparse array radar systems

（スパースアレイ・レーダにおける信号処理技術）

Submitted to

Graduate School of Environmental Studies
Tohoku University

by

Li Yi

Sendai, Japan, February 20, 2017

Supervised by

Prof. Dr. Motoyuki Sato

Dissertation Committee

Prof. Dr. Motoyuki Sato
Prof. Dr. Qiang Chen
Prof. Dr. Takatoshi Ito
Prof. Dr. Hiroyoshi Yamada
(Niigata University)

Abstract

Synthetic aperture radar (SAR) technique has been researched and applied for many years as an important remote sensing method on variant of environmental or engineering applications. It can not only achieve the high-resolution radar images of the terrestrial surface independent of weather and sunlight illumination with air-born or space-born SAR systems, but it also draws many attentions for the near-range microwave imaging research due to its high-resolution and penetrating ability, such as through-wall radar and ground penetrating radar (GPR).

However, a proper data acquisition standard need to be satisfied in order to generate the SAR imaging result, that the data need to be sampled well in both time/frequency domain and spatial domain under the Nyquist sampling criterion to prevent the result from imaging artifacts. In previous studies it is shown that such requirement is not practical to be achieved with the monostatic radar system because the scanning over a one or two-dimensional plane is necessary with high density depends on the operating frequency of the radar system. In order to simplify the data acquisition, multistatic array radar system is introduced. It can be used to acquire the dataset within a certain range without moving the system which can greatly enhance the data acquisition speed. But due to the limitation of hardware size or the cost, the spatial sampling may not fully satisfied the sampling criterion and imaging artifacts will be introduced to the imaging result. On the other hand, in previous studies we found that the special dataset used for velocity estimation can only be obtained by bistatic radar system can also be acquired by multistatic array radar system. However, it is difficult for precise velocity estimation when the sampling is too coarse and such problem is also similar to the imaging problem.

In the first part of this work, the imaging artifacts caused by the coarse sampling for near-range microwave imaging is mainly discussed. In order to build a better relation between the radar signal and the SAR imaging result, we focus more on the time-domain SAR processing algorithm. The relation between time-domain SAR processing algorithm and its extensions to frequency-domain or frequency-wavenumber domain is well discussed. It is pointed out that the time-domain SAR processing algorithm has the best accuracy for near-range imaging while the calculation cost is also the hugest. It is also shown that the main factors that related to the imaging artifacts includes the operating frequency bandwidth, which is shown as the waveform in time-domain, the sparsity of the array configuration and the imaging algorithm itself. The experimental system that mainly used in this work is introduced with one and two-dimensional sparse array configuration which is also means that the operating frequency and the sparsity of the array is already fixed. Based on this, our main aim is to solve the artifacts problem with signal processing techniques.

Three different type of the approaches are introduced to suppress the imaging artifacts and enhance the imaging resolution; the first type of the method is based on modifying the SAR processing operator, three sub methods are introduced in Chapter 3. These methods are based on the observation during the time-domain imaging and applied as the weighting function or filter within the conventional processing operator. All of these methods do not require too much extra calculation and the selection of the processing parameter is easy which means that these methods are more robust than complicated algorithms.

The second kind of method is based on solving the SAR processing as an inversion processing with least square approach. The least square solution with different regularization terms is well described in Chapter 4. It is concluded that l1 norm regularized least square method for SAR processing can be a good approach for its high image resolution and the ability of artifacts suppression. It is also pointed out that compressed sensing based SAR imaging method is just a special case of the l1 norm regularized least square method. Furthermore, some improvements and suggestions on solving l2 norm regularized least square method are also discussed.

The third type of the approach is a practical method that can enhance the conventional SAR imaging result. Based on the idea of the spatial filtering and pulse compression, we proposed to use the deblurring filter technique to remove the imaging artifacts caused by the sparse array. Mathematically we can obtain similar result with the least square SAR processing method. And since the deblurring filter is applied as a spatial variant local filter, the calculation is simplified by using the filtering instead of the iterative algorithm which can be a great benefit comparing with the least square SAR processing technique.

As for the velocity estimation problem, it is pointed out that this is similar to the SAR imaging problem but more practical. I proposed three advanced methods for the high precise velocity estimation with limited number of antenna elements which includes: An interpolation approach to reconstruct the common-mid point (CMP) dataset, a practical method based on the cross-correlation of two CMP datasets for simultaneous velocity estimation, and the velocity estimation method based on l1 norm regularized least square method. It is demonstrated that the real value of the velocity may still difficult to be estimated, while the slight velocity changes can be detected much easier and precisely with the proposed method.

In the end I introduced the multistatic array GPR system YAKUMO that is developed by our laboratory in 2012 for the large-scale environmental or engineering applications. The performance for the large-scale subsurface imaging is demonstrated with a field experiment. And the application for the airport taxi-way pavement inspection is mainly introduced with the precise velocity estimation techniques that I have introduced in Chapter 6. It is proved with the simulated dataset and the real dataset acquired with YAKUMO system at a model of airport taxi-way that the thin crack within the pavement can be detected with the slight velocity changes. The velocity profiles are also generated with the acquired dataset.

Contents

List of Figures

List of Abbreviations

SAR	Synthetic aperture radar
UWB	Ultra-wide band
CWD	Concealed weapon detection
CT	Computed tomography
MRI	Magnetic resonance imaging
GPR	Ground penetrating radar
UXO	Unexploded ordnance
NDT	Nondestructive testing
MIMO	Multiple-input multiple-output
PSF	Point spread function
FDTD	Finite-difference time-domain
CS	Compressed sensing
CMP	Common-mid point
RMS	Root mean square

Chapter 1 Introduction and background

1.1 Background

1.11 Application of Synthetic aperture radar (SAR) techniques

Synthetic aperture radar (SAR) is a powerful remote sensing technique that can provide high-resolution radar images of the terrestrial surface independent of weather and sunlight illumination.

The concept of synthetic aperture radar (SAR) was proposed by Carl Wiley of Goodyear Aerospace in 1951 [1] and the first practical fully polarimetric air-born SAR system is demonstrated in 1984 [2]. The SAR technique developed fast in recent decades and many new data acquisition modes and processing techniques have been successfully demonstrated, such as multi-looking-aspect SAR [3] circular SAR [4], bistatic SAR [5] and so on. These techniques are widely applied to different kind of environmental applications such as forest biomass estimation, hydrology, water resources measurements, land subsidence monitoring, agriculture management, geophysical and biophysical parameters inversion, natural disaster monitoring and so on [6][7].

1.12 SAR technique for near-range imaging with ultra-wide band (UWB) signal

Besides the SAR techniques that applied for far-field mapping, its potential on near-field imaging ability also attracts attention of researchers in different domains [8][9][10]. The far-field SAR technique is more like the optical photograph that the imaging result is obtained by a narrowband microwave imaging system, hence the distance will be collapsed onto the image plane and such imaging result is known as angle-angle image. While for near-range microwave imaging, much wider frequency bandwidth can be applied since the interference with other microwave system can be controlled. By employing a signal with bandwidth exceeding the lesser of 500 MHz or 20% of the center frequency, an UWB imaging system allows the imaging of both angular domain but also depth information [11]. Due to the penetrating feature of the electromagnetic wave, it is possible to image the targets that hidden behind or within the certain medium and this is consider to be one of the most important feature of near-range microwave imaging. For example, it can be used for the security applications such as concealed weapon detection (CWD) or thorough-wall radar [12][13]; the main aim of such application is to detect the targets that hidden inside the cloths or baggage, or the targets behind the walls at a certain distance. There are already many existing technique or products that are already applied in screening and surveillance applications. Microwave imaging technique is also applied for medical diagnosis especially for breast cancer detection [14][15]. The main attractions of using microwave is due to the harmless nature of microwave at low radiation level and the relatively lower cost comparing

to the existing medical screening techniques such as computed tomography (CT) or magnetic resonance imaging (MRI). Due to the limitation of the microwave property the microwave imaging has lower accuracy comparing to the existing medical techniques but the main aim of applying such technique is to assist the existing technique to reduce risks for early-stage patients [16].

The main activity and research work in our laboratory is focusing on the environmental or engineering of the microwave imaging. It is mainly related to the ground penetrating radar (GPR) systems [17][18]. GPR is a powerful tool used for subsurface exploration, characterization and monitoring. It is widely used in environmental and engineering applications, e.g. archaeological investigation, unexploded ordnance(UXO) and land mine detection, groundwater table localization, nondestructive testing (NDT), ice sounding, cave and tunnel detection, etc. It is a non-destructive detecting method that has the highest resolution among other method for subsurface imaging. Here we should notice that although the system is named as GPR, it does not limit its applications. In above I mentioned about the microwave imaging techniques applied for medical or thought-wall radar, but from the view of the system they have no difference with the GPR system and most of the signal processing techniques are also similar. The main difference is just the operation frequency bandwidth which specific its application. In previous research work we developed different GPR systems such as the ALIS system [19] hat combined GPR system together with the metal detector, it is specific system for the landmine detection; the 3DGPR system that we developed together with the university of Miami, which is combined GPR system with a high accuracy position system for the precise 3-dimensional GPR data acquisition [20].

With both experimental experience of our previous GPR system, and some reports of the previous application of microwave imaging, there is always a problem of the data acquisition speed. In order to generate the radar imaging result, the data have to be sampled under certain requirements. A straightforward way of acquiring the dense dataset is scanning with a single transceiver radar system together on a certain platform and such data acquisition is known as monostatic data acquisition. This is one of the most conventional way for radar data acquisition due to its low cost and dense data acquisition for air-born SAR system. However, the disadvantage of this system is also obvious especially for the near-range microwave imaging, when we suppose to acquire the dataset on a 2-dimensional plane, the data acquisition along the survey direction is convenient because the current hardware can acquire the dataset with tiny time interval and the data can be acquired densely, while the data acquisition in orthogonal direction will be a problem. For example, if we want to acquire the dataset with 5 mm interval of a 1 by 1 meter square, each radar scan can be fast, but we have to scan for 200 times. For the scientific research such data acquisition is acceptable, however it is difficult to achieve the real-time data acquisition for the practical applications of the system. In this case, using multiple radar elements together can be a better solution.

1.13 Array radar system and MIMO

It is obvious that by increasing the antenna elements on the platform can greatly reduce the data acquisition time. For example, if we consider the example that I mentioned in previous section, we can place a set of transceiver antenna pairs with 5 mm interval on the platform, we can finish the data acquisition with only one scan. And such straightforward approach has already applied to some medical scanning systems and GPR systems in previous research works [21][22][23]. However, such approach can hardly full fill the requirements of practical applications due to the limitations on hardware. Hence the next technological step is to apply the multiple-input multiple-output (MIMO) technique for array radar system. By using the combination of different antenna transmitter and receiver pairs and the digital beam forming technique it is already shown that the high resolution can be achieved with limited number of the antenna elements [24]. Many related works have already published and there are mainly two types of problem that attracted many researchers, the hardware design and the signal processing techniques [25][26]. It is already shown that by optimizing the antenna array the sidelobe can be greatly reduced and less antenna elements maybe required [27]. However here we should notice that the MIMO system is actually a kind of radar technique based on hardware synchronization, it may trigger several transmitters working together to realize the beam-forming of the radar signal. There is another similar data acquisition method that is known as multistatic data acquisition, it use only one transmitter at the same time so it does not consider the problem of the interference of different antenna. The beam forming is done by only signal processing technique and such technique is very similar to the seismic data processing which is known as the prestack data processing. The concept of the MIMO and multistatic is similar, while depending on the hardware design the processing of the signal can be different. More discussion on the effect of the different data acquisition will be given in Chapter 2.

In previous research work, comparing with the papers that related to the system design of the array system, there are not so many papers focus on the signal processing techniques with the multistatic system especially for the near-range imaging systems. Most methods or concepts are based on the far-field SAR techniques which is based on the frequency domain signal processing techniques [28][29]. There are also methods that are borrowed from other domain such as ultrasonic imaging or seismic imaging but the number is much smaller than the research on the far-field imaging techniques [30][31]. In general, the near-range imaging is still not attract much attention for the researchers working on microwave engineering domain. I think more detailed discussion towards the near-range imaging is still necessary and this is also the main topic of this work.

As I have mentioned above, such MIMO or multistatic array system is considered to be very useful for near-range microwave imaging system since it can provide high resolution image with limited number of the antenna elements and the array system make the real-time data acquisition possible. There are already some projects and product that have already published at different groups [32][33][34]. In our group we focus more on the development of the multistatic system, and a multistatic array GPR system name YAKUMO is already developed in 2012 for the environmental applications [35][36]. The main advantage of our system is the realization of the real-time data multistatic data acquisition of the 8 by 8 transmitter/receiver pairs. It is already applied for different cases such as archaeological survey, disaster mitigation and the inspection application of the pavement. Recently, another array based GPR system is also under investigating for the wooden structure inspection of the Japanese type wooden houses [37].

1.2 Research objective

As I have reviewed in above, currently there is still no so many researches that focus on the signal processing or imaging techniques of near-range imaging with the sparse array radar system. The previous research mainly based on the far-field SAR imaging technique that is based on the far-field assumptions and the targets are always point-like target, for the variant near-field imaging applications the condition may not satisfied. On the other hand, I think that the imaging techniques based on the frequency domain is not clear for the imaging applications since our real world is not in frequency domain but in time-domain, in another word, it is not easy to correlate the frequency domain signals with the physical model that we want to image while it is much easier to use the time-domain signal.

In this research work, I will mainly focus on the signal processing technique that based on the array radar system for the near-range imaging. There are mainly two topics will be discussed in this work: the first goal is the improvements of the imaging processing with the sparse array system; secondly is the development of the special array system for extra information extraction.

In order to achieve a straightforward relation of the radar signal and the imaging result, I will mainly describe the imaging process in time-domain. The relation between the time-domain imaging and frequency domain imaging will be clarified in Chapter 2. It is already described that sparse array will cause strong sidelobe and by optimizing the antenna configuration the performance of the imaging results can be improved. However, there will be still many imaging artifacts left especially for the near-range imaging cases and these artifacts are only caused by the imaging algorithm or the discretization of the signal. Since there are already plenty of the research works that improve the performance of the hardware or system design of the sparse array, we will mainly focus on solving the artifacts that are caused during the imaging processing. Furthermore, the imaging resolution or imaging quality can be enhanced by removing the imaging artifacts. However, for different

situations or conditions a certain processing method may not enough to solve all the problems. I think it is necessary to investigate multiple approaches from different point of view to achieve our goals.

On the other hand, by using the array configuration of antenna elements. The different variation of the antenna configuration can be investigated, the antennas can be placed for special data acquisition hence the extra information can be extracted. In later part of the research work I mainly focus on the electromagnetic wave propagation velocity estimation within the certain medium. In our laboratory we have already carried on the similar research many years ago. However the previous work is limited on pure research work and the technique is not applied for real application due to the limitation of the system. One of the main problem is also similar to the sparse array imaging system that due to the coarse sampling the conventional processing is not suitable for the coarsely sampled dataset. In our work, I hope I can fully use the limited antenna elements by using advanced signal processing technique.

1.3 Structure of the thesis

The structure of this thesis is shown in Figure 1.1. The dissertation is organized mainly into three parts. The first part is presented in Chapter 2 that the general problems of using the sparse array for near-range imaging is clearly described. Also the experimental equipment that is mainly used in this work is introduced, the effects on the imaging result which is determined by the system is also summarized in this part.

The second part is focusing on solving the imaging problem of using sparse array system by different processing approaches. I proposed mainly three different type of approaches to improve the imaging results in Chapter 3 to 5. These different type of approaches can be applied independently for the imaging processing. In each chapters I also introduced a few sub methods that belongs to a same type of approach. The detailed information will be given in below.

The last part is focusing on the velocity estimation with array configuration. The problem is similar to the sparse array imaging problem that I proposed several approaches to estimate high accuracy velocity information with limited number of the antennas in Chapter 6. And in Chapter 7 I introduced our YAKUMO array GPR system and further discussed on the velocity estimation on pavement inspection application.

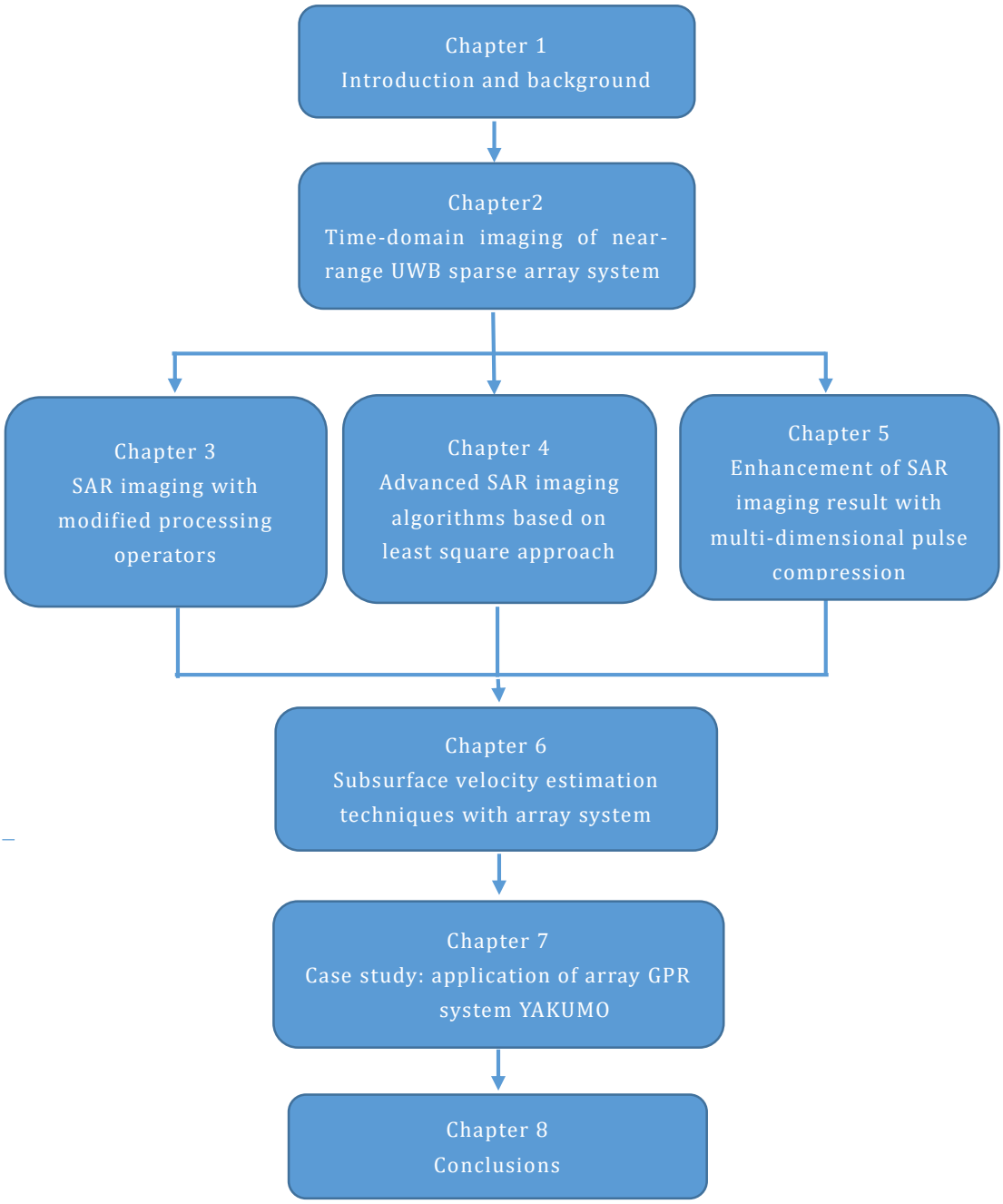

Figure 1.1 Structure of the thesis

Hereafter, the description of each chapter is provided:

Chapter 2: Since most of the proposed approaches in this work is based on the time-domain signal processing technique, a detailed introduction about the SAR processing in time-domain is given in this part. The relation of time-domain SAR processing and its development in frequency domain that is widely used in SAR research is well discussed. Based on this, the main factors that affect the near-range imaging result of sparse array system are summarized. The factors that decided by the system hardware are introduced

and some small improvements on antenna configuration design are introduced together with the experimental system and the antenna configurations that are used in later chapters.

Chapter 3: In this chapter the first type of SAR processing approach is introduced. There are three sub methods included in this chapter. In general, all the three methods are improved SAR processing method by using a filter or weighting factor within the conventional SAR algorithm. These factors includes a limitation on the processing aperture, a local low-pass filter and a semblance function as a weighting factor. They used some known physical fact as the factor to reduce the generation of the imaging artifacts. A comparison of these methods is also given in the end of this chapter to describe the advantage and disadvantage of different method. As a summary, this kind of approach is easy to apply and the effect on the imaging result is easy to understand hence these methods can be applied for the real acquired dataset robustly and these method can be considered to combine with other complicated methods as I introduced in later chapters.

Chapter 4: In this chapter a half inversion based method is introduced for the SAR processing algorithm. The core idea is to solve the SAR processing problem as a least square problem. A conventional way of solving the least square problem is under the $\ell 2$ norm regularization and this method is known as the least square migration in seismic research. I applied this method to near-range imaging problem to suppress the artifacts caused by the coarse sampling. In order to promote the sparsity and further suppress the artifacts I also used the $\ell 1$ norm regularization term and it gives good imaging results for both simulation and experimental dataset. Theoretically, I also proved that the solution of $\ell 1$ norm regularized least square method is just a general solution of the CS method that applied to SAR imaging. Furthermore, I generalized the least square problem in a more general form and some trials on improving the conventional least square method are also well discussed in the end of this chapter.

Chapter 5: In Chapter 4 I proposed to use the least square method to solve the accurate SAR imaging result. It is shown to have good performance with this approach, however the mathematic complicity is a huge problem for the practical use of this method. The pulse compression in time-domain is reviewed and a solution based on $\ell 1$ norm regularization is proposed in the beginning of this chapter. By combing the pulse compression method with the idea of deblurring filter introduced in imaging processing research, an imaging processing based deblurring filter method is proposed to reduce the imaging artifacts caused by the coarse sampling. The feature of the proposed method is well discussed and theoretically the estimated result of the least square solution can be achieved without the iterative calculation. However, the experimental result shows that this method is still difficult to apply for the real data which is far different from the idea data.

Chapter 6: The velocity estimation technique with bistatic radar is reviewed in the beginning. It is also pointed out that the fact of the velocity estimation is similar to the SAR processing. Different methods are introduced to use the limited number of antennas for the velocity estimation. An interpolation method and the ℓ1 norm regularized least square method are introduced for high accurate velocity estimation. Also a practical approach that based on cross-correlation of two different observation is also introduced for single layer structure monitoring. The slight velocity/thick ness changes can be detected simultaneously.

Chapter 7: The multistatic array GPR YAKUMO is introduced in this chapter. It is designed for the large scale engineering and environmental applications. The antenna configuration with different antenna polarization and its effects are well discussed. The performance of the system for the large-scale 3-dimensional data acquisition is demonstrated with a field experiment example. The continuous multistatic data acquisition made it possible for the large scale subsurface velocity estimation together with the methods that are introduced in Chapter 6. A case study on airport taxi-way pavement inspection with the YAKUMO system is demonstrated in detail. I introduced a method to detect the thin cracks within the asphalt layers by precise velocity estimation. The results are well discussed with the data acquired at the model of the taxi-way.

Chapter 8: This chapter summarized the main results of the thesis together with some discussions. Some recommendation of the future work is also included.

1.4 References

[1] I. G. Cumming and F. H. Wong, Digital Processing of Synthetic Aperture Radar Data: Algorithms and Implementation, Artech House, Boston, London, 2005.

[2] J. S. Lee and E. Pottier, Polarimetric Radar Imaging: From Basics to Applications, Boca Raton, US: CRC Press, 2009.

[3] F. Xu and Y. Q. Jin, “Automatic reconstruction of building objects from multiaspect meter-resolution SAR Images,” IEEE Trans. Geosci. Remote Sens., vol. 45, pp. 2336–2353, Jul. 2007.

[4] O. Ponce, P. Prats, M. Rodriguez-Cassola, R. Scheiber, and A. Reigber, “Processing of circular SAR trajectories with fast factorized back-projection,” in Proc. IEEE Int. Geosci. Remote Sens. Symp., Vancouver, Canada, Jul. 2011, pp. 3692–3695.

[5] M. Rodriguez-Cassola, P. Prats, D. Schulze, N. Tous-Ramon, U. Steinbrecher, L. Marotti, M. Nannini, M. Younis, P. Lopez-Dekker, M. Zink, A. Reigber, G. Krieger, and A. Moreira, “First Bistatic Spaceborne SAR Experiments With TanDEM-X,” IEEE Geosci. Remote Sens. Lett., vol. 9, pp. 33–37, Jan. 2012.

[6] Y. Q. Jin, Theory and Approach of Information Retrievals from Electromagnetic

Scattering and Remote Sensing, Berlin Heidelberg New York: Springer, Dec. 2005.

[7] C. Oliver, and S. Quegan, Understanding Synthetic Aperture Radar Images, Artech House, Boston, London, 1998.

[8] Y. Qi, Y. Wang, W.Tan and W. Hong, "Application of sparse array and MIMO in near-range microwave imaging", Proc. SPIE 8179, Czech Republic, Vol. 81790X, 2011.

[9] R. Appleby and R. N. Anderton, "Millimeter-wave and submillimeter-wave imaging for security and surveillance," Proceedings of the IEEE, Vol. 95, No. 8, 1683-1690, August 2007.

[10] D. M. Sheen, D. L. McMakin, and T. E. Hall, "Three-dimensional millimeter-wave imaging for concealed weapon detection," IEEE Trans. Microw. Theory & Tech., vol. 49, no. 9, pp. 1581-1592, September 2001.

[11] L. Y. Astin, A. A. Kostylev, Ultrawideband Radar Measurements - Analysis and Processing, 1997, The Institution of Electrical Engineers.

[12] S. W. Harmer, N. Bowring, D. Andrews, N. D. Rezgui, M. Southgate, S. Smith, "A Review of Nonimaging Stand-Off Concealed Threat Detection with Millimeter-Wave Radar: Application Notes", Microwave Magazine IEEE, vol. 13, pp. 160-167, 2012.

[13] G. L. Carvat, L. C. Kempel, E. J. Rothwell, C. M. Coleman, E. L. Mokole, "A through-dielectric radar imaging system", IEEE Trans. Antennas Propag, vol. 58, no. 8, pp. 2594-2603, Aug. 2010.

[14] M. Lazebnik, "A large-scale study of the ultra wideband microwave dielectric properties of normal benign and malignant breast tissue obtained from cancer surgeries", Phys. Med. Biol., vol. 52, pp. 6093-6115, 2007.

[15] E. Fear, S. Hagness, P. Meaney, M. Okoniewski, M. Stuchly, "Enhancing breast tumor detection with near-field imaging", IEEE Micro., vol. 3, pp. 48-56, Mar. 2002.

[16] X. Li, E. J. Bond, B. D. Van Veen, S. C. Hagness, "An overview of ultrawideband microwave imaging via space-time beamforming for early-stage breast cancer detection", IEEE Antennas and Propagation Magazine, vol. 47, no. 1, pp. 19-34, Feb. 2005.

[17] D. J. Daniels, Ground Penetrating Radar, IEE, 2004.

[18] H. M. Jol, Ground Penetrating Radar: Theory and Applications, 2009, Elsevier.

[19] K. Takahashi, M. Sato, "A hand-held dual-sensor system using impulse GPR for demining", Proc. IEEE Int. Conf. Ultra-Wideband, pp. 157-160, 2008.

[20] Mark Gransmueck, David A. Viggiano "Integration of Ground-Penetrating Radar and Laser Position Sensors for Real-Time 3-D Data Fusion" IEEE Trans. Geoscience and Remote Sensing, Vol. 45, No. 1, pp.130-137, Jun., 2007.

[21] J. E. McFee, V. C. Aitken, R. Chesney, Y. Das, K. L. Russell, "Multisensor vehicle-mounted teleoperated mine detector with data fusion", Proc. SPIE Detection and Remediation Technologies for Mines and Minelike Targets III, vol. 3392, pp. 1082-1093, 1998.

[22] Yarovoy, P. Aubry, P. Lys, L. Ligthart, "UWB array-based radar for landmine detection", Proc. of the 3rd European Radar Conference, pp. 186-189, 13–15 September 2006.

[23] R. Benjamin, I.J. Craddock, J. Leendertz, R. Nilavalan, A. Preece, "Experimental investigation of real aperture synthetically organised radar for breast cancer detection", Antennas and Propagation Society International Symposium 2005 IEEE, vol. 1B, pp. 179-182, 2005.

[24] A. M. Haimovich, R. S. Blum, L. J. Cimini, "MIMO radar with widely separated antennas", IEEE Signal Processing Magazine, vol. 25, no. 1, pp. 116-129, 2008.

[25] T.Takayama, Y. Tokieda, H. Sugawara, "MIMO Imaging Radar with Enhanced Range-Azimuth Sidelobe Suppression," Proc. IET Int. Radar Conf., 2012.

[26] P. Stoica, L. Jian, X. Yao, "On probing signal design for MIMO radar", IEEE Transactions on Signal Processing, vol. 55, pp. 4151-4161, 2007.

[27] A. De Maio, M. Lops, "Design principles of MIMO radar detectors", IEEE Transactions on Aerospace and Electronic Systems, vol. 43, pp. 886-898, 2007.

[28] Y. Yu, A. P. Petropulu, and H. V. Poor, "MIMO radar using compressive sampling", IEEE J. Sel. Topics Signal Process., vol. 4, no. 1, pp. 146-163, 2010.

[29] S. S. Ahmed, S. Andreas and L. P. Schmidt. "A Novel Fully Electronic Active Real-Time Imager Based on a Planar Multistatic Sparse Array" IEEE Transactions on Microwave Theory and Techniques, vol. 59, no. 12, pp. 567-576, 2011.

[30] B. Scheers, M. Acheroy, A. Vander Vorst, "Migration technique based on the time-domain model of the ground penetrating radar", Proc. SPIESurf. Subsurface Sensing Technol. Appl. III, pp. 111-119, 2001.

[31] I. Catapano, L. Crocco, R. Persico, M. Pieraccini, F. Soldovieri, "Linear and nonlinear microwave tomography approaches for subsurface prospecting: Validation on real data", IEEE Antennas Wireless Propag. Lett., vol. 5, no. 1, pp. 49-53, Dec. 2006.

[32] R. Solimene, A. D' Alterio, F. Soldovieri, "Determining Fresnel reflection coefficients in 3 D half-space geometry by GPR multistatic data", Near Surface Geophysics, vol. 9, pp. 265-275, 2011.

[33] J. Binningsbo, E.S. Eide and J.F. Hjelmstad, "3D migration of GPR array-antenna data," Proc. 8th International Conference on Ground Penetrating Radar, Gold Coast, Australia, 2000.

[34] T.G. Savelyev, X. Zhuge, A.G. Yarovoy, L.P. Ligthart, B. Levitas, "Comparison of UWB SAR and MIMO-based short-range imaging radars," Proc. 2009 European Radar Conference, pp. 109-112, Sept. 30-Oct. 2, 2009.

[35] M. Sato, "Array GPR “Yakumo” and its application to archaeological survey and environmental studies", in Proc. General Assembly and Scientific Symposium (URSI GASS) 2014, pp. 1-2, 2014.

[36] M. Sato, K. Takahashi, "Array GPR system “Yakumo” for Natural Disaster Mitigation", the International Workshop on Advanced Ground Penetrating Radar 2015 (IWAGPR), 2015.

[37] C. N. Koyama, K. Takahashi, Y. Iitsuka, M. Sato, "Polarimetric UWB SAR for subsurface imaging of building structures", Proc. of APMC 2014, pp. 1025-1027, November 4-7 2014.

Chapter 2 Time-domain imaging of UWB sparse array radar system

2.1 Introduction

In the past, there are mainly two types of theory for the array radar imaging; the monochromatic theory and the impulse theory. For the researchers who are mainly working on SAR techniques the most classical formulation is based on narrowband far-field assumptions. It states that the elements of the uniform array must satisfied to Nyquist criterion that the element interval should less than half wavelength [1]. The mathematical formulation can be greatly simplified and easy to understand, the details can be found in different articles [1] - [3]. The other type of theory is based on the ultra-wideband impulse theory which is very similar to the imaging theory for seismic exploration or ultrasound imaging [4][5].

In previous research works, some main features of the near-field array imaging are already well described in [2][6]. However, most of the conclusions are based on the far-field point-like target. When we consider the imaging quality of the distributed targets that are located within the near-field, the situation will be more complicated. For example, the analytical analysis in frequency domain will be very complicated, and also the PSF (point spreading function) of the distributed target is spatial-variant so that the stacked results of many PSF functions are difficult to predict [7].

In this study, I will analyze some of the main factors that will influence the imaging result of distributed targets in near-field. Since the response of the frequency domain is difficult to analysis, I will mainly focus on impulse theory analysis. One of the key factor that affects the imaging result is the bandwidth and the center frequency of the transmitted signal and it is already well concluded in [8]. Here I will evaluate this issue from the view of the time-domain waveform and its effect on the distributed targets. Secondary, the distribution of the antenna elements will strongly affect the imaging result, for the point target it is also will summarized in [9]. Here I will focus more on the redundancy of the antenna elements and the effect of the distributed targets. Finally, another main problem of the near-field imaging is that the strong artifacts may appear due to the coarse spatial sampling [10]. Similar problem is also well discussed for imaging processing, ultrasound imaging and seismic imaging issues and it is also pointed out that this issue is also closely related to the feature of the wavelet [11] –[14].

2.2 Comparison of SAR processing in different domains

2.21 Time-domain SAR processing and forward modeling

SAR processing is now widely used for both near-range and far-range microwave imaging systems. Originally it comes from the medical imaging and seismic exploration, and it include many different extended methods and sometimes for a same algorithm it can be named differently in other domains. Here I mainly focused on the most fundamental algorithm which is known as SAR processing. It also called back projection or diffraction stacking in different cases. Equation (2.1) and (2.3) shows the 2-dimensional time-domain and frequency domain of the SAR processing. In this work I will mainly focus on the time-domain of the processing. Here *x, y* and *z* is the coordinates of the imaging points and x_g y_g is the position of the transmitting/receiving antenna. *r* is the distance between transmitting/receiving antenna and the imaging point and *v* is wave propagation velocity in a certain medium. Equation (2.1) can be used for both monostatic case and multistatic case. The monostatic SAR processing sketch is shown in Figure 2.1.

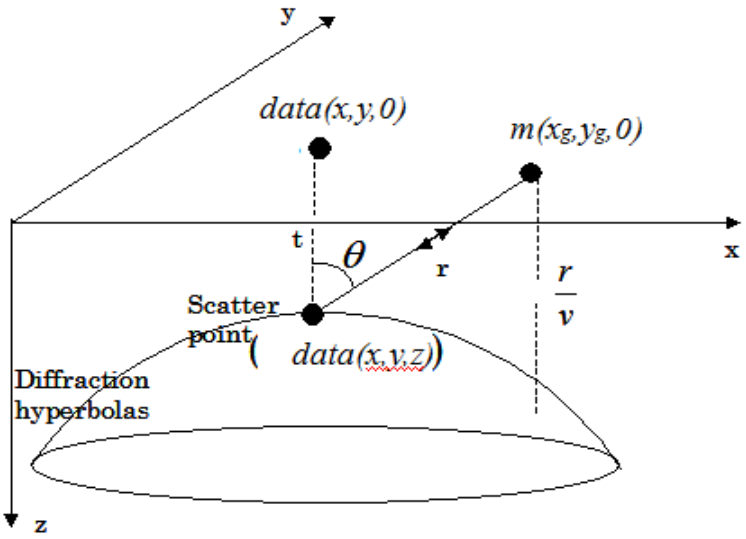

Figure 2.1 The schematic diagram of the 3-dimensional SAR processing

The physical meaning is quiet straight forward that is to assume that every imaging point can be a potential target, by calculating the travel time hyperbolic in the data domain, we can summing all the amplitudes along this trajectory onto the imaging point. When the imaging point really has a target, the summing energy can be enhanced so that we can get the real target position information from the radar signals. By changing the order of realizing the algorithm, we can also explain this processing as we spreading energy at each trace and arrival time on the hyperbolic trajectory.

$$m(x,y,z) = \iint d\left(t, x_g, y_g\right) \cdot \delta(t - \frac{r}{v}) dt dx_g dy_g \tag{2.1}$$

$$r = 2\sqrt{z^2 + \left(x - x_g\right)^2 + \left(y - y_g\right)^2} \tag{2.2}$$

Here we should point out that from (2.1) we can find that the position of the antenna element can be either regularly distributed or not. However, due to the bandwidth of the signal, we need to follow the spatial Nyquist sampling criterion that at least two points need to be sampled within one wavelength, otherwise spatial aliasing will appear.

Since the SAR processing can be seen as a simple inverse method, it is straightforward that there is also forward modeling exists. A simplified forward modeling of UWB pulse system based on ray tracing can be described as (2.3)

$$d\left(t, x_g, y_g\right) = \iint w(t) * g(x,y,z) \cdot m(x,y,z) \cdot \delta(t + \frac{r}{v}) dt dx_g dy_g \tag{2.3}$$

Where *g* include all the wave propagation factors such as radiation, dispersion and the effect of the antenna radiation pattern. *w* is the simulated waveform and we assume it is constant, usually we can use a Gaussian pulse or its second differential as the input because it is easy to control. Comparing to the (2.1) we can find that SAR processing is under the assumption of a station waveform, then the SAR processing is just the adjoint of the forward modeling given in (2.3). I will discuss more about this issue in later chapters.

There are actually many different ways for the microwave simulation, for example finite-difference time-domain (FDTD) is one of the most widely used numerical modeling techniques to simulate electromagnetic wave propagation for different cases [15]. Since FDTD algorithm explicitly solves Maxwell's curl equations using central finite differences in both time and space domain, it can solve different problems such as modeling the antenna elements or wave propagation through the medium accurately. However, FDTD forward modeling will make the imaging problem much more complicated because it include so many factors that is not considered in SAR algorithm. Since we are mainly focus on the imaging problem of SAR algorithm, I will use simple ray tracing for the forward modeling in this work. And I will pay more attention to make the acquired dataset more like the idea dataset with some preprocessing. For example, we can use the trace balancing technique based on antenna radiation pattern to make the energy more balanced and use pulse compression technique to make the waveform more like a pulse so that the input dataset satisfied more to the SAR processing assumptions which I will further discuss in Chapter 5.

G

2.22 Diffraction stacking and SAR processing

In previous section I have introduced the time-domain SAR processing that is known as the diffraction stacking. And I mainly explained its physical meaning in time-domain that is to assume that every imaging point can be a potential target, by calculating the travel time hyperbolic in the data domain, we can summing all the amplitudes along this trajectory onto the imaging point. When the imaging point really has a target, the summing energy can be enhanced so that we can get the real target position information from the radar signals. And the equation of its time-domain and frequency domain has given as (2.4), for simplicity here I only show the 2-dimensional equations.

$$m(x,z) = \iint d(t,x_0)\cdot\delta(t-\frac{r}{v})dtdx_0 \tag{2.4}$$

$$r = 2\sqrt{z^2+(x-x_0)^2} \tag{2.5}$$

$$m(x,z) = \iint d(\omega,x_0)e^{\frac{j2\omega r}{v}}d\omega dx_0 \tag{2.6}$$

Actually in previous explanations I explained this approach mainly from the knowledge of the seismic exploration and some of the terms and ideas are slightly different from the descriptions of the researchers working on electromagnetics or SAR applications. In this part we will further investigate some its expanded versions of the time-domain SAR processing and summarize its relation to the methods that build from the view of Maxwell equation.

First of all, based on (2.6) we can simply introduce the wave number that

$$\mathrm{k} = \frac{\omega}{v} \tag{2.7}$$

and then (2.6) can be rewritten in terms of integration as

$$m(x,z) = \iint d(k,x_0)e^{j2kr}dkdx_0 \tag{2.8}$$

Actually now (2.8) already point out that the diffraction stacking is equivalent to the range migration technique or synthetic aperture focusing technique introduced in [16].

Furthermore, we can also apply the Fourier transform on spatial domain to get the 2-dimensional Fourier transform of (2.9) as

$$m(x,z) = \iint f(k,k_x)d(k,k_x)e^{-jk_x x}e^{-jk_z z}d\omega dk_x \tag{2.9}$$

$$k_z = \sqrt{4k^2 - k_x^2} \tag{2.10}$$

$$f(k,k_x) = e^{j\pi/4}k\sqrt{2/(k_z^3\pi)} \tag{2.11}$$

Here we need to notice that $f(k,k_x)$ is an amplitude factor where $\sqrt{z}$ has been neglected. By substituting the frequency wavenumber k by the integration in k_z (2.11) can be recast as a double Fourier transform as

$$m(x,z) = \iint f(k,k_x)\frac{k_z}{\sqrt{k_x^2 + k_z^2}}d(k,k_x)e^{-jk_x x}e^{-jk_z z}d\omega dk_x \tag{2.12}$$

This is known as the Stolt migration method that has advantages in calculation because it can be done with FFT algorithm [17]. However, please notice that there is already some simplification and it requires data to be interpolated and resampled according to a rectangular grid in k domain which may introduce problems especially in sparse array case. Furthermore, if we ignore the amplitude factor, it is equivalent to the conventional SAR imaging algorithm that presented in [18].

Here I should mainly point out that actually time-domain migration is the relatively accurate imaging method. While frequency domain SAR methods that widely used for SAR applications are achieved by neglect some weighting factors that is not important under some certain cases such as far-field approximation or Born approximation so that the large scale calculation can be done much easier.

We may also apply some weighting factors to further compensate the amplitude changes due to the wave propagation or the imaging angle problem and one of the popular approach is known as the Kirchihoff migration [19]. However, in practical experiment or real applications, we always found that the complicate algorithm may has worse performance comparing to some simple methods. I think it is because that we sometimes may not understand the effect of the main factors. For a simple example, when we use an antenna that has a narrow radiation pattern for the SAR processing for a long range imaging, we need to limit the imaging aperture during the processing. Of course we can use Kirchihoff migration because it also somehow compensate the angle effect, but the result may not good than just limit the imaging aperture during the SAR processing according to the information of the antenna radiation pattern. For a specific imaging system we always need to find out what is the main factor for the imaging and chose the imaging condition properly. It always

give better results than using a complicate algorithm for a specific issue which is not related to our cases.

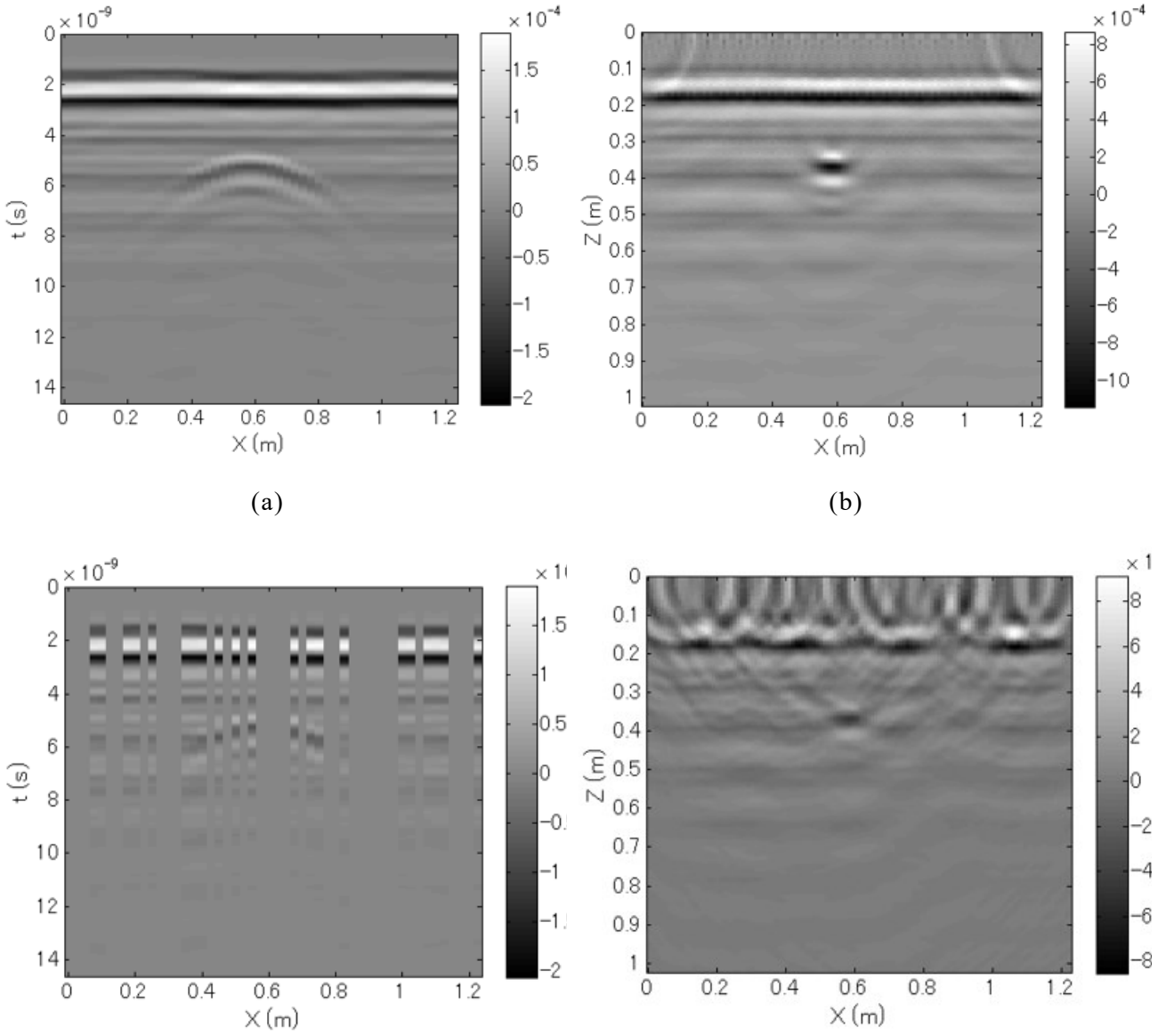

Figure 2.2 A 2-dimensional example for the imaging artifacts caused by the coarse sampling, (a) A 2-dimensional vertical slice with a point scartterer in the middle; (b) Conventional SAR imaging result of (a); (c) Randomly removed 50% of the traces in (a); (d) Conventional SAR imaging result of (c).

2.23 Relation between SAR imaging and the interpolation

In previous section I point out that frequency SAR processing is performed by some simplification and transformation of time-domain SAR processing. In another word, SAR processing result is closely related to the Fourier transform which means that some numerical problems in Fourier transformation will also appear for SAR processing in time-domain. One of the main effect is the sampling problem in Fourier transform. Nyquist sampling criterion rules that for a period we need at least two sampling points. Here we also need to notice that this is the most fundamental rule that it indicates in ideal case we can recover the signal by Sinc interpolation [20]. However if we only have two samples it is still very difficult to recover and practically we need 10 samples or even more to prevent the numerical problems happen. Furthermore, if we think about the irregular sampling the situation will be more complicated.

For the current radar system, the sampling in the time axis is quiet advance and we can even get hundreds point per period and there is almost no problem for time-domain signal processing. Therefore, as we explained above, the SAR processing is very similar to a 2-dimensional Fourier transform which means that we also need to follow the Nyquist sampling criterion in spatial domain. And vice versa we need at least two sample points within a wavelength. It means that for a transmitted signal with 3 GHz center frequency we need the distance between antenna elements less than 5 cm and if we think about a monostatic system the distance between each transceiver should less than 2.5 cm. Also such condition will be straighter for the UWB signal in near-field case as I mentioned before. In this case, if we want to design a 2-dimensional array for quick scanning, large number of antenna elements will be required. And also as I mentioned it is just the minimum requirement, there will be many problems happen without further interpolate the dataset. As I will mainly introduce in later section, the coarse sampling may cause severe problem during the SAR processing. As it shown in 1-dimensional case, the aliasing components will turn into artifacts after the SAR processing.

In early stage of this research work, I proposed an interpolation algorithm to use 3-dimensional interpolation method to interpolate the coarse dataset onto a uniform grid first and then do the SAR processing. The method is based on projection onto convex sets (POCS) and frequency-wavenumber zone-pass filtering to reconstruct the image from sparsely sampled data that violates the Nyquist criterion [21]. This method can fully use the 3-dimensional information and works well with irregularly sampled data. Comparing to other iterative interpolation method, the proposed method needs much less iterations and can avoid the aliasing.

And in later chapters I will mainly discuss how we can reconstruct the spatially sparse dataset to SAR image directly. This two method is somehow similar approach because SAR processing is just a special way to interpolate the acquired dataset. In Chapter 4 I will also introduce that SAR processing is just an adjoin calculation of the simple forward modelling.

It means that we can also apply the forward modeling to the SAR imaging result to reconstruct the acquired dataset in any required acquisition ways. If we forward modeling the SAR results on a uniform grid, it is just the interpolation the coarsely sampled data on a uniform grid. And based on the similarity of the SAR processing and the Fourier transform, we can conclude that SAR processing can be consider as a multi-dimension interpolation method that based on Fourier transformation.

While doing the iterative interpolation processing we are actually picking the unaliased frequency components at each iteration and reducing the high frequency aliasing components so that the dataset can be reconstructed. After that, the reconstructed dataset includes less aliasing during the conventional SAR processing so we can get better imaging result. This can be a good way to get the interpolated 3-dimensional data cube and we can directly check the horizontal slice of the data cube to find out the target we want. And mostly we do not have to worry about the artifacts caused by the SAR processing that may mislead us.

However, this processing is somehow a dumping processing and it is still time consuming. As I explained above, I think it is possible to find a way that dealing with artifacts during the SAR processing so that we can directly get the imaging results.

2.3 Data acquisition and array system

2.31 Data acquisition of SAR system

If we have multiple antenna elements, we can design any acquisition system that we want. There are mainly three different data acquisition methods; monostatic, bistatic and multistatic [22]. Here we should notice that these definitions come from the radar technique but it is slightly different because our target is not the moving target. The 2-dimensional case of these acquisition methods are shown in Figure 2.3.

If a transmitter antenna and a receiver antenna stay together as a transceiver, and we move it along a survey line. So that the data can be acquired at each position along this survey line. Such data is known as the monostatic data acquisition. Most of the air-born SAR systems and GPR systems are designed as monostatic system. This may be the most practical method for SAR data acquisition for its simplicity and flexibility. By fixing the antenna system on a platform we can acquire the dataset with different ways. However, less information can be extracted because there is only one propagation path between target and the transceiver at each position. For example, if we have multi targets, the targets close to the system may block the other targets behind it. Figure 2.4 shows a simulation example of monostatic SAR imaging. We simulated a point scatterer at 0.5 m away and we used the Gaussian pulse with 3 GHz center frequency as the source. The imaging aperture is 1.2 m long and the spatial sampling interval is 5 cm.

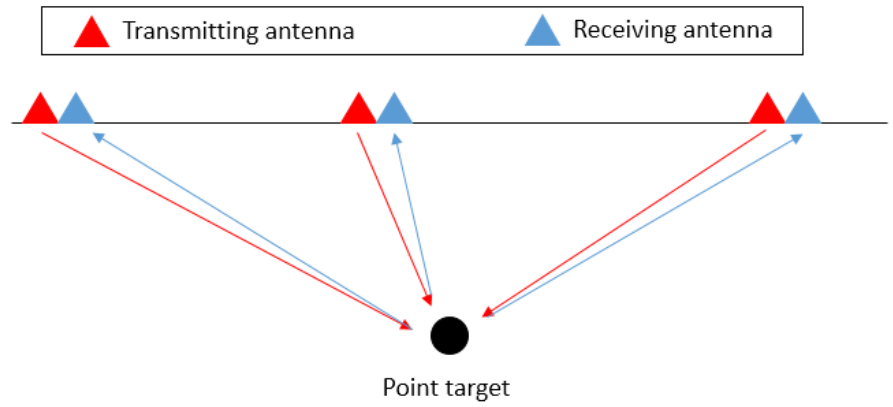

(a)

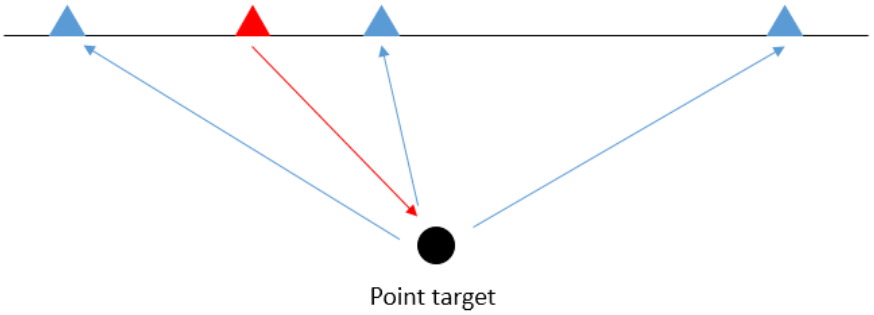

(b)

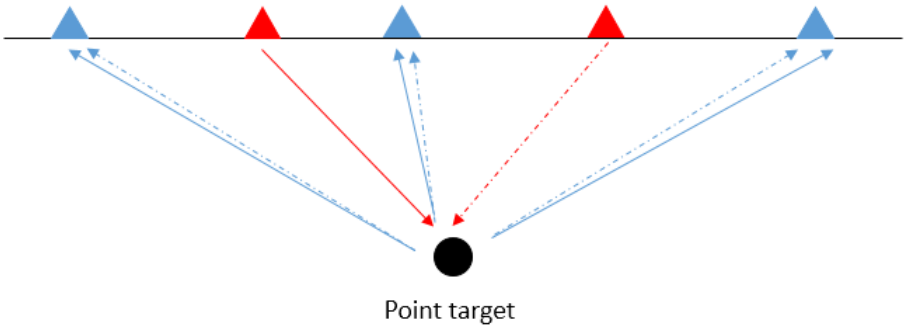

(c)

Figure 2.3 Data acquisition with different antenna configurations, the red triangle indicates the transmitting antenna and the blue one indicates the receiving antenna, (a) monostatic data acquisition; (b) bistatic data acquisition; (c) multistatic data acquisition.

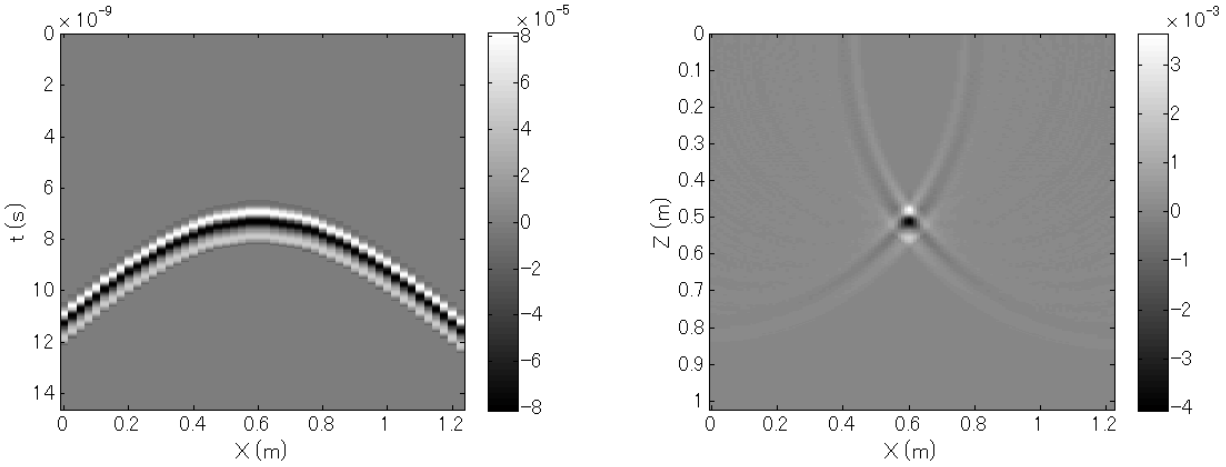

(a) (b)

Figure 2.4 2-dimensional simulation data of monostatic data imaging, (a) simulated radar profile; (b) conventional SAR imaging result of (a).

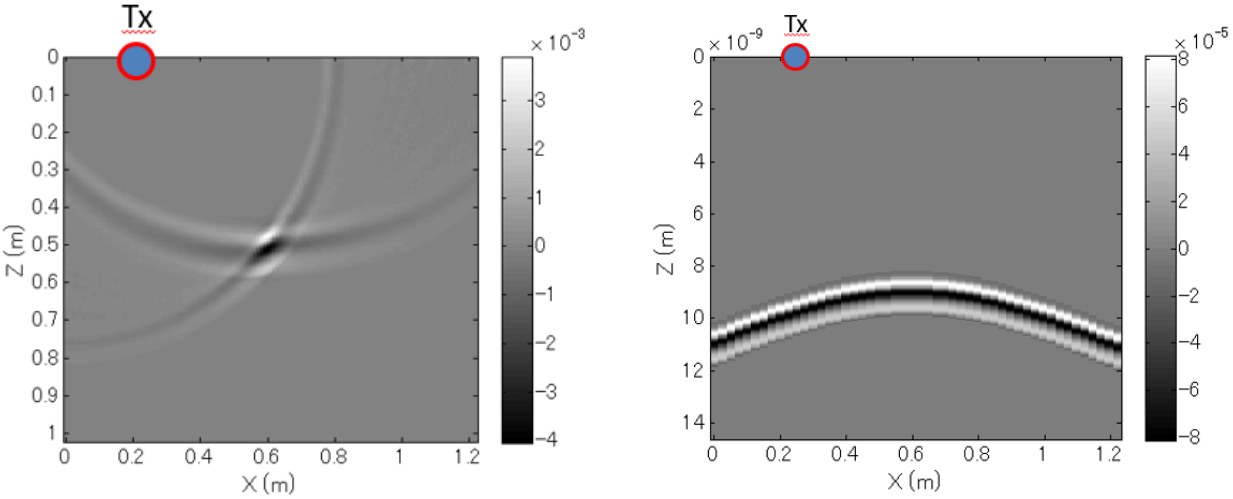

(a) (b)

Figure 2.5 2-dimensional simulation data of bistatic data imaging, (a) simulated radar profile; (b) conventional SAR imaging result of (a).

If we fix a transmitter antenna or receiver antenna while moving another one along a survey line, it is known as the bistatic system. From the view of the information quantity, there is no extra information comparing with the monostatic case if we place the antenna elements as in Figure 2.5 (a) and Figure 2.5 (b). Actually, if we think about the SAR processing and assume the target is a point scatterer or a horizontal reflector, the resolution will be worse

than monostatic case as it shown in Figure 2.6. Because under such situation we can actually consider a transceiver in the middle of the transmitter and receiver antenna is equivalent two this antenna pair. Hence the imaging aperture is actually half of the monostatic case and the spatial sampling interval is also half. We may also notice in Figure 2.5(b) the imaging result is affected the shift of the imaging aperture.

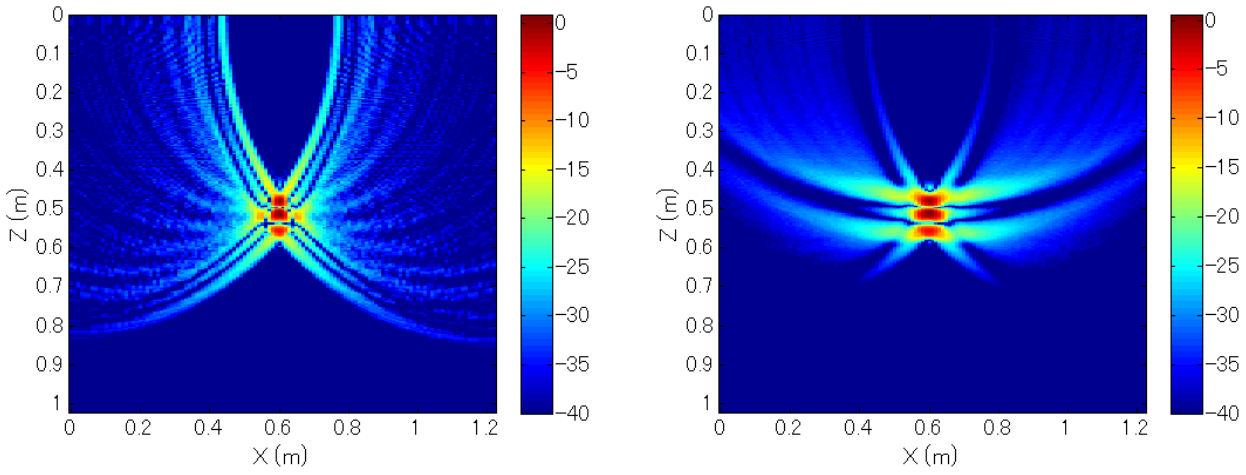

(a) (b)

Figure 2.6 2-dimensional SAR imaging results with different configuration, (a) monostatic imaging result; (b) multistatic imaging result.

Multistatic acquisition is similar to bistatic case, but after the bistatic acquisition we will also move the fixed antenna to other position and repeat the data acquisition. Here I should emphasis that multistatic acquisition is not equivalent to the multi-input multi-output (MIMO) data acquisition because we do not transmit signals at same time with multi transmitters. We should always consider the situation that there is only one source working at one time. In the case the bistatic data is just a part of the multistatic data. If we consider the SAR imaging of the multistatic case, we are actually stacking all the bistatic SAR results together. Since each bistatic SAR result has the different imaging aperture, we can expect that the trend of the artifacts or noise of each bistatic SAR result will be different. However, the response form the main target is more constant. While stacking all the bistatic SAR results together, the response from the main target will be enhanced and the artifacts or noise can be suppressed. In Figure 2.6 I also shows the imaging result of the multistatic case and monostatic case with same aperture width, In order to compare the details I used dB scale to show the results here. We can found that the wing shape imaging artifacts are reduced due to the stacking but the resolution is slightly worse than monostatic case. If we comparing the imaging aperture the resolution should be equivalent, practically, when we do the stacking process the artifacts surround imaging target may blur the final results. Multistatic SAR processing is also known as the prestack migration in seismic exploration, and these features are also pointed out in [23].

In previous study, I did many works with monostatic system. As I mentioned in Chapter 1, it is widely used for the large scale imaging such as air-born SAR system or GPR survey. With the positioning system we can actually acquire dense dataset along the survey lines, however, the problem is that for the 2-dimensional survey we can acquire dense data on the survey lines but it is difficult to acquire dense data across the survey direction. So the monostatic system is still not enough for large scale 2-dimensional survey in near-field case such as GPR applications.

Now if we consider the relatively small area for 2-dimensional survey, for example the wooden structure inspection that I introduced in Chapter 1. Same problem also happens if we use monostatic system for data acquisition. In this case, a straightforward idea is just make many transceiver pairs and arrange is along the cross direction of the survey direction so the 2-dimensional survey can be reduced to 1-dimensioal survey. Or we can do it even cleverer that make a 2-dimensional antenna array so we can acquire the data without moving the system. However, if we just simply put transceivers follow the Nyquist sampling criterion that elements spacing is less than half wavelength, then the cost may extremely huge. For example, if we want to make a 0.5 m by 0.5 m 2-dimensional array with about 6 GHz center frequency, 0.05 m element spacing is required and it need more than hundred antenna elements. Also the size of the antenna will be another problem for producing such 2-dimensional array. In this case we need better solutions for the 2-dimensional array design.

2.32 Experimental equipment and array configuration

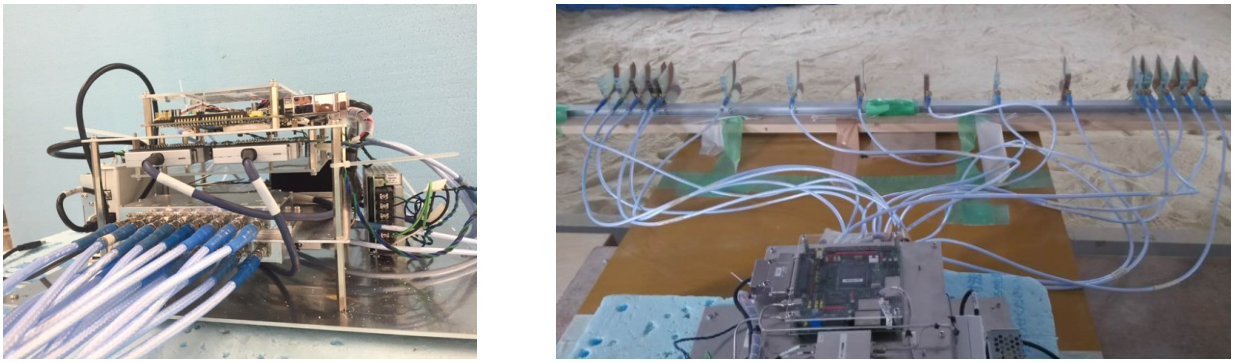

(a) (b)

Figure 2.7 SFCW radar system for our experiment. (a) Control unit of the system; (b) combined system with a 1-dimensional linear sparse array.

Figure 2.7 shows the experimental equipment that is using for the experimental data acquisition for this thesis. It is a stepped frequency system that works from 3.81420 GHz to 8.0674 GHz. Here we should delight that the operating frequency bandwidth is directly related to the time-domain waveform. More detailed conclusions will be given in section 2.41.The system can support eight transmitters and eight receivers work together as a

multstatic system. As the Figure 2.9(7) shows we can arrange the antenna elements in different way as an array radar system. Currently we are using the vivalid antenna for the data acquisition and a trace signal with one of the transceiver pair is shown in Figure 2.8. We put a metal sphere as the target and in Figure 2.8(b) we can observe the direct coupling at about 2 ns and the reflected signal from the metal sphere at about 6 ns. The wavelet of the reflected signal is complicated and we think it is caused by the drop of the high frequency components. Further discussion will be given in later section.

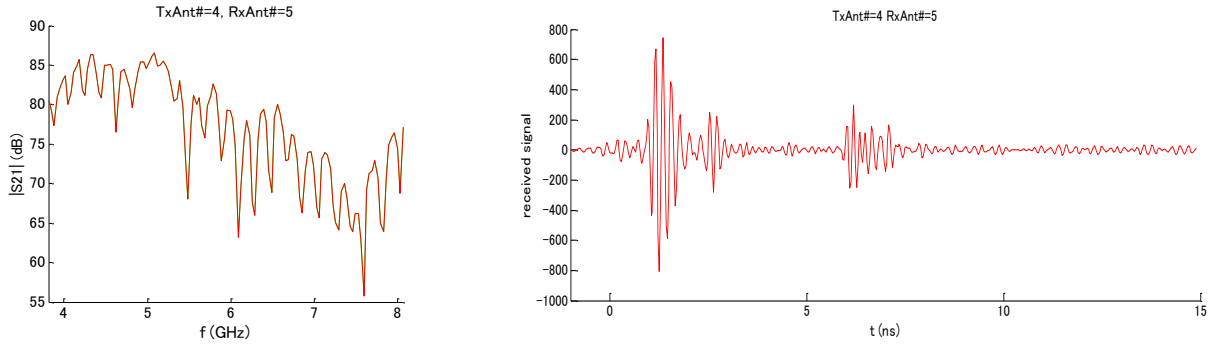

(a) (b)

Figure 2.8 An acquired dataset with a transceiver pair of our system, (a) frequency spectrum; (b) time-domain signal;

In order for the quick data acquisition and to overcome the hardware limitation, we designed the sparse array systems as it shown in Figure 2.19. There are two kinds of the sparse array system that are used for the experimental data acquisition of this thesis, a 1-dimensional linear sparse array and a 2-dimensional sparse array. The conceptions of the sparse array design is already well discussed in previous research works [24] and our lab members designed these array system based on the mid-point assumptions that introduced in [24]. It assume there is a virtue monostatic radar located in the middle of a transceiver pair. For the 2-dimensional array case, the coverage area is 0.6 m by 0.6 m, and the imaging targets are considered to be within 0.5 m. In Figure 2.10 we plotted the middle point of each antenna pair. When the target is a plane reflector, the sparse array is equivalent to a monostatic array that has transceiver elements at these middle points. We can also find that these middle points is somehow uniformly distributed and there are some overlapped middle points included.

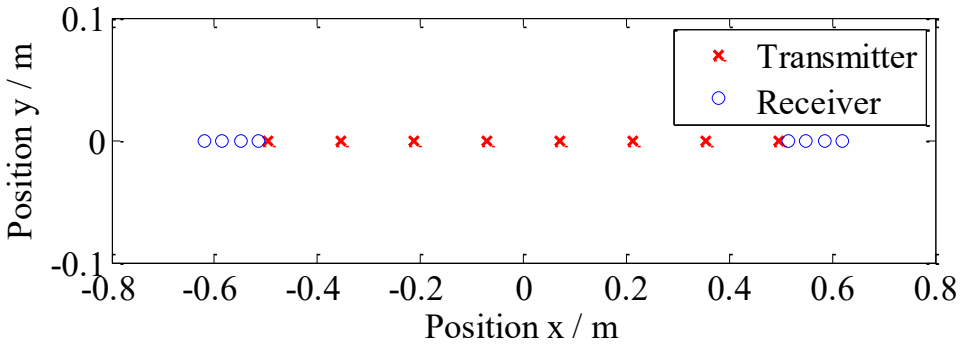

(a)

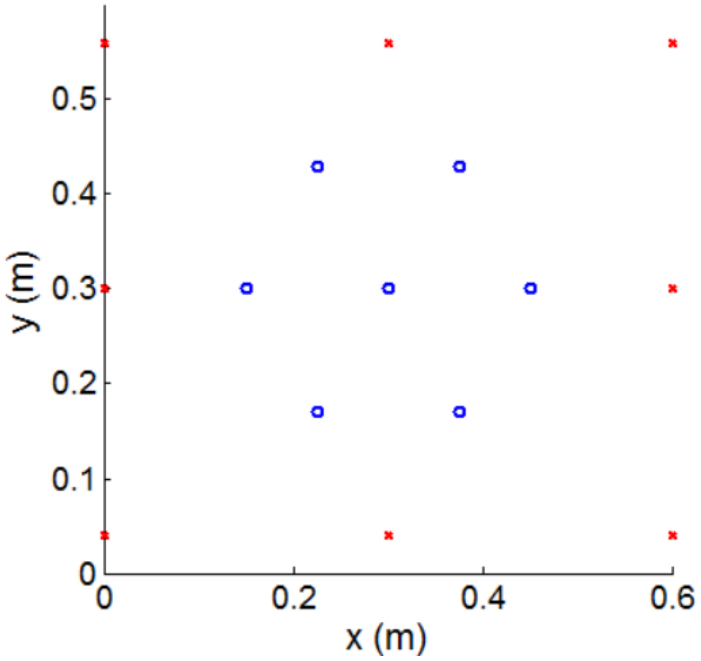

(b)

Figure 2.9 Two different sparse array configurations, (a) 1-dimensional linear sparse array; (b) 2-dimensional sparse array, the red crosses indicate the transmitters and blue circles indicate the receivers.

Here we should notice that the average interval between each mid-point is about 8 cm which is much larger than the half-wavelength of the operating frequency of our system, and this is the main problem that we need to solve for the imaging algorithm with this system. More discussion about this issue will be given in later sections.

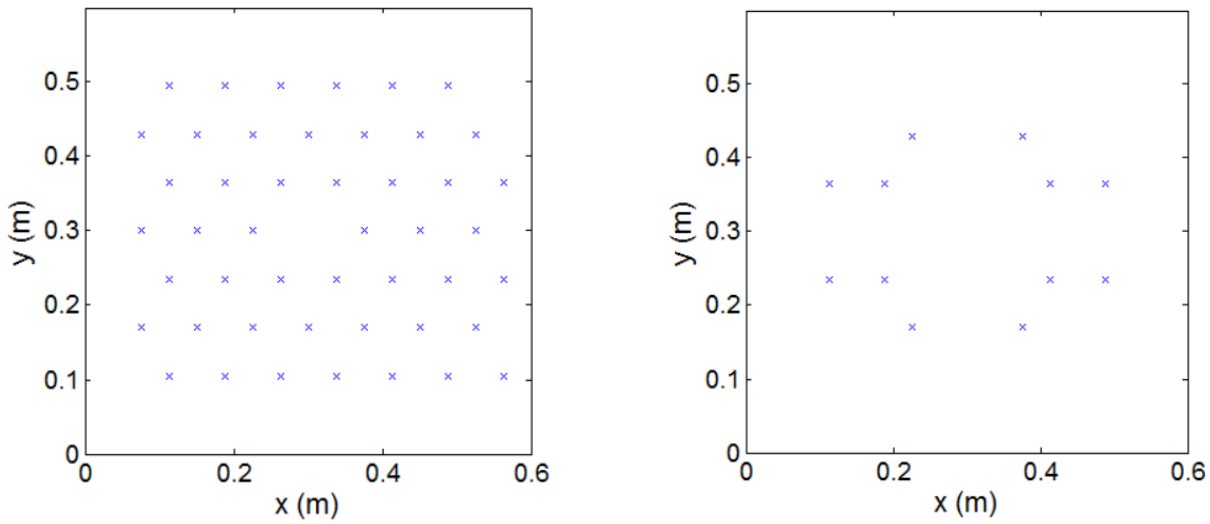

Figure 2.10 The 2-dimensiona sparse array mid-points, (a) distribution of the middle points of each antenna pair; (b) the distribution of the overlapped middle points.

2.4 Hardware factors for multistatic near-range array imaging

2.41 Effect of the waveform

In general, the waveform is directly related to the frequency components of the signal. If we consider the SAR processing in time-domain, it is predictable that the spatial resolution and artifacts are closely related to the waveform of the signal. During the SAR processing we are actually spreading a waveform at a certain depth to an assumed hyperbolic trajectory, the cancelation or the summation of all the waveforms from different traces will decide the final imaging result. Figure 2.11 shows and simple case when the hyperbolic trajectory is above a horizontal reflector. It is straight forward that while the data is well sampled, the summed energy along this hyperbolic trajectory can be well canceled due to the positive and negative part of the waveform. When the spatial sampling is coarse, the energy along the hyperbolic cannot be canceled well and it is predictable that for the irregular sampling case this problem can be more severe.

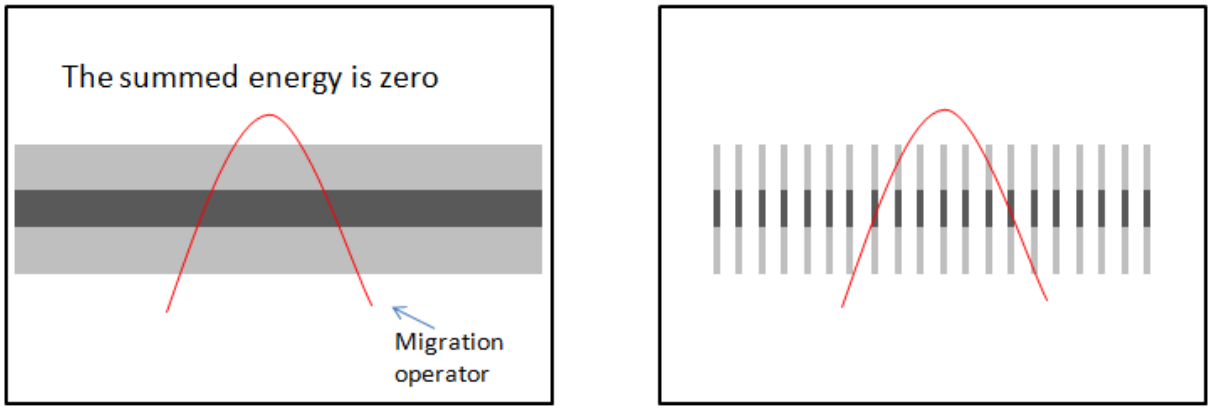

(a) (b)

2.11 The schematic diagram of imaging artifacts, (a) the summation hyperbola cross the properly sampled horizontal reflector; (b) The summation hyperbola cross the coarsely sampled horizontal reflector.

As it concluded in [8], if we assume that the data is spatially well sampled and there is no noise. We can find that the resolution of the image is mainly related to the center frequency when the bandwidth is fixed, but at the same time the sidelobe will be enhanced. If we fix the center frequency, the sidelobe will be decreased and the resolution is constant while increasing the bandwidth. The time-domain signal analysis is more significant. For example, when we fix the bandwidth the signal pulse length in time-domain is fixed. And the mainlobe of the wavelet will be narrower if we increase the center frequency. When we do the SAR imaging, the sharpened mainlobe will provide higher resolution especially in the near-range. At the same time, the sidelobe of the time-domain wavelet will be increased. The simulated results of the PSF response of different waveform is shown in Figure 2.12 (a) - (f). And the PSF response is generated with the sparse array that is shown in (g)- (i).

Please notice that if the system is well sampled, these sidelobes will just cancel to each other. However, when the system is sparse, these energy cannot be canceled well and the pattern of the artifacts depends on the antenna elements distribution of the sparse array system. And these sidelobes can be seen as other reflection from different depth, then there will be a similar problem happens as shown in Figure 2.11. It suggests us that we should use simple waveform in time-domain for the imaging processing.

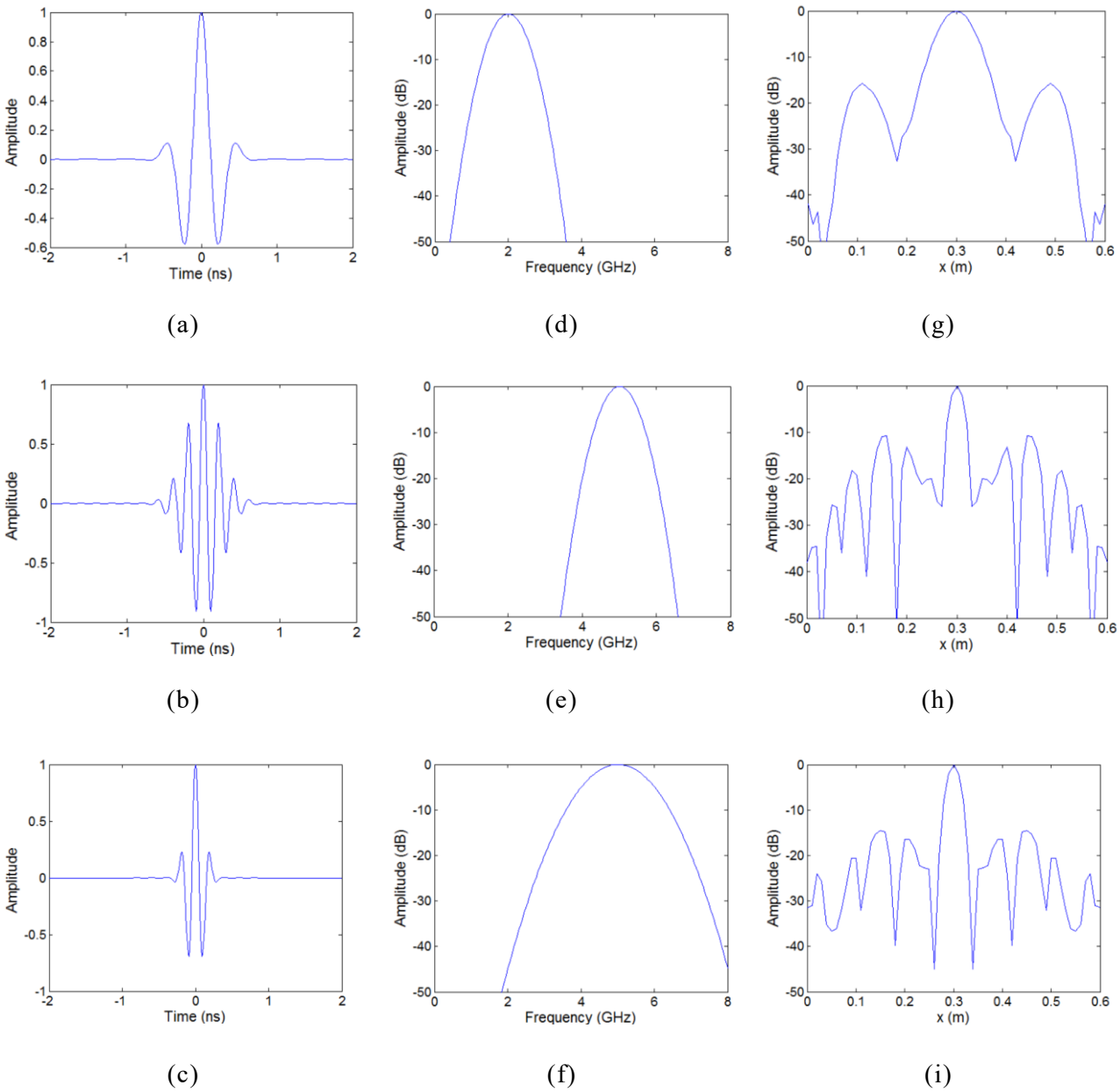

Figure 2.12 From the left side to right side shows the simulated spectrum, time-domain waveform and its PSF response of different frequency components; (a)(d)(g) is the Gaussian signal with 2 GHz center frequency and 1 GHz bandwidth; (b)(d)(e) is the Gaussian signal with 5 GHz center frequency and 1 GHz bandwidth; (c)(f)(i) is the Gaussian signal with 5 GHz center frequency and 2.5 GHz bandwidth.

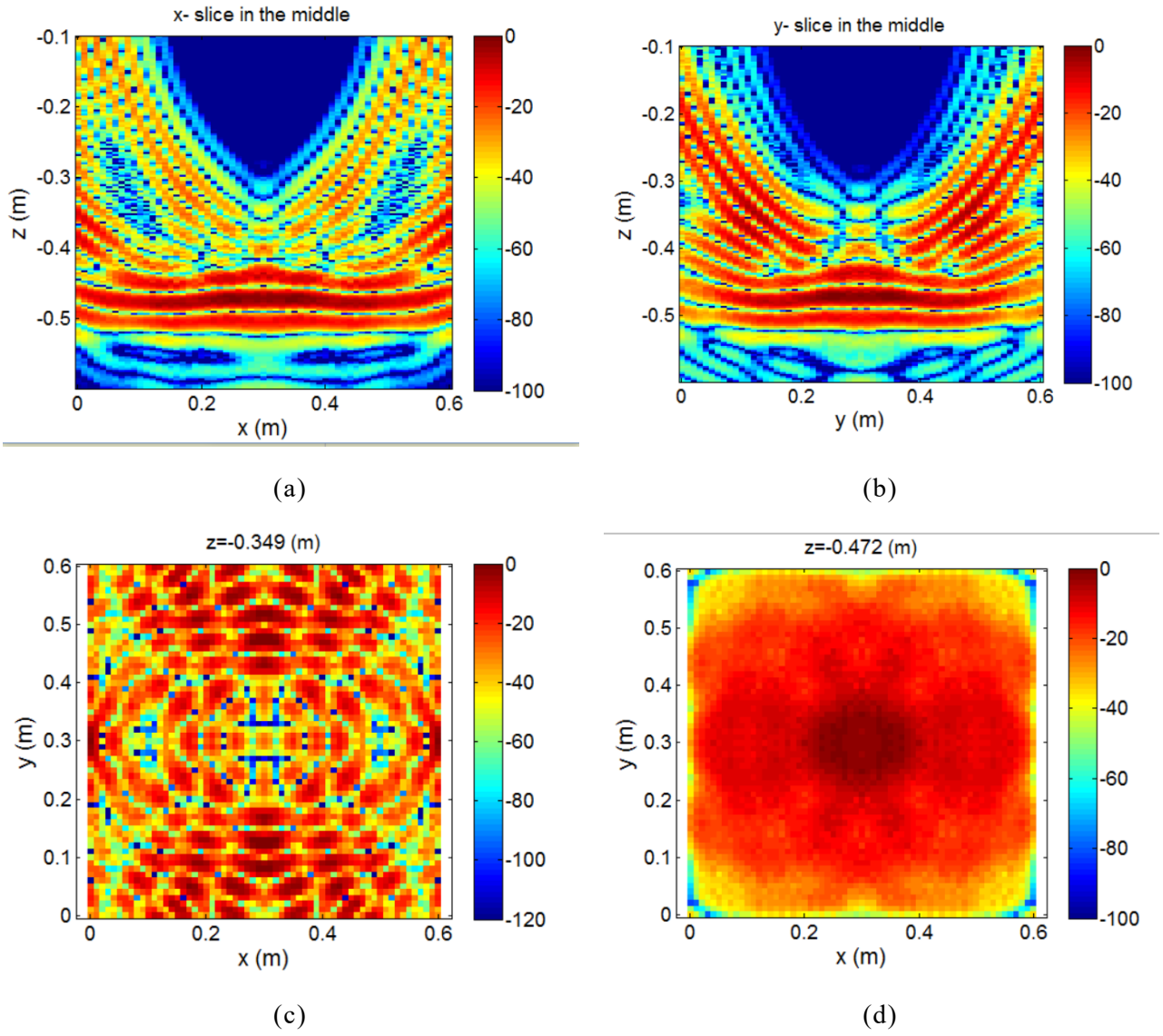

Figure 2.13 simulated 3-dimensional imaging of a horizontal reflector at 0.47 m with sparse array; (a) vertical slice in x direction; (b) vertical slice in middle of the y direction; (c) horizontal slice at shallower depth about 0.35 m; (d) horizontal slice at the corresponded depth of the horizontal reflector.

When we think about the imaging of the distributed target, we can find that the imaging result is hard to be predict. For a certain antenna array, the PSF response is spatial variant and the final imaging result of a distributed target can be approximate to many point targets distributed at different places. Which means that the final result is not only decided by the antenna array but also strongly affect by the target itself. And this is the main reason that sometimes the imaging distributed result does not follow the conclusions of the point target imaging. Because for a single point target there is no interaction from other targets while for the distributed target, the imaging will not only suffer from the artifacts caused by the sparse sampling but also suffer from the artifacts from the other targets at different position. Figure 2.13 shows one situation that imaging a layer reflection with the sparse array after

3-dimensional SAR processing. The target is a horizontal reflector at 0.48 m away and we can find this reflector is lightly distorted. And such distortion is less severe at lower part of the reflector. As I mentioned above, it is because that the lower part correspond to the sidelobe of the reflected wavelet and while spreading the energy from this part of the signal, it will mainly distort the upper part of the imaging area.

Another problem is that we can find when we add other target in shallower region, the artifacts from the lower reflector will cover the reflected signal from the upper target. Such problem always happen for the near-range inspection of the inner wall structures.

As the example shows, firstly we should try to use simple waveform as the transmitted signal so that less artifacts will be introduced due to the sparse sampling. Here we should emphasis that only for the sparse array the simple waveform is important because the fluctuations can be well canceled if we use spatially well-sampled dataset. Then we need to try to reduce the artifacts that introduced in shallower region of a distributed target.

As it shown in Figure 2.11, we can find that when the bandwidth is close to center frequency the waveform can be quiet simple because there is only one notch appears. However, such idea signal is difficult to be achieved due to the limitation of the transmitted frequency band or the hardware and antenna. In this case we may need signal processing methods such as deconvoluiton or wavelet shaping filter to improve the signal waveform.

2.42 Effect of the Antenna redundancy

As it also mentioned in [8], for the far-field antenna array design it is common to calculate the array response by convoluting the transmitting array and the receiving array. However it is not that proper for the near-range imaging because the distance between antenna elements is so large comparing to the distance to the target and the summation trajectory during the SAR processing changes dramatically for the different imaging points. It will cause many numerical problems during the SAR processing which are not significant for far-field imaging. Figure shows the case of a PSF response of a point target in 2-dimensional case. Such PSF response indicates the summation trajectory the imaging point on that point target. From the view of the time-domain imaging, these trajectory are clearly correspond to the antenna array distribution. As I mentioned in previous part, they are decided by antenna array distribution and also spatial variant. Rather than using the convolution approximation for far-field case, we may use mid-point approximation to simplify the array imaging.

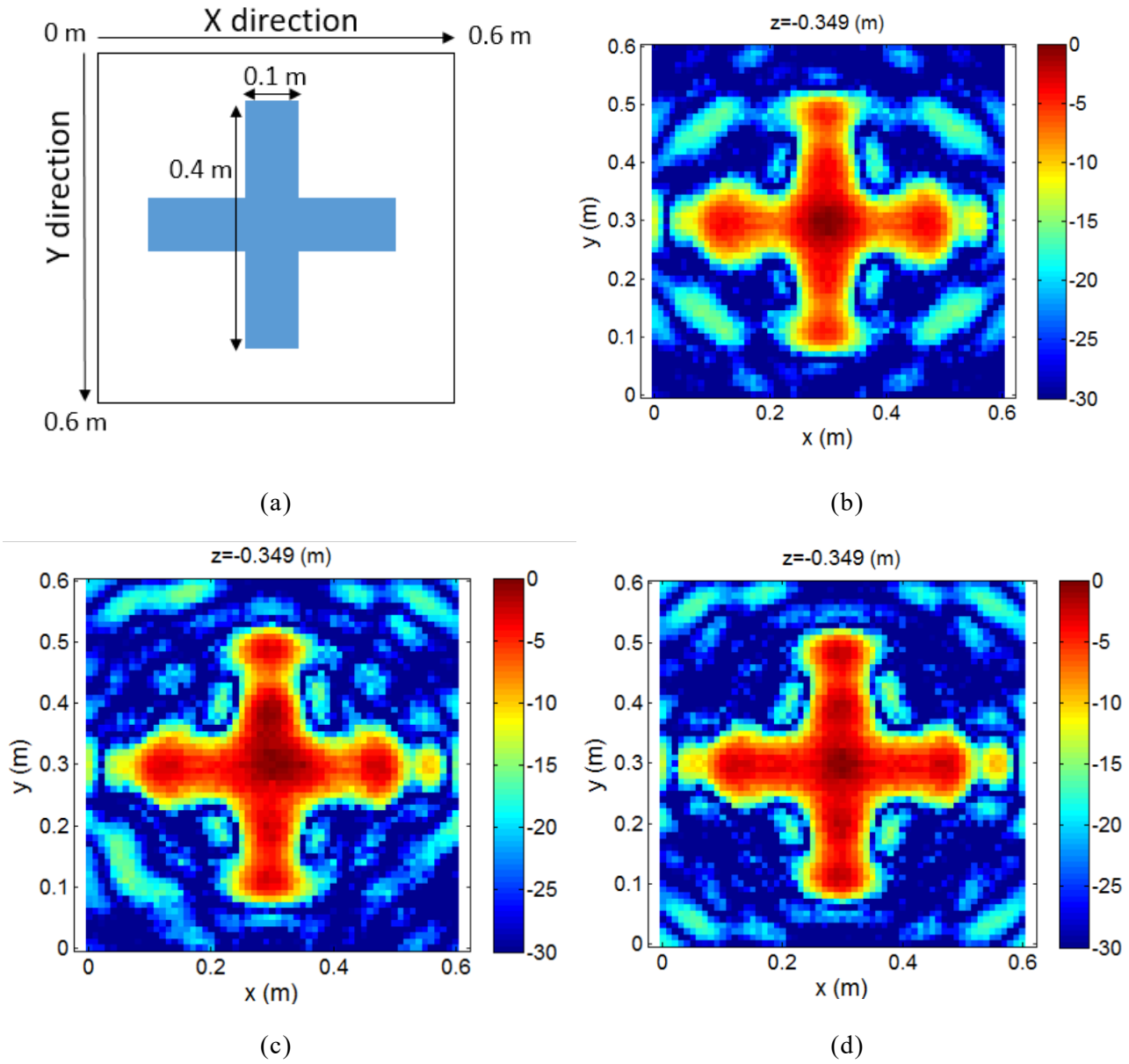

Figurer 2.14 Simulated 3-dimensional SAR imaging of the cross target; (a) model of the cross target;(b) horizontal slice of the target with all antenna pairs; (c) horizontal slice of the target after random redundancy middle point removal; (d) horizontal slice of the target after symmetric redundancy middle point removal;

If we know the position of the imaging point, and the wave propagation velocity, we can correct the response of a transmitter receiver pair to the response of a transceiver that located in the middle of the transmitter receiver pair. It is also pointed out in [8] that such problem but there is not clear conclusion of this problem. Actually this problem is also appears for seismic exploration, and it is suggested to make the stacking number on each overlapping points to be as uniform as possible. While for antenna array system usually we only have few times of overlapping at each mid-point, we can predict that if there is only

few points are overlapped it may introduce strong artifacts due to the cancellation of the SAR processing trajectories. As we discussed above, such effect will be more significant for sparse array imaging. In previous section we showed the sparse array system that designed for relatively uniform mid-points in Figure 2.10. And there are 17 overlapping points that are indicate in Figure 2.10(b). Here in Figure2.14 shows the horizontal slice of a cross model with/without removing the overlapped mid-points. And the simulated waveform is generated with the Gaussian wavelet ranged from 3 GHz to 6 GHz. We can find that by removing the overlapping points the shape of the cross become more accurate and the surrounded artifacts also become weaker. Figure 2.14(c) shows another case that we remove the overlapped mid-points randomly, the result is somehow worse than removing these points symmetrically. It also leave us a question, if the random spatial sampling can provide better imaging results or not? However, in both cases we can find that the surrounded artifacts can be greatly reduced. With many simulated experiment we found that by removing these redundant traces the imaging result can be improved.

2.5 Summary

In this chapter I reviewed the basics of SAR imaging and clarified its relation with the migration processing in seismic. I have shown that the time-domain SAR imaging algorithm which is also known as migration is most accurate method for SAR imaging, while the calculation is very huge and it can be greatly simplified with FFT that applied in frequency domain by some mathematical simplifications. And the algorithms in frequency domain is widely used in SAR imaging techniques. However, I still think it is better to use the time-domain algorithm for near-range imaging since many far-field assumptions are not satisfied and I think the wavelet shape has significant effect in near-range imaging. Similarly, it is also pointed out that the SAR processing is a kind of interpolation of the coarsely sampled data.

Different kinds of data acquisition synthesis are introduced. And I introduced the multistatic SFCW radar equipment that is mainly used in this research work with two different sparse array configuration that applied for 2-dimensional imaging and 3-dimensional imaging. The array radar system that I discussed in our work is not MIMO system but multistatic system, it transmit signals independently which is similar to the pre-stack technique in seismic exploration.

The main problem of the SAR imaging with the sparse array radar system is well discussed. There are many factors that caused the imaging artifacts during the SAR processing and one of the main problem is caused by the coarse spatial sampling which is related to the sparsity of the antenna elements. Also I discussed the effect of the operating frequency range which is presented as the wavelet shape of the time-domain signal. I think it is clearer to discuss the imaging problem in time-domain since there is only time-domain signal exist in the real world. From both microwave imaging point of view and the mathematic point of

view I think we should use simple wavelet form to reduce the imaging artifacts. I also discussed the effect antenna redundancy and I think the unity of the overlapped point can be important especially for near-range imaging issue.

These factors are somehow decided with the observation system. Hence In later chapters I will further discuss on artifacts removal methods with signal processing technique based on the fixed antenna configuration, antenna elements selection, and the fixed signal wavelet.

2.6 Refereces

[1] F. Anderson, W. Christensen, L. Fullerton, B. Kortegaard, "Ultra-wideband beamforming in sparse arrays," IEE Proceedings-H., vol. 138, pp. 342-346, Aug. 1991.

[2] J. D. Taylor, Ultra-Wideband Radar Technology, Ed, CRC Press, 2001.

[3] T. T. Wu, "Electromagnetic missiles," J. Appl. Phys., vol. 57 (7), pp. 2370- 2373, 1985.

[4] V., Schmitz, S., Chakhlov, W., Müller, "Experiences with Synthetic Aperture Focusing Technique in the Field," Ultrasonics, vol.38, pp.731–738, 2000.

[5] O. Yilmaz, Seismic Data Processing, Tulsa, Society of Exploration Geophysicists, 1987.

[6] A.G. Yarovoy, T.G. Savelyev, P.J. Aubry, P.E. Lys, and L.P. Ligthart, "UWB Array-Based Sensor for Near-Field Imaging", IEEE Trans. Microw. Theory Tech., vol. 55, no. 6, pp. 1288-1295, Jun. 2007.

[7] X. Zhuge, T. G. Savelyev, A .G. Yarovoy, "Assessment of Electromagnetic Requirements for UWB Through-Wall Radar," in Proc. International Conference on Electromagnetics in Advanced Applications (ICEAA), Sep. 2007, pp. 923-926.

[8] X.zhuge, 2000, "Short-Range Ultra-Wideband Imaging with Multiple-Input Multiple-Output Arrays," doctoral thesis, Delft University of Technology.

[9] H. F. Harmuth, R. N. Boules, M. G. M. Hussain, Electromagnetic Signals: Reflection, Focusing, Distortion, and Their Practical Applications, Kluwer Academic/Plenum, New York, 1999.

[10] Vittorio Murino, Andrea Trucco , Alessandra Tesei, "Beam pattern formulation and analysis for wide-band beamforming systems using sparse arrays," Signal Processing, vol. 56, pp. 177–183, 1997.

[11] B. L. Biondi, "Kirchhoff imaging beyond aliasing," Geophysics, vol. 66, no. 2, pp. 654–666, 2001.

[12] F. J. Herrmann, "Randomized sampling and sparsity: Getting more information from fewer samples," Geophysics, vol. 75, no. 6, p. WB173-WB187, Nov. 2010.

[13] P. M. Zwartjes and M. D. Sacchi, "Fourier reconstruction of nonuniformly sampled,

aliased seismic data," Geophysics, vol. 72, no. 1, pp. V21–V32, Jan. 2007.

[14] J. Dmochowski, J. Benesty, and S. Affès, "On spatial aliasing in microphone arrays," IEEE Trans. Signal Process., vol. 57, no. 4, pp. 1383–1395, 2009.

[15] S. S. Zivanovic, K. S. Yee and K. Mei, "A subgridding method for the time-domain finite difference method to solve Maxwell's equations," IEEE Trans. Microwave Theory Tech., vol. MTT-39.No.3, pp. 471-479, March 1991.

[16] C. Cafforio, C. Prati, E. Rocca, "SAR data focusing using seismic migration techniques", IEEE Transaction on Aerospace and Electronic Systems, Vol.27, No.2, pp.194-206, March 1991.

[17] H. Stolt, "Migration by Fourier transform,"Geophysics, vol. 43, no. 1,pp. 23–48, 1978.

[18] M. Soumekh, "Signal Subspace Fusion of Uncalibrated Sensors with Application in SAR and Diagnostic Medicine," IEEE Transactions on Image Processing, vol. 8, no. 1, pp. 127-137, January 1999.

[19] X. Zhuge, A. G. Yarovoy, T. Savelyev, L. Ligthart, "Modified Kirchhoff migration for UWB MIMO array-based radar imaging," IEEE Transactions on Geoscience and Remote Sensing, vol. 48, no. 6, pp. 2692–2703, 2010.

[20] H. Feichtinger and K. Gröchenig, "Theory and practice of irregular sampling," in

Wavelets: Mathematics and Applications, J. Benedetto and M.Frazier, Eds. Boca Raton, FL: CRC, 1994, pp. 305–363.

[21] L. Yi, K. Takahashi, and M. Sato, "A Fast Iterative Interpolation Method in f-k Domain for 3-D Irregularly Sampled GPR Data," IEEE Journal of Selected Topics in Applied Earth Observations and Remote Sensing, Vol.9, no.1, pp. 9-17,January 2016.

[22] D.R. Wehner and B. Barnes, High Resolution Radar Second Edition, Artech House, 1995.

[23] G. J. O. Vermeer, "3D symmetric sampling of sparse acquisition geometries," SEG Tech. Progr. Expand. Abstr. 2010, pp. 3796–3801, Jan. 2010.

[24]W. Feng, L. Zou and M. Sato, "2D Imaging by Sparse Array Radar System", IEICE Tech. Rep., vol. 116, no. 309, EMT2016-49, pp. 65-70, Nov. 2016.

Chapter 3 SAR imaging with modified processing operators

3.1 Introduction

In previous chapter I discussed about the SAR imaging algorithm and an imaging problem caused by the coarse sampling in spatial domain. For the far-field SAR imaging research, it is already proved that the distance between the antenna elements should be less than half wavelength to prevent the imaging results from artifacts. There are many articles in SAR processing that dealing with the imaging artifacts caused by coarse sampling which is also known as the sidelobe suppression [1][2][3] . However, for the near-field imaging the condition will be straighter because some of the far-field assumptions are not satisfied for near-field case. I will introduce in later sections that many of the artifacts generated in near-field imaging is not really considered for classical far-field narrow-band imaging case.

In this chapter I will mainly discuss on different methods that deal with the near-field imaging artifacts caused by coarse sampling form the view of time-domain imaging. All of our approaches are designed by using a filter or a weighting factor within the SAR processing operator. From the view of practical application, these methods are easy to apply and do not require too much extra calculation. On the other hand, due to the simple form and clear physical meaning of using these weighting factors, the processing results are predictable and the performance are robust. So these methods can be applied to harsh or complicated dataset such as GPR dataset. Another advantage for its simple form so that we can consider to use these improved SAR processing operators for more complicated processing such as within the least square method. I mainly discussed three methods that can directly applied to SAR processing operator.

The first method is about the limitation on SAR processing aperture. This approach is borrowed from seismic imaging processing to deal with the strong artifacts generated in near-field imaging [4]. It Is pointed out in [5] that the imaging artifacts can be reduced by limiting the effect aperture during the SAR processing. Here I should delight that this method is only dealing with the artifacts that caused by coarse sampling during the SAR processing, and actually we are removing the artifacts by sacrificing the effective aperture size for targets at different positions. The other method comes from the doubt of the half wavelength limitation that always mentioned in radar array imaging [2]. For conventional SAR imaging we did not consider about the spatial variation of the PSF on surface because the height is constant and we have enough virtual aperture length. However for the near-range SAR imaging we may care about the distance or depth of our targets. If we consider the PSF function of the point target, it is more like spatial variant rather than constant, which means the far-field assumption is not fully correct in near-field case. Similar problem is also well-discussed in seismic imaging and known as the aliasing problem [6] [7], which

is borrowed from imaging processing techniques [8]. The core idea is consider the artifacts problem from the view of spatial Nyquist sampling criterion so that the imaging resolution can be related to the frequency components of the wavelet. If we can calculate the maximum frequency that do not violate the spatial Nyquist sampling criterion, we can low-pass the dataset properly to remove the imaging artifacts. It is somehow similar to previous method that we have to sacrifice part of the high frequency components to remove the artifacts. In another words, both of these method reduced the imaging resolution to suppress the imaging artifacts.

3.2 Limitation on SAR processing aperture

We will start from the simplest form of the filter applied to SAR processing operator that deal with the virtue range of the processed aperture. As it is shown in Figure 3.1(a), targets can be well detected only when it is located within the antenna radiation pattern of both transmitting and receiving antenna. Here we should notice that the beamwidth of the antenna radiation can be defined by the angle θ, it does not means that we cannot "see" the target even if the target is out of the beamwidth, but the amplitude can be very weak which means that we may not see a complete hyperbolic within the aperture as it shown in Figure 3.1(b). Since the SAR processing algorithm does not count for the radiation pattern of the antenna, it will assume that we can always observe the complete hyperbolic. In this case, the missing hyperbolic will turn to imaging artifacts when the sampling is coarse. It is simple to compensate this issue by using a limited aperture φ within the SAR processing operator and the equation can be given as (3.1)

$$m(x,z) = \iint H_{\varphi} \cdot d(t,x_0) \cdot \delta(t - \frac{r}{v}) dt dx_0 \tag{3.1}$$

Here H_{φ} Indicates the threshold filter that ignore the hyperbolas that exceed the limited aperture φ, while d indicates the radar data and m indicates the imaging result. This φ can be selected by the means of the antenna beamwidth θ. Here we should notice that such filtering processing includes two different meanings. Firstly, it compensate the difference between the observed dataset and the SAR processing algorithm as we described on above; secondary, it will actually limit the appearance of the hyperbolic artifacts caused by the coarse sampling. We will further discuss this issue with a simulation example next.

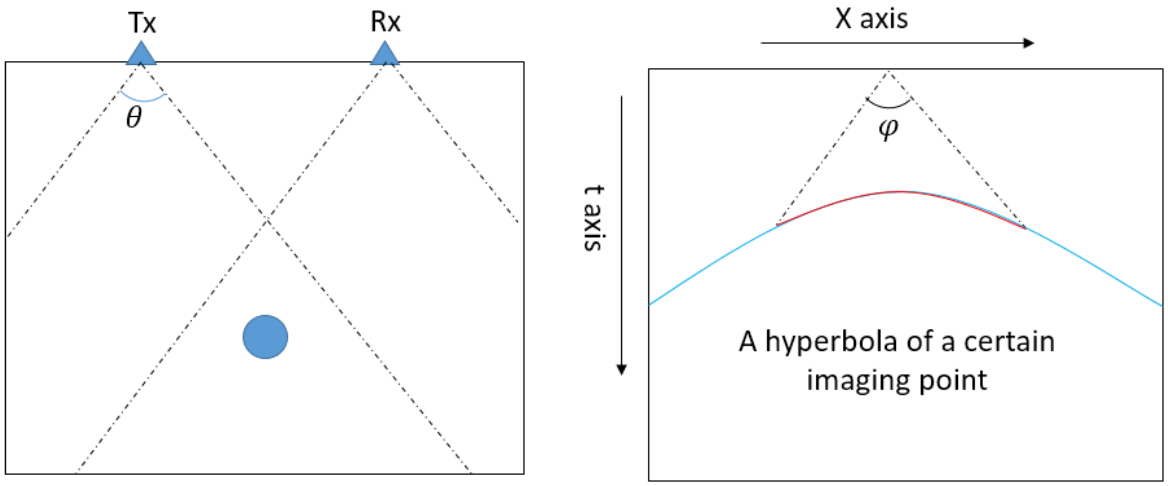

(a) (b)

Figure 3.1 effective aperture in phyjsical model and data space; (a) the antenna beamwidth ploted in model space; (b) the limited aperture for SAR processing in data space.

In order to analyze the performance and the effect of the method, we will use a simple 1-dimensional monostatic simulation case to demonstrate the different methods. The model and the simulated data are shown in Figure 3.2. Here we should point out that all the simulations for imaging problems are done with simple ray tracing and convoluted with a Gaussian wavelet that is introduced in Chapter 2. We do not use the complicated simulation method such as FDTD method because we are focusing on comparing the different imaging methods. As we described in Chapter 2 that the SAR method is just focusing the energy on different hyperbolas, which means that the SAR processing are not considering the complicated effect such as the multiple reflection, wavelet changes caused by attenuation or dispersion. Hence we can purely comparing the performance of different imaging algorithm with the ray tracing simulation.

The model is shown in Figure 3.2(a), it include two point scatterers and a horizontal layer reflection in middle of the point scatterers and the upper scatterer has weaker amplitude. As I mentioned in Chapter 2, we choose the simulated wavelet as a Gaussian wavelet ranged from 4 GHz to 8 GHz. After we resampled the dataset to 5 cm spatial interval, we can observe clear artifacts as it is shown in Figure 3.2(d). We can observe many hyperbolas appears on the horizontal reflector as the artifacts. Figure 3.3 shows the processed result by limiting the processing aperture with 45 degree. As the result, most of the hyperbolas artifacts disappeared. As the example shows, these artifacts are only caused by the coarse sampling and due to the SAR algorithm, when we summing the energy at shallower depth the summation hyperbolas may across with the reflected signals in deeper part and these energy will appears as the hyperbolic artifacts. After we applied the limitation angle on

processing aperture as it is shown in Figure 3.1(b), these energy will no longer appear in shallower depth as the artifacts. As the drawback, since the scatterer in shallow depth has shaper hyperbolic reflection, most of the energy may cut off by the limited angle hence the point scartterer is almost disappeared in Figure 3.3(b).

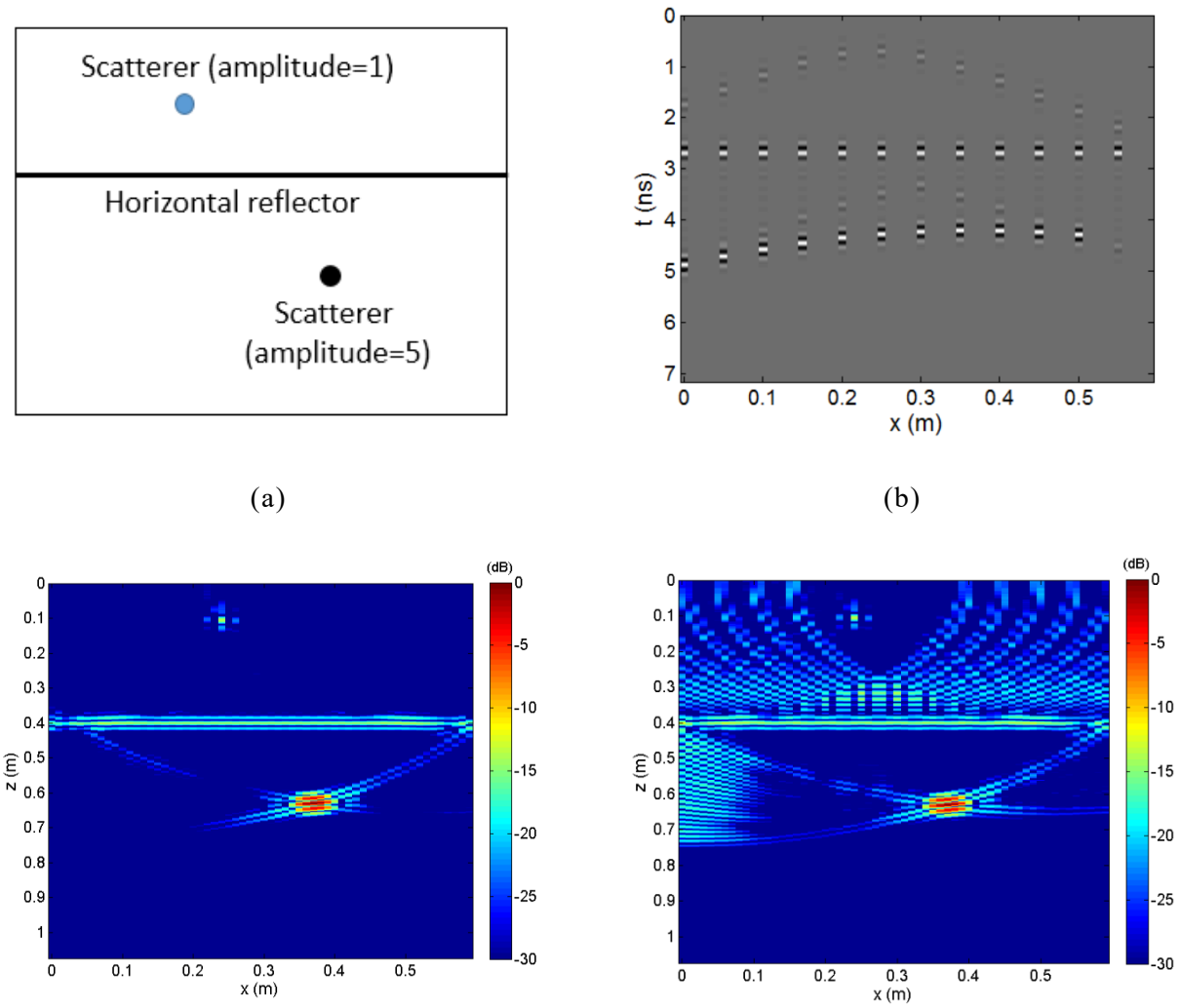

Figure 3.2 2-dimensional simulation for artifacts removal experiment, (a) physical model; (b) simulated radar profile after resampling to coarse condition; (c) conventional SAR imaging result with well-sampled data; (d) conventional SAR imaging result with coarsely samped data.

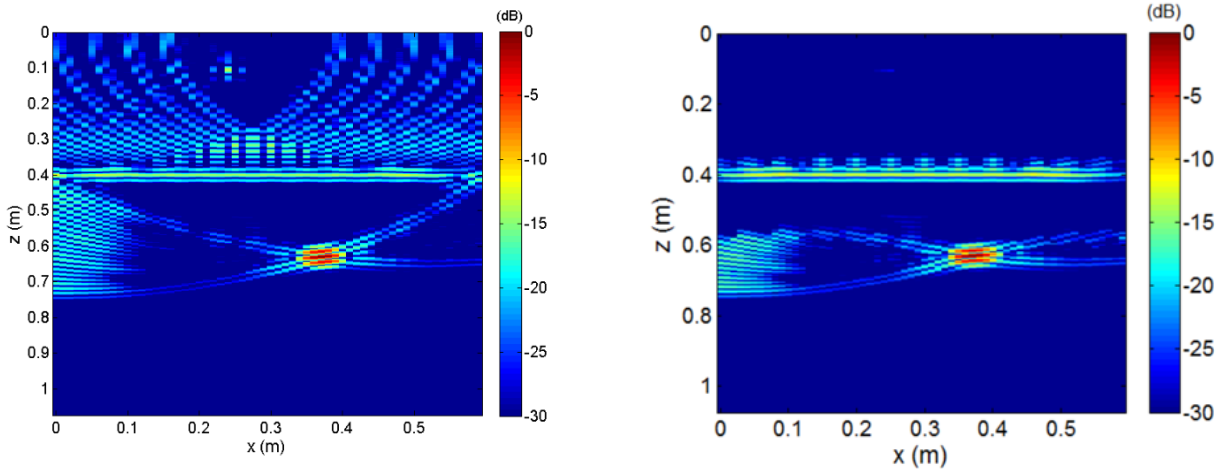

(a) (b)

Figure 3.3 SAR processing with limited processing aperture, (a) without aperture limitation; (b) with 45 degree limitation on aperture.

3.3 Artifacts removal by using the semblance weighted SAR processing

From some of our near-range system results we found that in most of the cases the wavelet shape is quiet constant. It means that we can use the phase information as the weighting parameter. An analysis method for velocity analysis in seismic data processing which is known as semblance is introduced in [9][10]. Semblance is a mathematic definition and it defines in (3.2), it describe the uniformity of a vector q. In another word, when the values in the vector q are constant or nearly constant, the output s will be large; while the values are not uniform the output will be small.

$$s = \frac{\left[\sum_{n=1}^{N} q(n)\right]^2}{\sum_{n=1}^{N} N q^2(n)} \tag{3.2}$$

For our case, s is the semblance value of a certain hyperbolic trajectory, N is the number of the sampled points along the hyperbolic and q is each of the amplitude along this trajectory. The semblance is just one of the practical way of measuring the coherency of a vector. The physical meaning is straightforward, when the values along this hyperbolic trajectory have same value, it will return as maximum value and when the values are different to each other it will return a small value.

As it is shown in Figure 3.4, the dash line indicates a focusing hyperbolic that across with the reflected signal. It will turn to an artifact point as we already described in previous

section. If we use the semblance instead of the stacking processing in SAR processing, even if the hyperbola is not complete and has many missing in between as it shown in Figure 3.2(b), the output will not affect by the missing energy. Figure 3.5 shows some results that comparing the conventional SAR processing and the SAR processing that use semblance instead of the stacking.

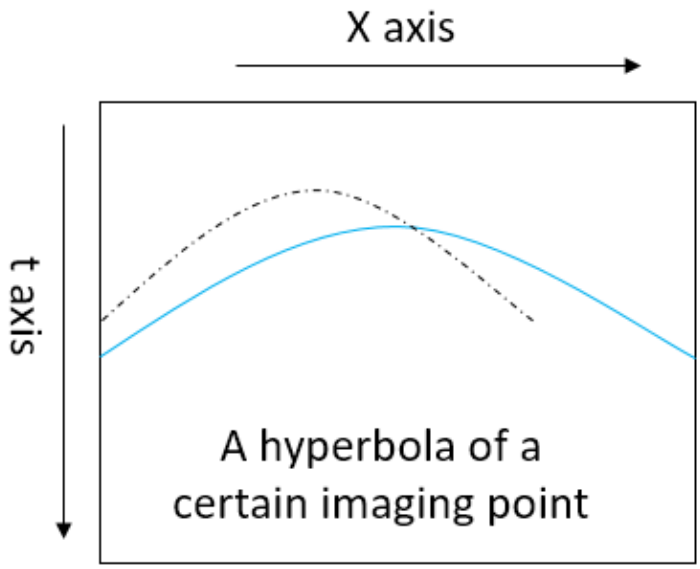

Figure 3.4 sketch of the stacking hyperbolic that across the reflected signal, dash line indicates a focusing hyperbolic and the blue line indicates the reflected signal of a scatterer.

From Figure 3.5 we may found some interesting feature of using semblance for SAR imaging. For both of the well-sampled dataset and coarsely sampled dataset it seems that conventional diffraction stacking has better performance. But it is interesting to point out that semblance image will lose the amplitude information and both upper and lower scatter gives almost same response.

It indicates that semblance is very sensitive to the stationary of the phase information and stacking is relatively stable. Hence we can try to use the semblance as the weighting factor of each summation hyperbolic trajectory. The formulation is shown in (3.3), S indicates the semblance along a focusing hyperbolic as a weighting factor.

$$m(x,z) = S \iint d(t,x_0) \cdot \delta(t - \frac{r}{v}) dt dx_0 \tag{3.3}$$

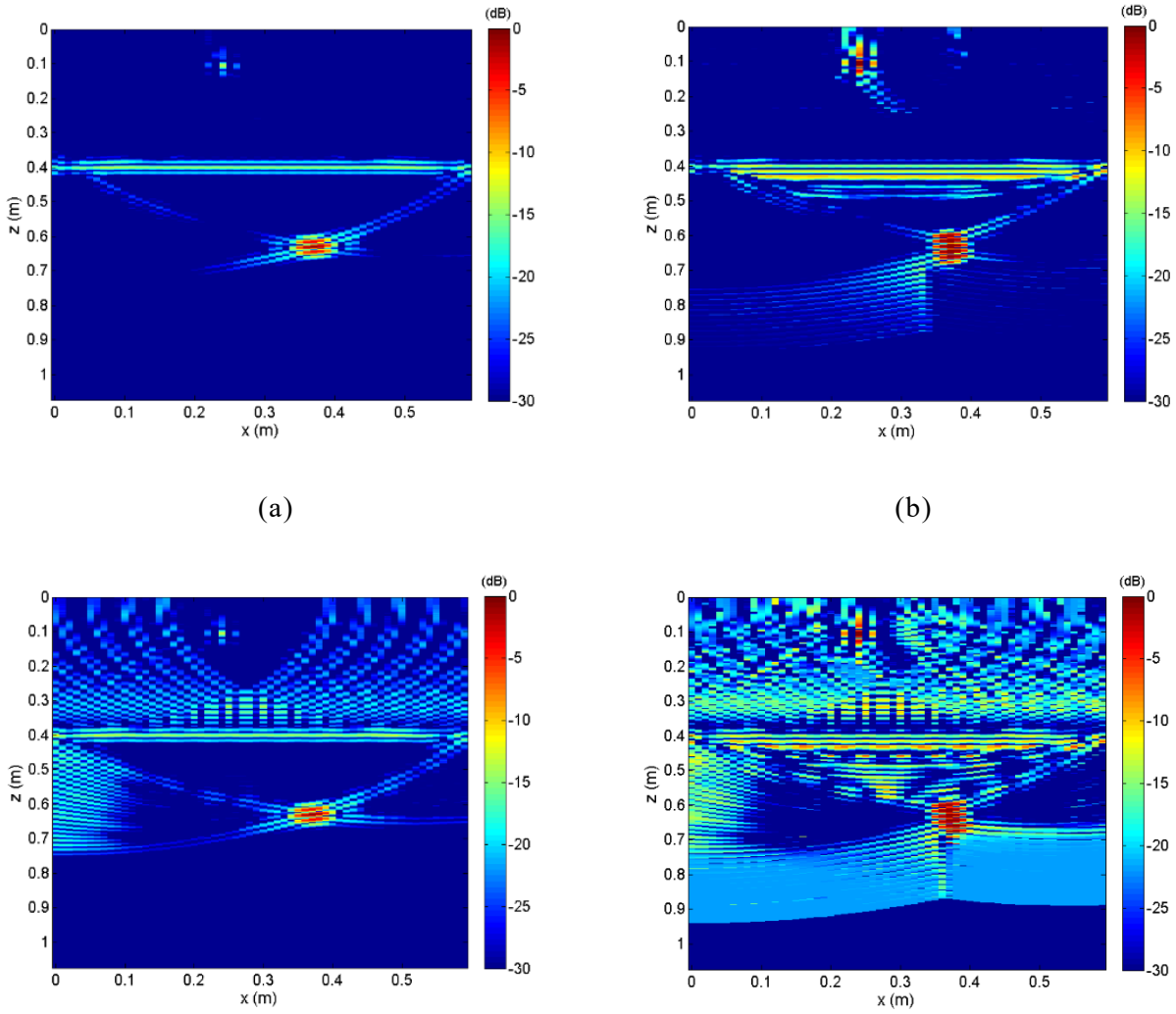

Figure 3.5 Comparison of conventonal SAR processing and the SAR processing using semblence instead of the stacking, (a) well-sampled SAR processing result; (b) well-sampled SAR processing with semblance; (c) SAR processing with coarsely sampled data; (d) SAR processing with semblance on coarsely samppled data;

Figure 3.6 a shows the results for well-sampled and coarsely sampled dataset. As we can expect that the point target is perfectly reconstructed and almost all the artifacts are removed. However, the layer reflector become much weaker. It is because that for each diffraction hyperbolic that near to the layer reflector, the coherency along the assumed hyperbolic is much weaker than a point target. As the result, this approach has excellent performance for the point like targets but it may has problem for distributed target imaging.

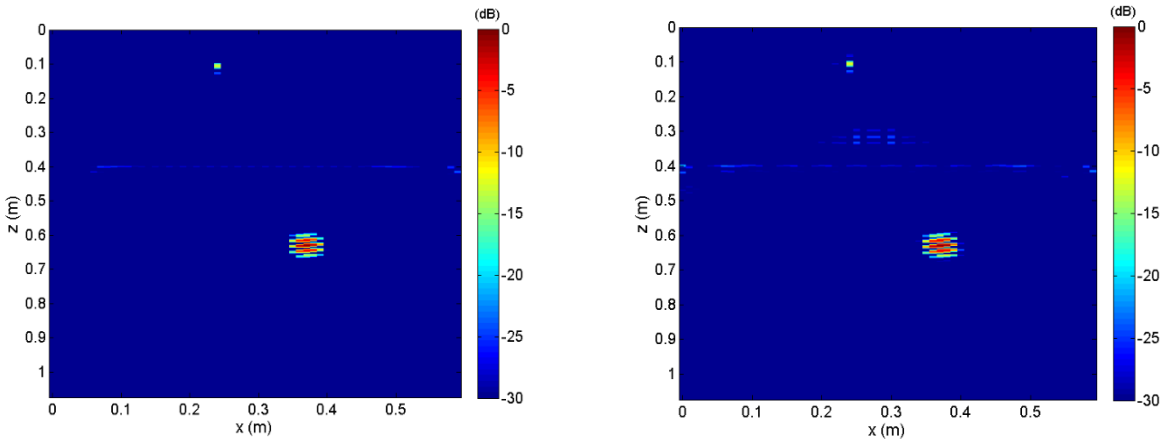

(a) (b)

Figure 3.6 artifacts removal with semblence weighted method, (a) processed with the well-sampled dataset; (b) processed with the coarsely sampled dataset;

3.4 local low-pass filter for artifacts removal

3.31 Nyquist sampling theorem in spatial domain

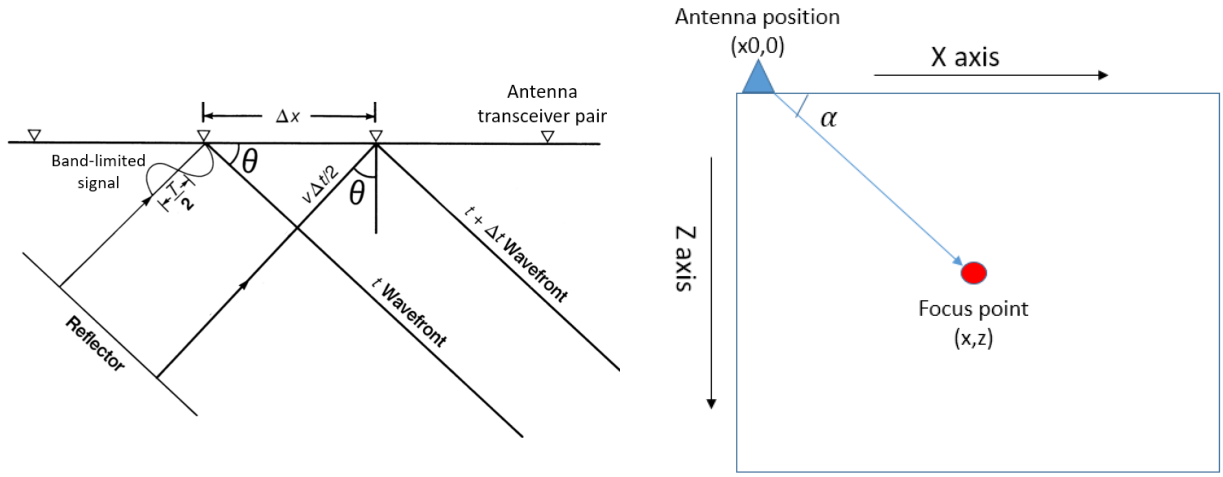

(a) (b)

Figure 3.7 Spatial sampling requirements with reflectors located in near-filed case, (a) the spatial sampling requirment in real space; (b) corresponded situation in data space.

As it is shown in Figure 3.7(a), the reason of the spatial aliasing is caused by the possibility

of distinguish the time delay difference from the nearby signals that reflected from a same target. As I mentioned above, it is related to the angle of the reflector and also during the SAR processing it related to the position of the imaging point. Usually for the near-range SAR case, the problem is mainly caused by the SAR processing because there are not so many tilted reflectors. As it shows in Figure 3.7(a), this angle can be calculated by the geometry relation as

$$\sin\theta = \frac{v\Delta t}{2\Delta x} \tag{3.4}$$

Where θ is the reflection angle of the reflectors and v is the propagation velocity of wave, Δx is the spatial interval between the transceiver pairs and Δt is the time delay difference of adjacent transceiver pair. Also as the Nyquist sampling theory required that the Δt should be less than the half of the dominant period T.

$$\Delta t < T/2 \tag{3.5}$$

With (3.4) and (3.5) we can get the maximum cut-off frequency f_{max} for a tilted reflector as

$$f_{max} = \frac{v}{4\,\Delta x \sin\theta} \tag{3.6}$$

Here we need to point out that the aliasing condition that I mentioned above is quiet in general case. And once the data is acquired, these aliasing cannot or almost impossible to be removed. However, when we do the SAR processing these aliasing will turn into artifacts. Also, even if the data is well-sampled, the operator aliasing may still appears for some imaging points especially in near-field. Fig. 8 explains how these aliasing appears. Here we should notice that if we think about the SAR processing aliasing, the angle α should be defined as the local incident angle that defined by the antenna position and the imaging point. It indicates that depends on different imaging points, the requirement of the aliasing condition will be changed. And in this case (3.6) will become

$$f_{max} = \frac{v}{4\,\Delta x \cos\alpha} \tag{3.7}$$

$$\cos\alpha = \frac{x_0 - x}{\sqrt{(x_0 - x)^2 + z^2}} \tag{3.8}$$

3.32 artifacts removal with local low-pass filter

If we simply low-pass all the signal with the half wavelength condition, many of the useful

high frequency components will be lost. Here we should notice that actually by reducing the frequency components we will partially loss some spatial resolution. As it shown in (3.7), the targets that close to the antenna array has higher spatial resolution but also suffers more from the aliasing problem.

A simple 2-dimensional tests are shown in Figure 3.8, we use same model with previous section. Here we can find that the artifacts mixed to near region are greatly reduced by using the filter. From this result we may notice that 2-dimensional artifacts is not so dangerous because it is somehow easy to be distinguished. However, the pattern of the artifacts is strongly depends on antenna array and the target itself and they may much difficult to be recognized. Also for 3-dimensional horizontal slice these artifacts may just cover the reflections in shallow depth.

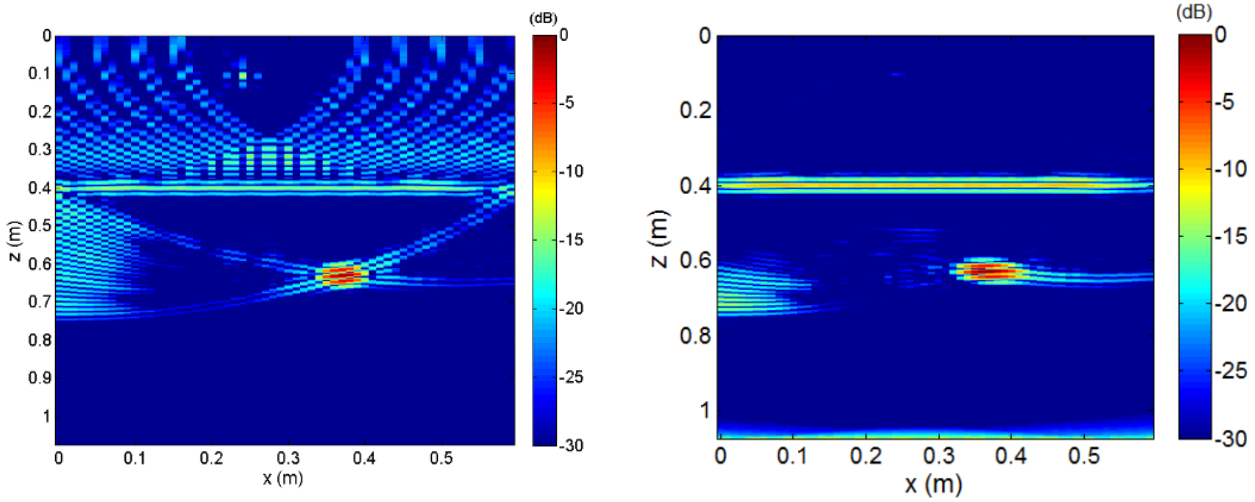

Figure 3.8 SAR processing result with local low-pass filter, (a) Conventional SAR imaging result; (b) SAR processing with local low-pass filtering.

However, the maximum cut-off frequency is easy to be defined in 2-dimensional monostatic case while it is much difficult to be define for the 3-dimensional multistatic case. Because when we are summing the energy in 3-dimension with a hemi-spherical the aliasing appears in different spatial direction. There are already some research works discussed about this issue but there is still no clear conclusion. One of the way is to calculate the average spatial interval of both transmitting antenna and receiver antenna. And the maximum cut-off frequency can be given in (3.9)

$$f_{max}=\frac{v}{2\,\Delta\rho(cos\alpha+cos\beta)} \tag{3.9}$$

Where $\Delta\rho$ is the average spatial aliasing and α,β are the local angle of transmitting antenna and receiving antenna.

But when the elements are distributed sparsely and irregularly such approach is still not correct. In this case, we designed our sparse array with such consideration that make the middle point of each antenna pair spatially uniform as possible and use this middle point distance as the average spatial interval of the array. We also tried some other methods to evaluate the maximum frequency that introduced in [11][12], while the maximum frequency calculated with (3.9) give best results for our 2-dimensional sparse array system. More precise mathematical analysis for this issue is still necessary.

3.33 Practical application of the local low-pass filter

The local low-pass filter is a relatively good method to compensate these artifacts. (3.7) indicates that the maximum cut-off frequency is changing at different position for each imaging point. In this case we can use the local low-pass filter to remove the high frequency components to reduce the aliasing or imaging artifacts while do not loss so much resolution. We can achieve it by conventional low-pass filter in frequency domain, however, for each data acquired by an antenna pair we need to apply different low-pass filter for many times. So the calculation can be very large. Here we used a mathematical simplification that is introduced in [13] on seismic imaging. The filtering in time-domain can be given as

$$f(t)=x(t)*w(t) \tag{3.10}$$

Where x is the input signal and f is the output and w is the filter. The triangle filter in time-domain is a simple low-pass filter and it can be given as

$$w(t)=\begin{cases}1-|t|/k & |t|\le k\\ 0 & otherwise\end{cases} \tag{3.11}$$

Here this k is the width of the triangle filter and it can be related to the cut-off frequency of the low-pass filter. Because in frequency domain this filter can be given as

$$W(f)=k\left(\frac{sin(\pi kf)}{\pi kf}\right)^2=ksinc^2(\pi kf) \tag{3.12}$$

For the linear calculation like convolution we can change the order of the integral/deferential hence (2) can also be give as

$$f(t) = \tilde{x}(t) * w''(t) \tag{3.13}$$

Where

$$\tilde{x}(t) = \iint_{-\infty}^{t} x(t)dt \tag{3.14}$$

For the quadratic differential of the triangle filter it can be given as three delta function located at both side of the triangle and its middle point. Hence the output at a local position can be simplified as

$$f(t) = \frac{\tilde{x}(t-k) + \tilde{x}(t+k) - 2\tilde{x}(t)}{k^2} \tag{3.15}$$

By using this method the local low-pass filter can be calculated easily without adding too much calculation. In most of the cases this method can get almost same result with the convolution method, while the cut-off frequency is less than center frequency numerical error will happen. Such case is quiet rare but we still need to keep it in mind.

3. 5 Comparison of different methods

Figure 3.9 shows the 3-dimenasional simulated model for 2-diemnsional sparse array. We put a cross shape at 0.35 m depth and a horizontal reflector at 0.45 m depth. And the simulated waveform is generated with the Gaussian wavelet ranged from 3 GHz to 6 GHz. The simulated waveform is designed to be similar to our experimental system that is introduced in Chapter 2, the frequency bandwidth is slightly narrower than the real system. It is adjusted based on the observed result since the real signal is not an ideal Gaussian wavelet and the frequency spectrum is not same. Here we simulated with the 2-dimensional sparse array configuration that we have introduced in Chapter 2 and the antenna configuration is shown in Figure 2.9(b). Figure 3.10(a) shows the conventional SAR imaging result at the correct depth. The artifacts caused by this horizontal reflector will cover the cross target in shallow depth in horizontal slice as we have discussed at the end of previous chapter. We can see many strong artifact and the cross shape become not continuous. The performance of different processing methods are shown in Figure 3.10 and Figure 3.11. The aperture is limited to 45 degree for the processing aperture limitation method, the average spatial interval is set to be 7 cm for local low pass filtering method. It

is easier to compare with the horizontal slice at the correct depth of the cross shape reflector as it is shown in Figure 3.10. In general we can find that the local low-pass filtering method has relatively better performance than the other methods although we still can observe the distortion at the edge of the cross shape. While SAR process aperture limitation method result in Figure 3.10(b) can also greatly improve the imaging result that the artifacts from the lower plate reflector are most eliminated but the shape of the target is not clear comparing to the Figure 3.10(c). The semblance weighted method does not show a good result for this model. As we already introduced in section 3.3. This method is designed base on point target, for a distributed target this method will enhance the edge of the target which include some scattering effect hence the shape of the target may become discontinuous. In Figure 3.11 we can observe some other features of the proposed methods. In Figure 3.11(b) we can find that the limitation on processing aperture will prevent the SAR processing by bring the energy to the upper part of the summation hyperbola so that the artifacts can be suppressed. In this case some targets that close to the antenna which have sharp summation hyperbola may become much weaker after processing or vanished from the imaging result. Similar problem may also happen to the local low-pass filter method because we also need to calculate the cut-off frequency depending on the position of the imaging point. When the target is close to the antenna the cut-off frequency will be very small which means these targets may not image clearly. Also, we may notice from Figure 3.11(c) that not only the spatial resolution, but also the time resolution is reduced due to the low-pass filtering.

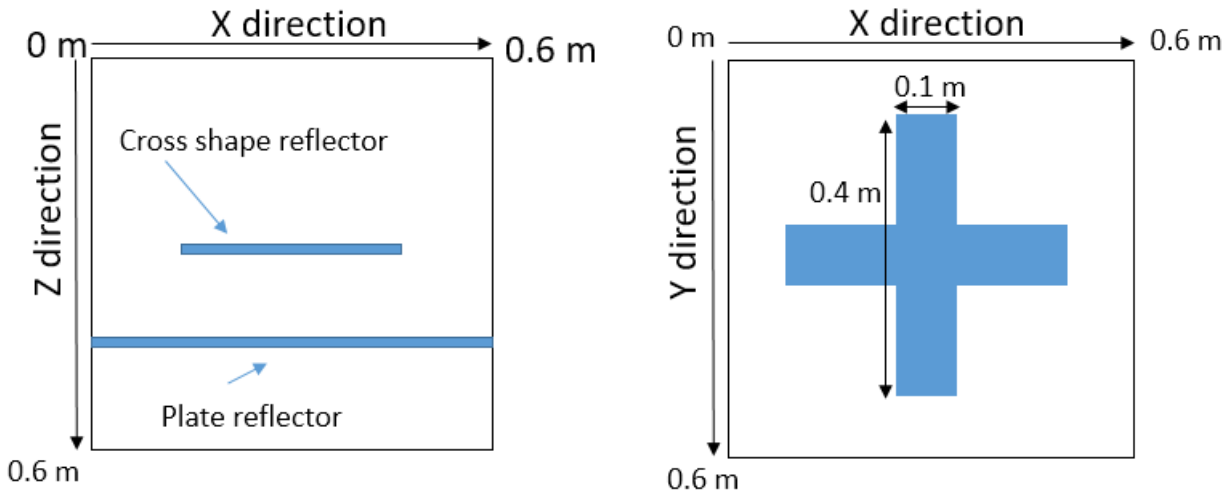

(a) (b)

Figure 3.9 3-dimensional model for the local low-pass filter test; (a) vertical slice; (b) horzontal slice;

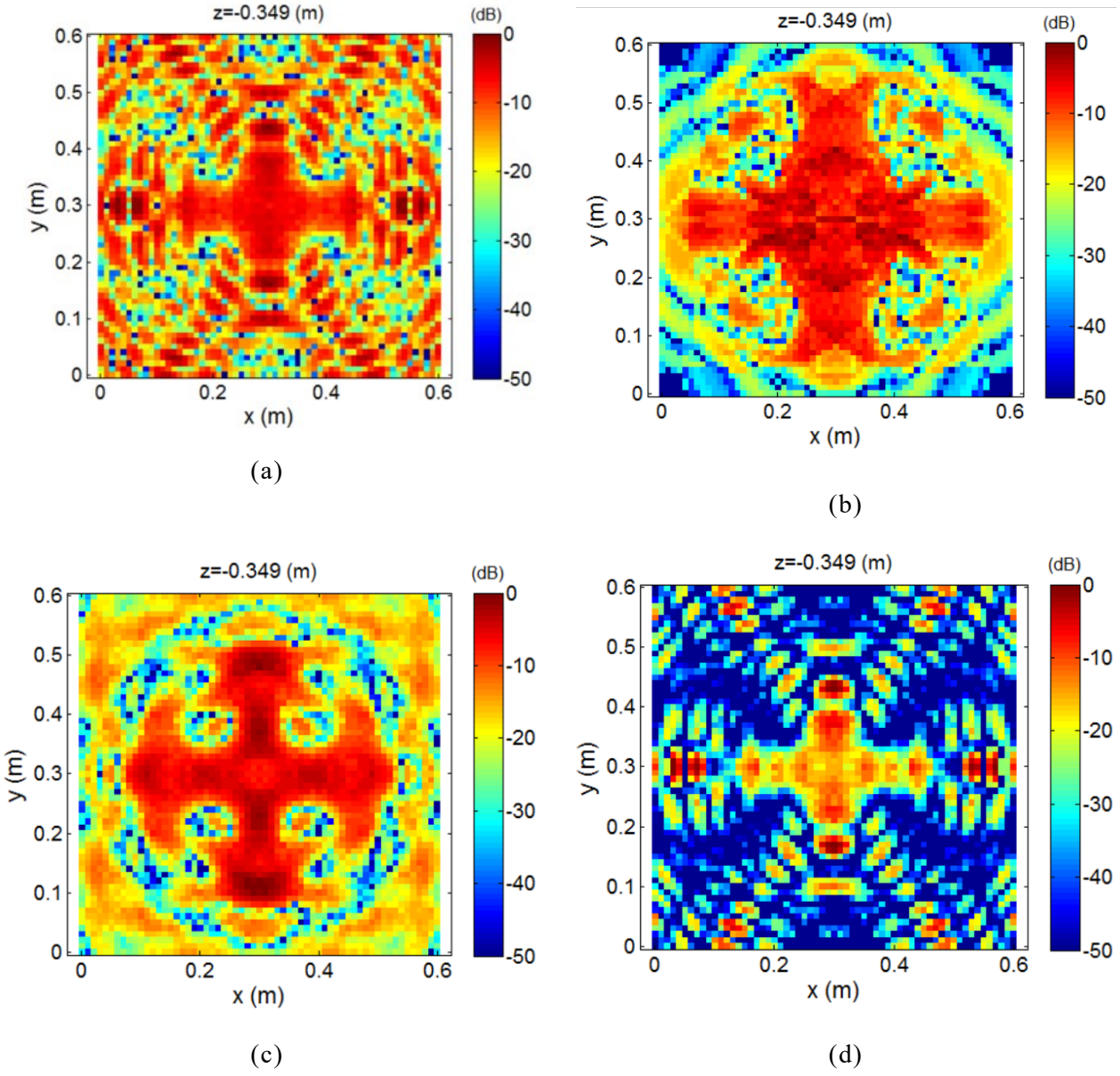

Figure 3.10 Horizontal slice comparison of different artifacts removal methods for 2-diensional sparse array, (a) conventional SAR imaging result; (b) SAR imaging with limited processing aperture (c) SAR imaging with the local low-pass filter; (d) SAR imaging with the semblence weighted.

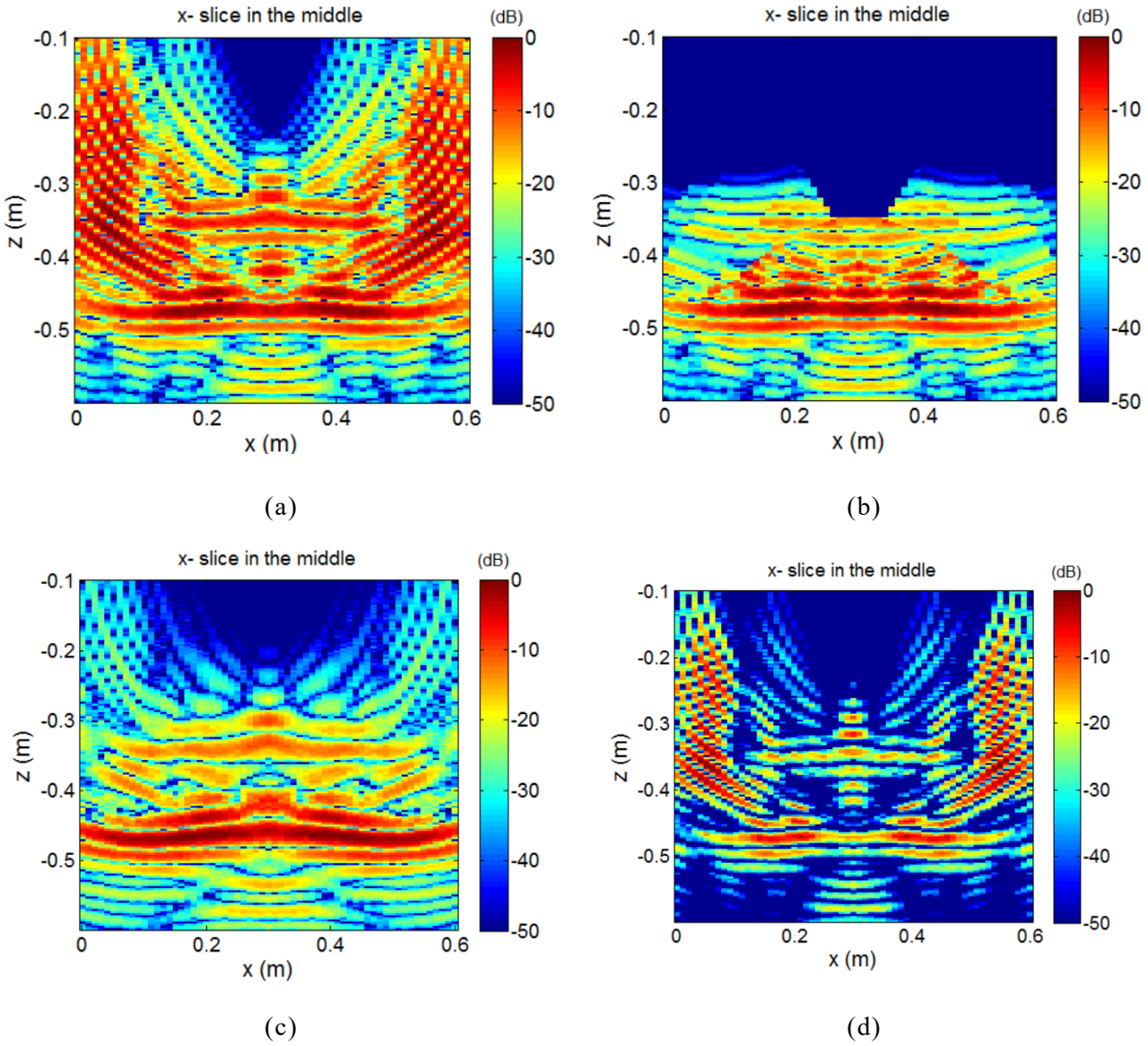

3.11 Vertical slice comparison of different artifacts removal methods for 2-diensional sparse array, (a) conventional SAR imaging result; (b) SAR imaging with limited processing aperture (c) SAR imaging with the local low-pass filter; (d) SAR imaging with the semblence weighted.

3.6 Summary

In this chapter I introduced three different approaches to remove the imaging artifacts that can applied as a filter or weighting factor within the conventional SAR processing. All of these methods do not require too much extra calculation and the selection of the processing parameter is easy which means that these methods are more robust than complicated

algorithm such as CS method that I will introduce in Chapter 4. The general idea of these methods are trying to deal with the impropriate summation of the energy along the summation hyperbola during the SAR processing, while the approaches are different to each other.

The limitation on processing aperture is related to the antenna radiation beamwidth but actually it is reducing the artifacts by reducing the effective aperture. Hence the spatial resolution maybe reduced and the targets with sharp hyperbola response may lost.

The semblance weighted SAR processing has good performance against the point like targets while it is not designed for distributed target. If we can make sure that there is only point scartterers this method can be the most effective way to reduce the imaging artifacts.

The local low-pass filtering method has relatively robust performance for different applications. It uses a spatial variant low-pass filter to cut-off the high frequency components that may turn into artifacts during the SAR processing. The main disadvantage of this method is that the effective spatial interval which is used for calculating the maximum cut-off frequency cannot be clearly defined for multistatic system. And it remains to be a future work of this research.

The main aim of using this operator based artifacts removal methods is that it can be combined with other advanced processing technique such as iterative based algorithm that I will introduce in Chapter 4. And also we can consider to combine themselves together for example we can actually combining the processing aperture limitation and the local low-pass filter together. This kind of trial is still continue.

3.7 References

[1] D.H. Turnbull, F.S. Foster, “Beam Steering with Pulsed Two-Dimensional Transducer Arrays,” IEEE Trans. Ultrason., Ferroelectr. Freq. Control, vol. 38, pp. 320-333, Jul. 1991.

[2] G.R. Lockwood and F.S. Foster, “Optimizing the Radiation Pattern of Sparse Periodic Two-Dimensional Arrays,” IEEE Trans. Ultrason., Ferroelectr. Freq. Control, vol. 43, pp. 15-19, Jan. 1996.

[3] J. L. Schwartz, B.D. Steinberg, “Ultrasparse, Ultrawideband Arrays,” IEEE Trans. Ultrason., Ferroelectr. Freq. Control, vol. 45, pp. 376-393, Mar. 1998.

[4] S., Phadke, Imaging crustal diffraction zones and seismic tomography, Ph.D Thesis, Department of physics, University of Alberta, 1988.

[5] J. Gazdag, P. Sguazzero, "Migration of seismic data", Proc. IEEE, no. 10, pp. 1302-1315, Oct. 1984.

[6] R. Abma, J. Sun, and N. Bernitsas, “Antialiasing methods in Kirchhoff migration,” Geophysics, vol. 64, no. 6, pp. 1783–1792, Nov. 1999.

[7] S. H. Gray, “Spatial sampling, migration aliasing, and migrated amplitudes,” Geophysics, vol. 78, no. 3, pp. S157–S164, 2013.

[8] J. Dmochowski, J. Benesty, and S. Affès, “On spatial aliasing in microphone arrays,” IEEE Trans. Signal Process., vol. 57, no. 4, pp. 1383–1395, 2009.

[9] R. J. Castle, "A theory of normal moveout", Geophysics, vol. 59, no. 6, pp. 983-999, 1994.

[10] O. Yilmaz, “Migration,” in O. Yilmaz, Seismic Data Processing, Tulsa, Society of Exploration Geophysicists, 1987.

[11] J. C. Bancroft, “Aliasing in prestack migration,” CREWES research report, vol.7, 1995.

[12] Y., Zhang, J. C., Sun and S. H. Gray, “Aliasing in wavefield extrapolation pre-stack migration,” Geophysics, vol.68, pp. 629-633, Jan. 2003.

[13] D., Bevc, and J., Claerbout, “Choice of integration method for anti-aliased Kirchhoff migration,” SEP research report, vol. 77, pp. 295-302, 1993.

Chapter 4 Advanced SAR imaging algorithms based on least square approach

4.1 Introduction

In Chapter 2 I state our problem on near-range imaging with the spare array radar system and I introduced several ways to compensate the imaging artifacts with the imaging operator. However, we can also treat this problem as the sparse reconstruction problem.

In order to solve the problem, Compressed Sensing (CS) is a hot topic that has attract attentions from many researchers and it is widely applied in different domains, such as imaging processing or medical imaging [1][2]. The theory of CS has been clearly explained in [3][4]. And until now there are already plenty of papers that applied CS technique for imaging with sparse array system [5][6][7]. These results already shown that CS technique is can be a good way to reduce the cost of the data acquisition and also can used to deal with the artifacts caused by the coarse sampling. However, most of the applications have to assume that the targets are sparse point target and we found it is difficult to apply these methods for near-range imaging. A lot of details are not described for far-field SAR applications while there are not so many success applications of the near-range imaging are reported. On the other hand, I will also explain in later section that CS is not really applied for the sparse array application.

Instead of starting with the CS topic, I will introduce another approach that based on solving inverse problem. An imaging technique that is known as the least square migration that is used for seismic exploration [8][9]. It is already shown that least square migration has better spatial resolution than the common SAR processing and it can compensate the artifacts by the coarse sampling. Also many advanced methods are already introduced for better or faster solution than the conventional least square migration method. However, the cost is still much larger than other imaging method so it is not practically used for seismic industrial.

In later section I will introduce this approach and apply it to our sparse array imaging application. Furthermore, I will point out the relation between least square imaging method and CS imaging method and give a general form of solving least square problem with different regularization term. With the simulation dataset of the 2-dimensional sparse array configuration and the experimental dataset, I would compare the imaging results with different regularized least square methods.

In the end of this chapter, I proposed several ways to improve the least square algorithm. The key point is to use the improved SAR operator as I proposed in Chapter 3. Some experimental results and the discussion is given in this part.

4.2 least square method for SAR imaging

4.21 ℓ2 norm regularized least square method for SAR imaging

First we start with a simple imaging model that how we can acquire the radar dataset from a given model. If the physical properties of the targets and the surrounding media properties are known, the measured data *d* can be uniquely determined by an operator *G*. The size of this operator is related with the model, it means with more known parameters of model we will have a larger operator and at the same time the acquired dataset is more close to the real situation. This relation is known as forward problem or forward modeling, it can be written in matrix form as (4.1)

$$d = Gm \tag{4.1}$$

If the inverse of the operator G can directly be acquired, the model *m* can uniquely be determined by the measured data *d*. However, the inverse of *G* is very difficult to acquire because in most cases the operator is non-linear problem [10]. Solving such problem is known as the inverse problem (4.2)

$$m = G^{-1}d \tag{4.2}$$

Another way to solve this problem is to use the adjoint matrix instead of the inverse matrix, hence we can acquire the estimated model $\widetilde{m}$ as shown in (4.3). This result can not indicate the accurate value of the physical properties and some artifacts may be introduced.

$$\widehat{m} = G^{H}d \tag{4.3}$$

For the radar image reconstruction, if the operator is a forward model operator by ray tracing, the adjoint matrix G^H is SAR processing. In time-domain the 2-dimension SAR algorithm can be given given as (4.4)

$$m(x,z) = \iint d(t,x_0)\cdot\delta(t-\frac{r}{v})dtdx_0 \tag{4.4}$$

Here *x* and *z* is spatial coordinates in *x* and *z* direction, *t* is the two-way travel time and x_0 is the coordinates of the measurements.

The misfit function of least square problem can be formulated as

$$J(m) = \|Gm - d\|^2 \tag{4.5}$$

In order to prevent from the ill-pose problem, some constrain condition is necessary to make the equation robust. For example, a common approach is applying a ℓ2 norm constrain on the processing result m, and the problem is given as (4.6)

$$arg\ min\|m\|_2\ s.t.\|Gm - d\|_2 < \epsilon \tag{4.6}$$

From the view of the mathematical solution, the ℓ2 norm regularized least square solution is trying to estimate the inverse solution. In this case we can expect that least square method can increase the spatial resolution than conventional SAR processing and also can suppress the artifacts caused by the coarse sampling. In seismic imaging applications, this method is already applied to enhance the spatial resolution and dealing with the missing traces during the data acquisition. However, due to the huge calculation cost, this method is not practical for industrial application. In our case, since the sparse array does not include so much dataset and the imaging area is limited, I think it is possible to apply such complicate algorithm for imaging applications.

4.22 Solution of ℓ2 norm regularized least square method

As I mentioned in previous section, the operator *G* is equivalent to forward modeling and its transpose is just SAR processing. Here we just consider the simplest case that ignores other factors such as limitation on aperture or weighting factor. In order to solve the equations many solvers or mathematical approaches can be applied [11]. Here we will introduce one of the most common method known as conjugate gradient method for solving such problem.

If we want to solve a general form of (4.1) which given as the linear equation

$$b = Ax \tag{4.7}$$

Mathematically $\boldsymbol{A}$ should be a real, symmetric, positive-definite matrix (please notice it may not true for our application). The input vector x_0 can be an approximate initial solution or 0. The pseudo code of conjugate gradient method can be given as

Initialization

$r_0 = b - Ax_0$

$p_0 = r_0$

$k = 0$

Do while r_{k+1} is smaller than a misfitting constant value

$$\alpha_k = \frac{r_k^T r_k}{p_k^T A p_k}$$

$x_{k+1} = x_k + \alpha_k p_k$

$r_{k+1} = r_k - \alpha_k A p_k$

$$\beta_k = \frac{r_{k+1}^T r_{k+1}}{r_k^T r_k}$$

$p_{k+1} = r_{k+1} + \beta_k p_k$

$k = k + 1$

End

Table 4.1 pseudo code of CG method

There are also many improved method based on it such as Biconjugate gradient method (BiCG), Conjugate residual method and Nonlinear conjugate gradient method. They may have some improvements for some special cases but this is not the main topic of our research, for more details it can be refer to [11]. In this section we only applied this conventional conjugate gradient method. However, we can find out from this example that no matter which solver we will use, the key factor is the construction of the operator G.

No matter what there are two ways for solving the problem; we can either use a function to calculate the output of the Ax (in most of the cases we also need to calculate $A^H x$) or directly calculate the explicit matrix form of the operator G. The final result of both method should be same and each of the method has its own advantages and disadvantages; If we construct the function to directly calculate the output, the coding is much simple because the forward modeling and backward (SAR processing) coding is straightforward so it is also easy to apply filter or weighting factors with the imaging algorithm. Each iteration may include forward and backward processing and it does not require large storage. On the other hand, if we construct the explicit matrix form of the operator it is much efficient especially for maltab program since the forward and backward processing is just the multiplication of two matrixes. However, it requires large storage because the constructed

matrix will be much larger than the input and output data. For example, if we assume both model space and data space is a 2-dimensinal matrix with same size M*N, then the size of the operator *G* will be M*M*N*N. It is obvious that for 2-dimensional case the operator is already very huge, and it will be extremely large for 3-dimensional case. Also the construction is quiet tricky and it may cause some problems if we want to apply the filter or weighting factors. More detailed information on constructing the explicit matrix operator can be found in [12].

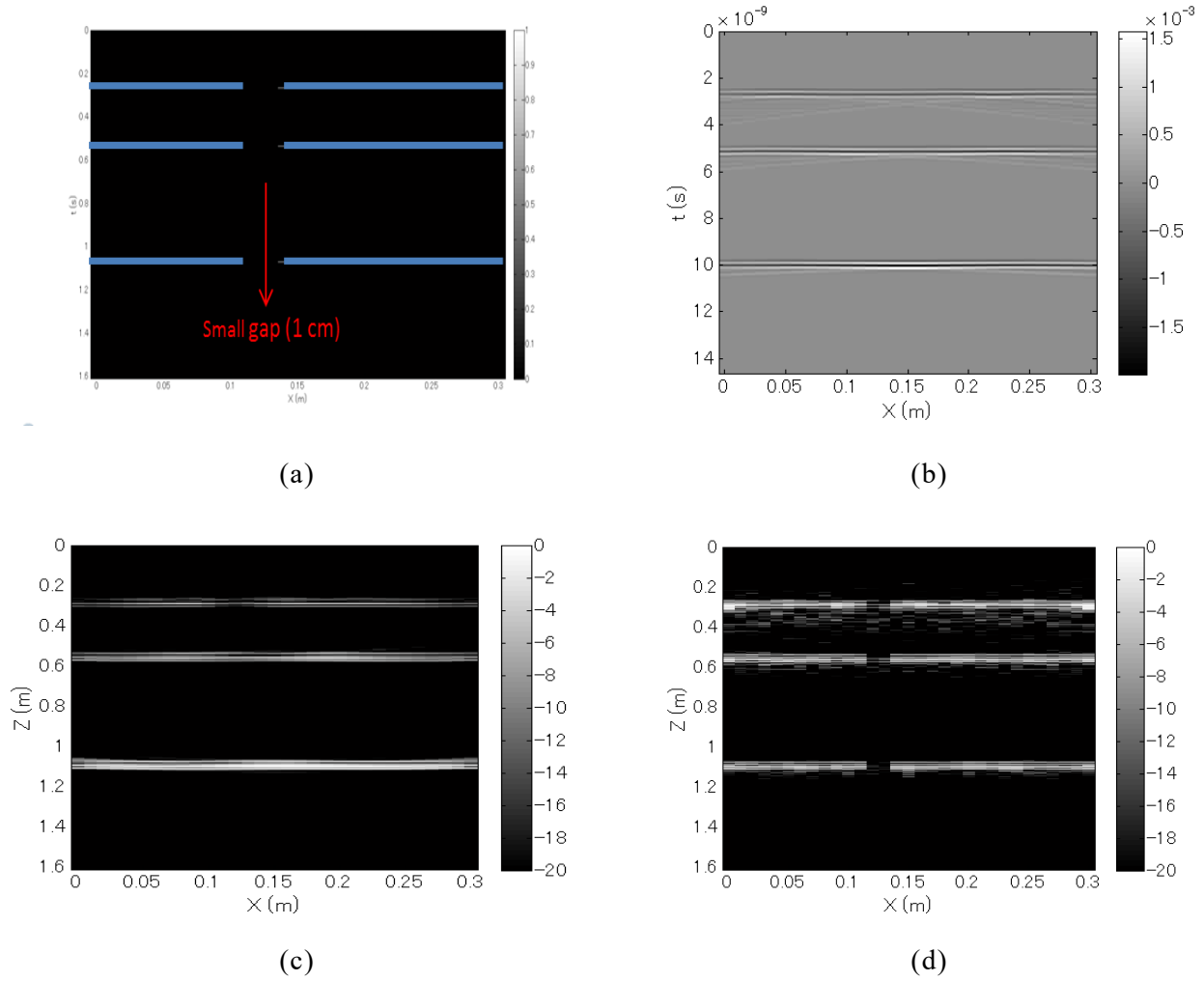

Figure 4.1 The conventional SAR result and least square imaging result with a synthetic data, (a) the reflectivity model; (b) the simulated radar profile; (c) conventional SAR imaging result; (d) least square imaging result.

Figure 4.1 shows the processing results of a simulated data with both SAR processing and least square imaging. There are three layer reflections with a 1 cm gap in between. The center frequency is 2 GHz and the target is relatively far. Due to the diffraction at the edge, the gaps cannot be seen with vertical slice directly. The horizontal resolution of SAR

processing will decrease with the distance so that only the gap at the first layer can be distinguished with the SAR processing result. But all the three gaps can be distinguished with the least square imaging method. It shows that this method gives much better spatial resolution than the coventional SAR processing. However, this method is extremely expensive for the iterative algorithm, usually equal to hundreds times of common SAR algorithm.

4.3 CS approach

Many researches in signal processing found that most of the signal can be represented in another form where it has a sparse or compressible representation, by transform coding. By sparse signal it means that most of the information in the signal is contained in a very small number of its components. We also introduced an example in Chapter 2 that by using the Fourier transform the time-domain signal can be sparsely presented in frequency domain and there is some advantages of using the randomly sampled dataset and we proposed an iterative interpolation method that based on f-k filtering, it shows good performance with irregularly distributed data for this reason. And this is just the core idea of compressed sensing that with the mathematical approaches we can use small amount of the sampling which violet the Nyquist sampling criterion to reconstruct the perfect results. CS uses randomization to turn coherent sub sampling related interferences such as aliasing into relatively Gaussian noise which are easy to suppress. According to the CS theory, the noise level depends on the degree of sub sampling and transform domain sparsity. Consequently, sampling is no longer fully determined by Nyquist, but by transform domain sparsity which make the sparse reconstruction become possible.

The general idea of CS can be given as follows

$$x = D\alpha \tag{4.8}$$

x is the original signal that can be represented sparsely in another domain by an operator D. Here the operator D can be any transform operator (e.g. Fourier transform, curvelet transform, convolution operator, migration operator, etc) as long as it can promote the sparsity that satisfy:

$$\|\alpha\|_0 < K \tag{4.9}$$

Here the $\ell 0$ norm is the number of the non-zero elements, and K is a specific number that is much smaller than the data dimension.

$$y = Rx \tag{4.10}$$

Y is the measured signal that resampled by a sensing matrix R. Another important condition is that the sample matrix R is incoherent with the operator matrix D, then the original signal x can be reconstructed by solving (4.11)

$$min\|\alpha\|_0 \ \ s.t. \quad y = RD\alpha \tag{4.11}$$

Here we use the CS reconstruction condition as the constrain to the least square imaging algorithm as (4.12) shows

$$arg\ min\|m\|_0\ s.t.\ \|Gm - d\|_2 < \epsilon \tag{4.12}$$

Here G is the transform operator which is also known as forward modeling, m is the data after SAR processing, and d is the observed data. The misfit ϵ controls the iteration number of the algorithm. Usually we set this value depends on the quality of the data.

Mathematically, it is very difficult to solve the $\ell 0$ norm regularized least square problem directly. While the key point of CS approach is that when the sensing matrix is random and it is incoherent with the compress matrix, the $\ell 1$ norm constrained solution is equal to $\ell 0$ norm. In this case we need to solve (4.13) instead of (4.12) and this problem is also known as basis pursuit denoising problem [11]. Comparing to the $\ell 0$ norm constrain, it has good performance even when the signal is noised, which made this constrain is more suitable for the SAR image.

$$arg\ min\|m\|_1\ s.t.\ \|Gm - d\|_2 < \epsilon \tag{4.13}$$

There are many ways to solve (4.13), such as the SPG$\ell 1$ solver that is introduced in [13]. It is wrote with matlab and has good performance with large scale calculation and we are mainly using this solver for the simulation and experimental data imaging in our work.

Also we shows a simple simulation results to compare the $\ell 2$ norm regularized least square method and CS based method. There is only a scatterer in the middle and the wavelet is a Gaussian wavelet ranged from 3 GHz to 6 GHz. In Figure 4.2(c) we can find that with $\ell 2$ norm least square method, after 20 times iteration the imaging artifacts can be reduced comparing with the conventional SAR processing result. In Figure 4.2(d) we randomly resampled 10% of the data and applied CS approach, we can find the target is reconstructed to a point perfectly.

However, here we should notice that actually the sensing matrix R in (4.10) is fixed by the distribution of antenna array and usually it is not really random matrix. In previous example we create the random sampling matrix by ourselves hence the result has a good performance. While in practical case, it is almost impossible to have a real random sensing matrix. In this case, we are actually solving the $\ell 1$ norm regularized least square problem but not CS

problem. Since the ℓ1 norm regularization can promote the sparsity of the solution, I think it is still quiet acceptable for our application case. More details will be given in later sections.

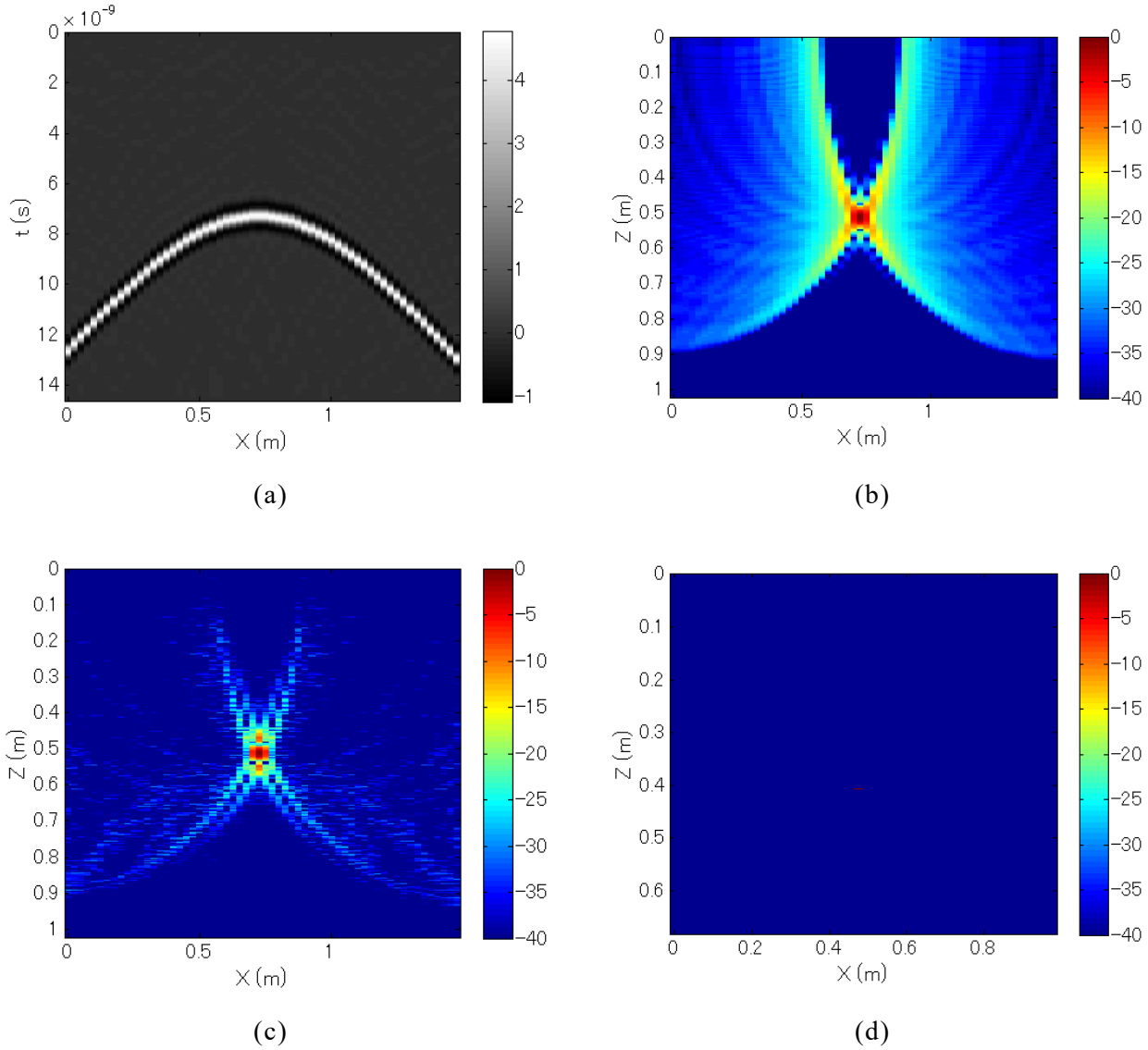

Figure 4.2 Imaging results of the simulated data with different methods, (a) simulated radar profile with a scartterer in the middle; (b) conventional SAR imaging result; (c) ℓ2 norm regularized least square imaging result; (d) ℓ1 norm regularized least square result.

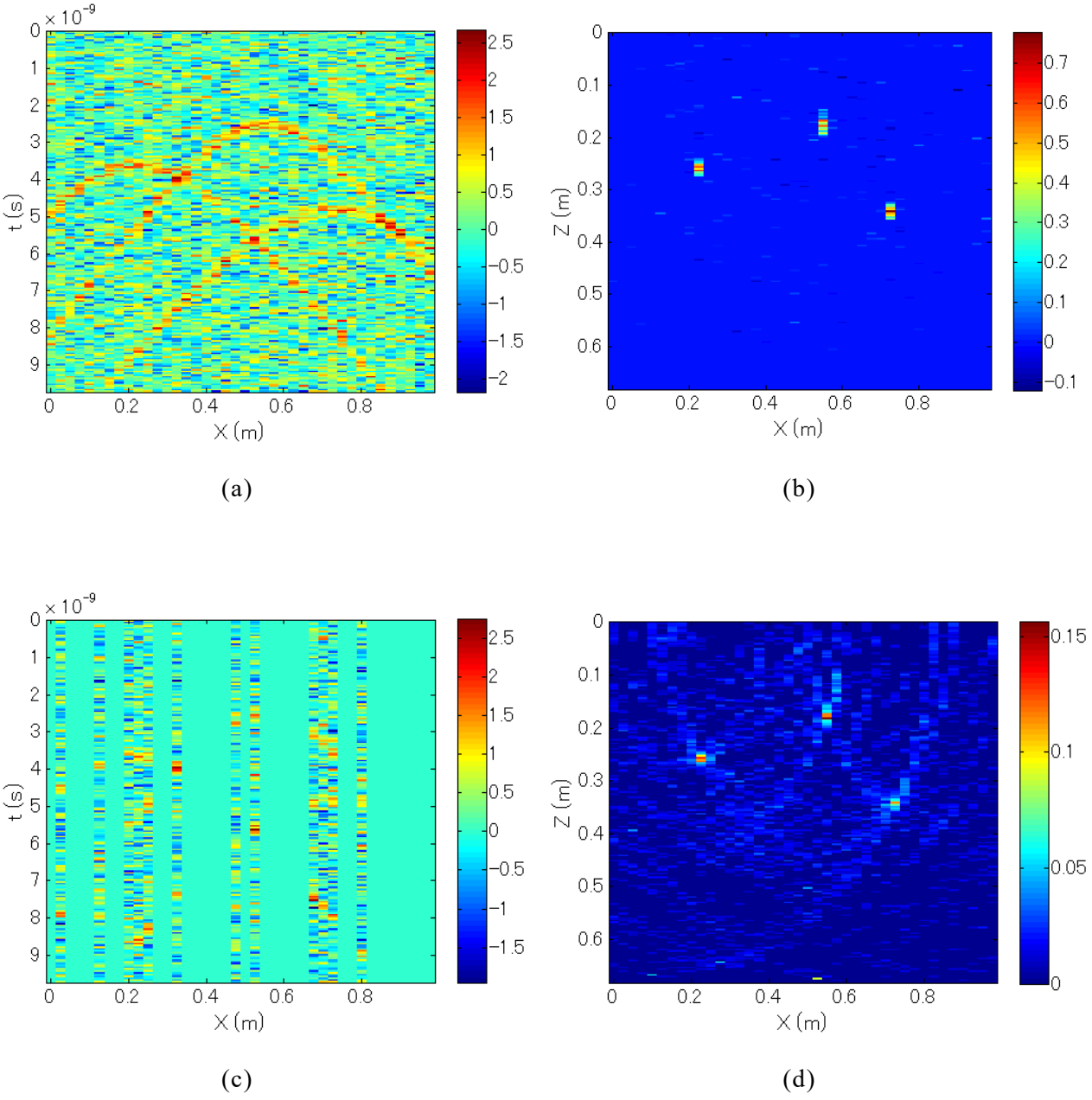

Figure 4.3 The ℓ1 norm reglarized least square imaging with noise and trace resampling, (a) the simualted radar profile with -3db noise; (b) ℓ1 norm regularized imaging result of (a); (c) the sumulated radar profile with trace resample based on (a); (d) ℓ1 norm regularized imaging result of (c).

In Figure 4.3 we shows the simulated result with ℓ1 norm regularized least square method. Here we should notice that in this case we are not using the random sensing matrix so it is not CS method in definition although we are also solving (4.11). We also use a simple model that includes three scatterers so that the solution can be converged quickly. Depends on the complicity of the data, the iteration number can be reduced from hundred times to only a few times to reach at a same residual. Here we shows both using the full dataset and the dataset only resampled in spatial domain which is similar to sparse array data

acquisition. The three point targets still can be well reconstructed when 70% of the traces are randomly removed and we added -3 dB noise. Here we should also point out that comparing the ℓ1 norm regularized least square solution is quiet tricky. In Figure 4.3(b) and (d) we used same parameter for calculation which is not proper in mathematical sense, by selecting the parameter carefully we can improve the result in Figure 4.3(d) and it will looks similar to (b). Then it is difficult to compare the methods, similar problem also happens to later comparisons of least square methods. A discussion on calculation parameter will be given in later sections of this chapter.

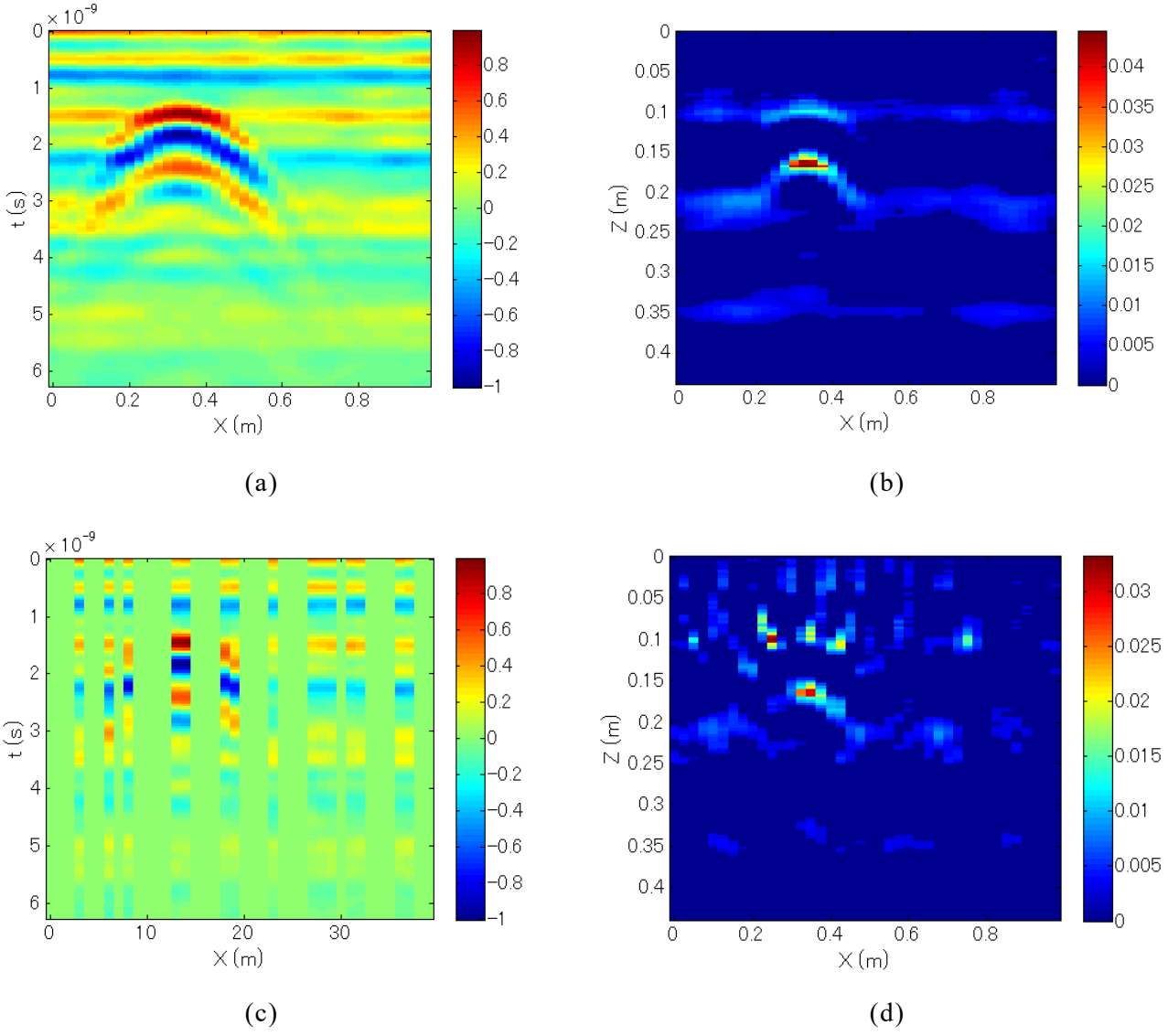

Figure 4.4 The ℓ1 norm regularized least square imaging for real GPR data, (a) acquired radar profile with a metal sphere burried at 20 cm depth; (b) ℓ1 norm regularized imaging result of (a); (c) trace resample based on (a); (d) ℓ1 norm regularized imaging result of (c).

If we consider the calculation step of the ℓ1 norm regularization and ℓ2 norm regularization, a main difference is that ℓ1 norm regularization includes the soft-threshold within the calculation [13]. And this is the main reason that ℓ1 norm regularization can be used for denoising application and can improve the sparsity of the solution. In our application, it means that ℓ1 norm regularization has better possibility to image our main targets when the dataset is incomplete or include much noise. Figure 4.4 shows the experimental results with real data that acquired by the 1 GHz bowtie antenna. A metal sphere is buried at 20 cm depth. After 60% of the traces are randomly removed, the reconstructed result still indicated the correct position. It shows that ℓ1 norm regularized least square method may have good potential on sparse array imaging.

4.4 Relation between least square migration and CS imaging method

In previous section we have already shown that at the end the equation for least square migration and CS based SAR imaging is very similar to each other. The main difference is just the regularization term. In previous research on solving the least square problem, it is already addressed the importance of the regularization term.

Regularization methods provide a procedure to guarantee the stability and uniqueness of the solution of an inverse problem. In more general case, the minimizing function can be written as

$$J(m) = \|Gm - d\|^2 + \mu \mathrm{R(m)} \tag{4.14}$$

Where G is a matrix of weights proportional to the inverse data covariance matrix and the second term in equation (4.14), $R(m)$ is called regularization term. Mathematically, we have quadratic regularization term and non-quadratic regularization term.

Sacchi [8] already explained that conventional least square migration that use ℓ2 norm as the regularization term is just quadratic regularization. While ℓ1 norm regularization and Cauchy norm regularization is known as the non-quadratic regularization term. Cauchy norm regularization imaging method is also introduced in [9][14] and it is shown that it has similar performance with ℓ1 norm regularization which can improve the sparsity of the results.

Hence we can conclude that the compressed sensing approach is actually a special case of least square problem. It requires ℓ1 norm regularization and also random sampling of the observed dataset. Practically, CS based SAR imaging can provide super high resolution because it promotes the sparsity of the result. In another word, it tries to compress the waveform into a pulse during the imaging processing and ignore the small artifacts so that the imaging result can be very clean. However, when the target is distributed target or multiple targets it will cause more problem. While ℓ2 norm regularization has more

advantages for distributed target imaging of our sparse array system as it pointed out in [8]; First, the problem can be treated as a Bayesian inference problem where a priori information about the unknown image and observations can be included and used to minimize unwanted artifacts. Secondly, weighting matrices in data space can be used to minimize the influence of missing observations. Practically, we need to choose proper regularization term for the least square imaging method with the different purposes which is target dependent.

4.5 experimental results applied with 2-dimensional sparse array

In Figure 4.5 we show the simulated result with the 2-dimensional sparse array configuration that we introduced in Chapter 2. It is a stepped frequency system that works from 3.81420 GHz to 8.0674 GHz with eight transmitting antennas and eight receiving antennas. The antenna arrangement is shown in Figure 2.9 and the interval between each midpoint of transceiver pair is about 8 cm. And the model is shown in Figure 4.5(a). We set up a cross-shape reflector at 65 cm away from the array and the Gaussian wavelet with 3-6 GHz frequency bandwidth is used for ray tracing simulation. After the conventional SAR process we select the horizontal slice around 65 cm as it is shown in Figure 4.5(b). We can find the shape of target can be imaged while the edges are slightly distorted, and also we can find many artifacts distributed at the spaced area. These artifacts is only caused by the imaging algorithm since there is no other target within this model.

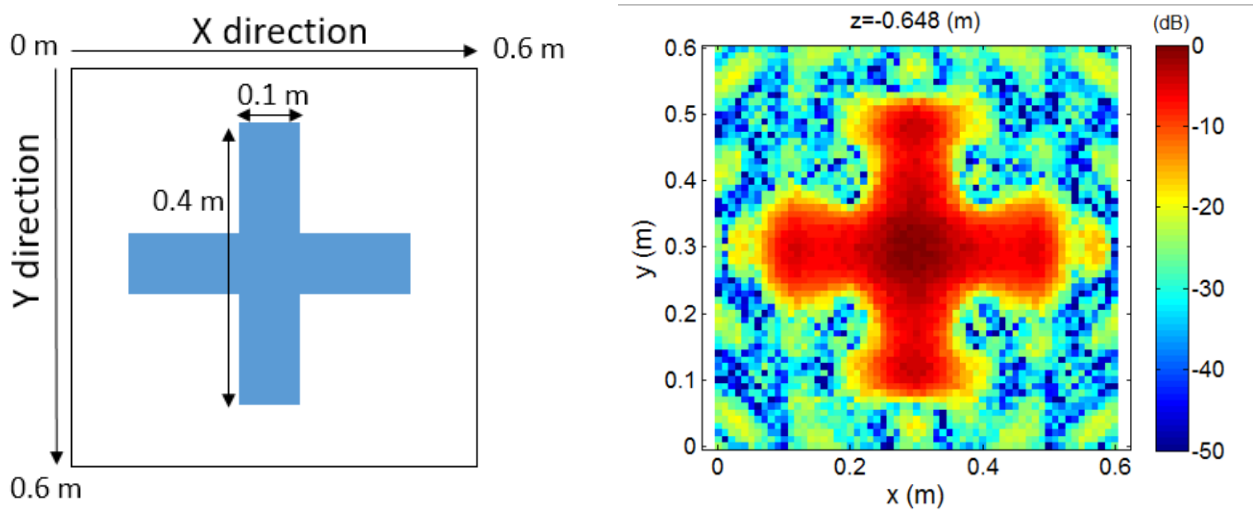

(a) (b)

Figure 4.5 simulation results with the 2-dimensional sparse array configuration, (a) physical model; (b) depth slice of the conventional SAR imaging result.

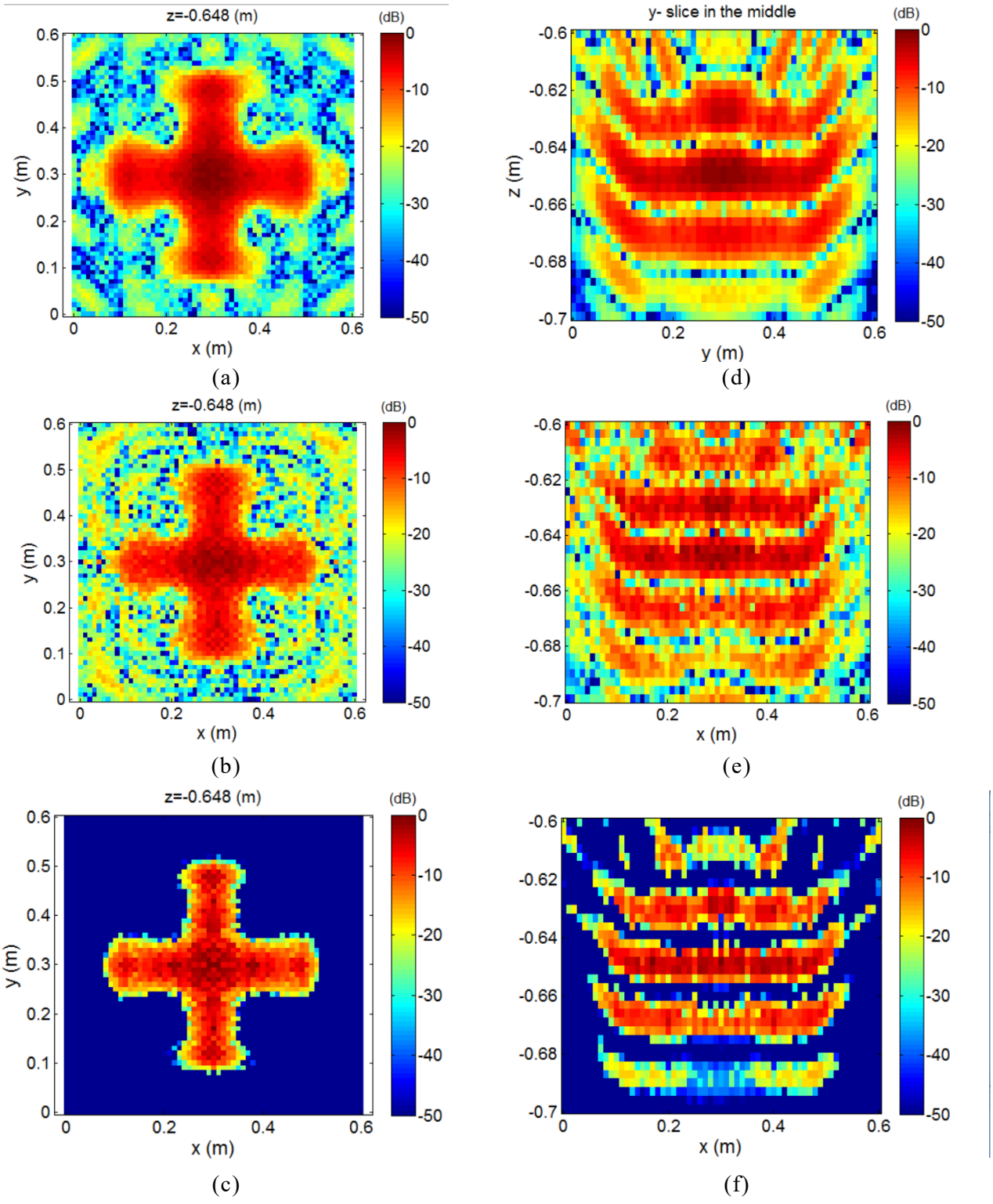

Figure 4.6 Comparision of different imaging methods with depth slice(left) and vertical slice (right), (a)(d) conventional SAR imaging method; (b)(e) ℓ2 norm regularized least square method; (c)(f) ℓ1 norm regularized least square method.

In Figure 4.6 we compared the processing results with ℓ2 norm regularization and ℓ1 norm regularization. From the horizontal slice we can find that ℓ1 norm regularization gives good performance, the target has less distortion and almost all the imaging artifacts are well removed. For the ℓ2 norm regularization result, the shape of the target is slightly better than conventional method but the artifacts remains. We can find that distribution of the artifacts is changed and in this model the artifacts become stronger than the conventional SAR imaging result. We also tried with other different models and this problem happens case by case. It shows a general problem of the ℓ2 norm regularized least square solution that when the target is distributed target, some of the imaging artifacts can be considered as noise. When the algorithm minimize the ℓ2 norm these part of the energy cannot be eliminated but replaced to "better" position that can minimize the ℓ2 norm. Hence there is a general feature of the ℓ2 norm regularized solution that when we use extremely large iteration number, the final solution will turn all the targets into the noise for imaging problem.

We also applied the proposed methods with the real experimental dataset acquired by the 2-dimensional sparse array radar system that we have introduced in Chapter 2. The results are shown in Figure 4.7. A metal pipe with 60 cm length and 5 cm diameter is used for the imaging experiment. We can find that for the real dataset that include noise and clutters the ℓ1 norm regularized least square method also gives the best result, most of the artifacts can be removed and the resolution of the imaging result is enhanced. While in this case the performance of the ℓ2 norm regularized least square method looks worse than conventional method, the artifacts seem to be increased. As we have already discussed in previous part I think it is caused by the strong noise and clutter included in the acquired dataset. With the data acquired with different targets we found that ℓ1 norm regularized least square method has good performance against the noise and clutters, however, in order to achieve to a good result the calculation parameter need to be selected carefully and it is very difficult to define automatically. We will further discuss about this issue in later sections.

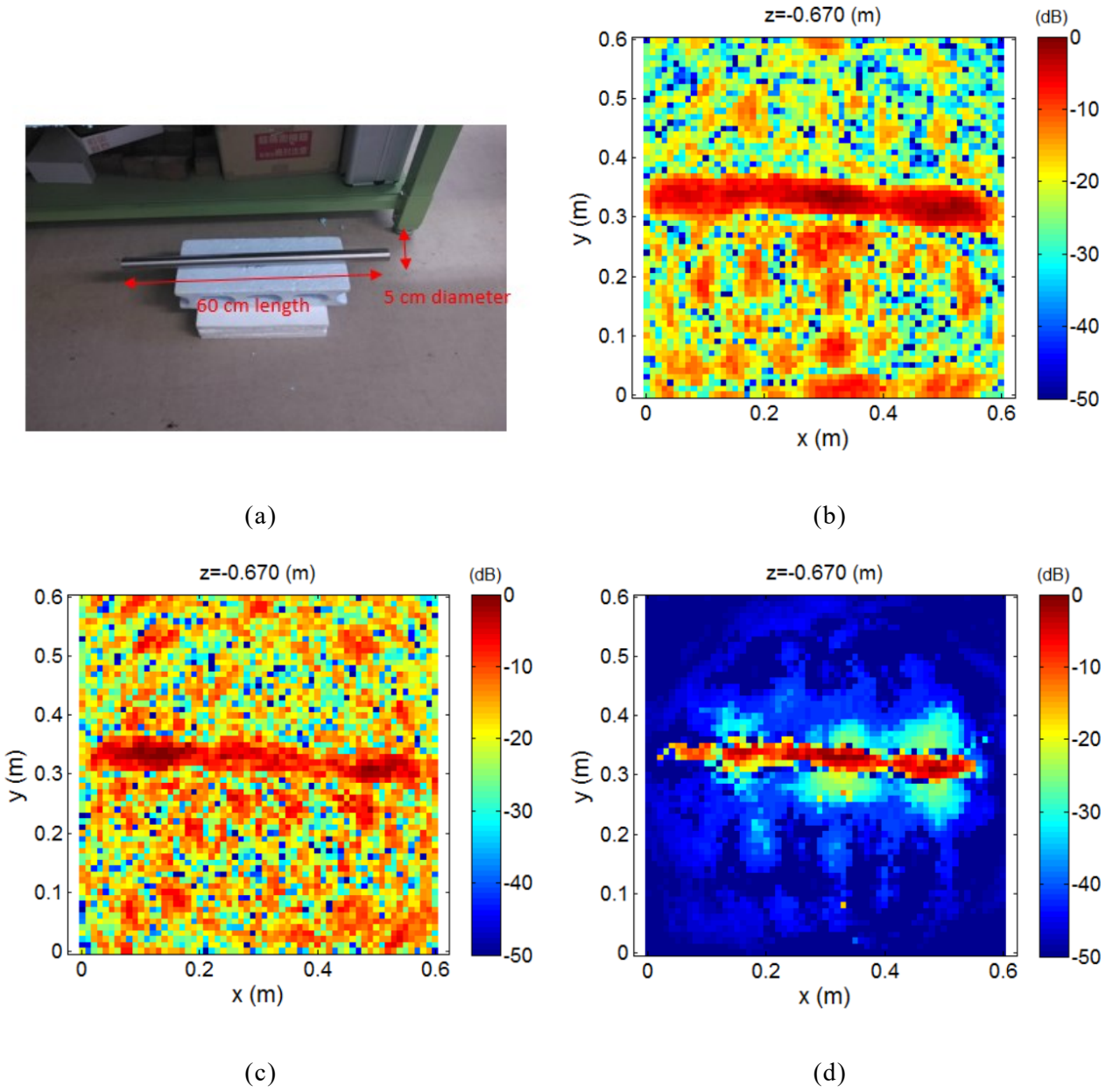

Figure 4.7 Comparision of different imaging methods with experimental dataset acquired with 2-dimensional sparse array system, (a) target for the imaging experiment; (b) conventional SAR imaging method; (c) ℓ2 norm regularized least square method; (d) ℓ1 norm regularized least square method.

4.6 Prospective on practical calculations of least square method applied for SAR imaging

4.61 Selection on calculation parameters

In previous imaging experiment for both simulated data and the real dataset we did not

mention about the detail parameter settings. The main reason is that these parameter is not unique for different solvers or different datasets. If we consider about the objective function as it is shown in (4.13), the only parameter that we need to solve the problem is the ϵ which is known as a parameter that closely related to the SNR of the signal [8][11]. However, for different target or different imaging operator it is difficult to define the "noise", in an extreme case, for $\ell 0$ norm regularized problem when the number of the target is defined, all the other clutters will be the "noise" for solving the problem. As we have also mentioned in previous examples, $\ell 1$ norm regularized least square imaging results are more sensitive to the parameter. We may achieve totally different results only by changing the parameter during the calculation. Furthermore, the parameter will be very different depending on the targets or imaging area from our experimental results.

On the other hand, the different methods also require different parameters based on the ϵ in (4.13). Beside the SPG$\ell 1$ solver that is used in our research, there are also different methods can be used for solving (4.13), such as DALM and FISTA that are introduced in [14][15]. With different mathematic solver the methods may requires several parameters and there is no deterministic way to calculate these parameters, most the other articles that applied these method by selecting the parameters with experience and test [5][6][16]. In our experimental results, we also chose these parameters mostly depends on test results. In this case, actually it is not fair to compare the $\ell 1$ norm regularized results and $\ell 2$ norm regularized results together.

I think currently one of the main problem that limited the $\ell 1$ norm regularized least square method or CS based methods for SAR imaging is caused by the determination of the calculation parameter. Since the imaging result will be changed due to the different parameter, it is difficult to apply these algorithm for real application or products. Actually there are some methods for determining the parameter as it concluded in [17], however it is also depends on the different regularization term as we discussed in section 4.4 and also the operator that we used in calculation. For our application we still did not find a good way to calculate the regularization parameter accurately depends on the input radar dataset and it remains to be a main question of our research work.

4.62 improvements on least square method for SAR imaging

If we consider the process of least square method, we found it may possible to improve the calculation of the iteration process. The analytical solution of (4.6) can be given as

$$m = (G^H G + \mu I)^{-1} G d \qquad (4.15)$$

Here I is the unity matrix and u is the weighting parameter. From (4.15) we can get an important conclusion that if the $G^H G = I$ or $G^H = G^{-1}$, the imaging result will be same with the inverse result. $G^H G$ is known as Hessian matrix, and many mathematical research

have been done on trying to diagonalize the Hessian matrix [12]. By diagonalization of the Hessian matrix, the effect of the wavelet and the artifacts can be suppressed. This is the main reason that least square imaging method has a good performance against the noise and the artifacts [12]. From the imaging point of view, G^H will become similar to G^{-1} when we can focus the hyperbolas to a point without generating other artifacts and such modified G^H operator is just introduced in Chapter 3.

I tried to apply the local low-pass filter and the processing aperture limitation operator within the least square method. However, we found the result may not stable and we show an example in Figure 4.8. Here we applied the conventional ℓ2 norm regularized method and the ℓ2 norm regularized method together with the local low-pass filter. In this example we set the maximum iteration number to be 30 and used same regularization parameter for the calculation. Actually from this result we can find that the proposed method has good performance, I think it is mainly because of the simplicity of the model. As I mentioned in above that G^H will become similar to G^{-1} when there are less artifacts introduced, and this condition only satisfied when there is point scartterer and we cannot guarantee that such assumption is mathematically correct for the distributed target.

On the other hand, if we check the residual curve that is shown in Figure 4.8(f) we can notice that the curve is not converged constantly comparing to the conventional ℓ2 norm regularized method in Figure 4.8(d), and I think it is also the main reason that the proposed method is not always work.

Beside this approach, we also tried another simple approach based on this idea. If we can remove the artifacts during the each iteration, I think it is also "forced" the convergence of the least square problem and the artifacts removal can be considered as a regularization term based on physical idea of SAR processing. I tried a simple threshold during the iteration processing as in (4.16) that we introduced in table 4.1, here H_s is a threshold that reduce the artifacts caused by SAR operator at each iteration. We found the method has a good performance and can greatly reduce the iteration number than the conventional ℓ2 norm regularized least square method. However, later we found this approach is already mathematically presented in [15] that by using a properly designed soft-threshold function instead of H_s, we can obtain the ℓ1 norm regularized solution instead of the ℓ2 norm regularization.

$$m_{k+1} = H_s(m_k + \alpha G^H(Gm_k - d) \tag{4.16}$$

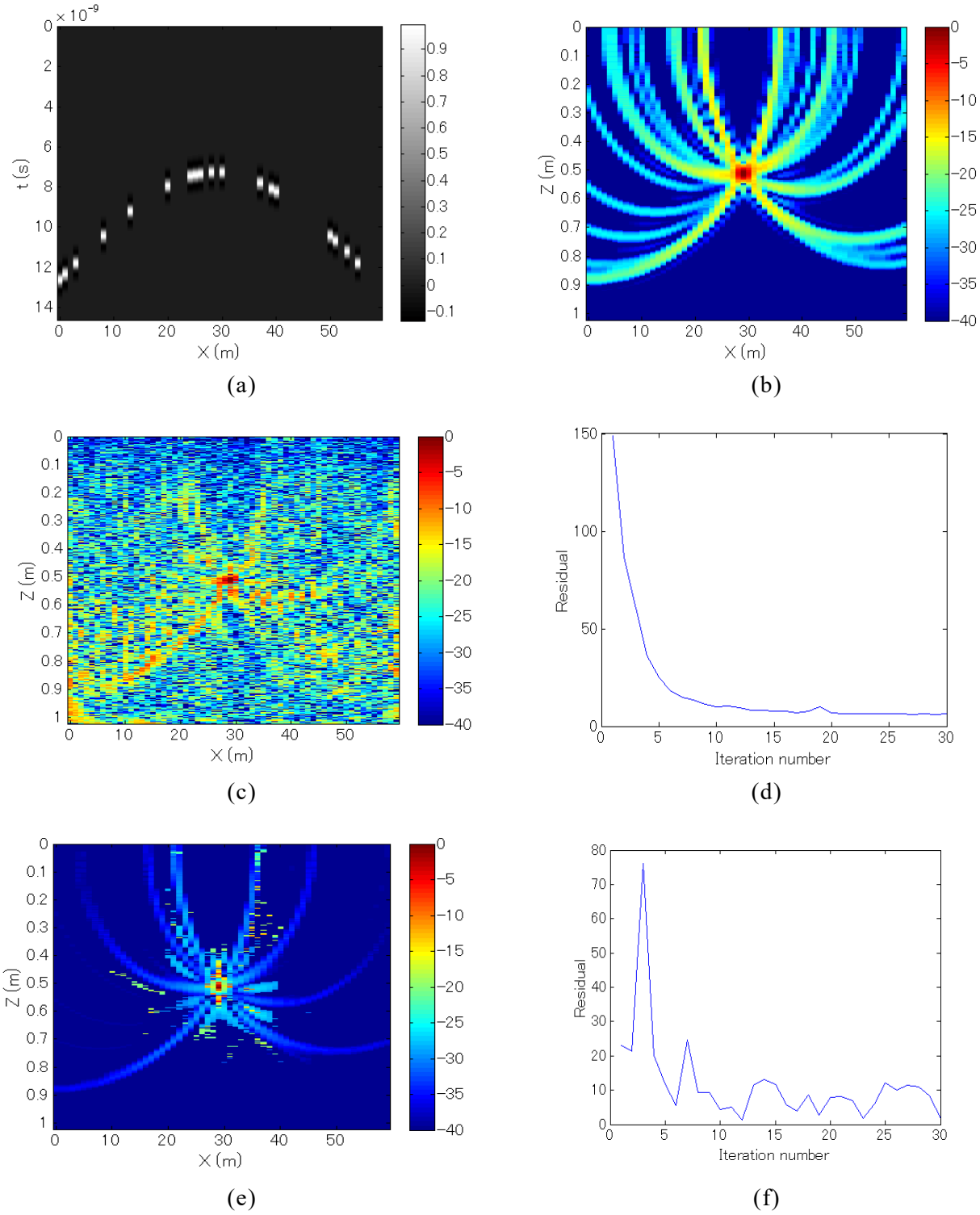

Figure 4.8 Simulated example for applying the local low-pass filter on ℓ2 norm regularized least square method, (a) simulated radar profile of a point scartterer with trace resampled; (b) conventional SAR imaging result; (c) result of ℓ2 norm least square method; (d) residual of each iteration of (c); (e) result of ℓ2 norm least square method with the local low-pass filter; (f) residual of each iteration of (e).

4.7 Summary

In this chapter I represented the idea to reduce the imaging artifacts and enhance the imaging quality by using the least square method for SAR imaging problem. I introduced $\ell 2$ norm regularized and $\ell 1$ norm regularized least square method for near-range SAR processing with 2-dimensional sparse array and from the simulation and experimental results I think $\ell 1$ norm regularized least square method is a good method for sparse array imaging. It can greatly reduce the imaging artifacts and enhance the imaging resolution. I also clarified the relation between the CS based imaging method that is already widely used for far-field SAR imaging and the proposed methods that CS is actually a special form of $\ell 1$ regularized least square method. However, I also pointed out that due to the difficulty of determining the regularization parameter for different dataset, the iterative method is still difficult to apply to the real system practically and it remains to be the main aim of our further research aim.

On the other hand, in order to reduce the huge calculation cost of the iterative algorithm for this problem, I tried to improve the $\ell 2$ norm regularized least square method by using the physical constrain conditions to make it fit better for the near-range SAR imaging application. The core idea is to remove the artifacts during solving the $\ell 2$ norm regularized method so that the least square solution is more like the inverse solution and we can expect better convergence speed. For example, the artifacts removal methods applied with the SAR operator that I introduced in Chapter 3 can be used for the least square method. However with the proposed approach I found the solution is not robust due to the violence on mathematical assumptions for solving the least square problem. Another simple approach that use a threshold during the CG iteration is success but I found it already known as a mathematical approach for solving the $\ell 1$ norm regularized solution. However, I think the least square methods still has much potential for solving the SAR imaging problem and I am still trying to improve it.

4.8 References

[1] M.F. Duarte, M.A. Davenport, D. Takhar, J.N. Laska, T.Sun, K.F. Kelly, and R.G. Baraniuk, “Single-pixel imaging via compressive sampling,” IEEE Signal Processing Magazine, 25(2) pp. 83-91, March 2008.

[2] M. Lustig, D. Donoho, and J. M. Pauly, “Sparse MRI: The application of compressed sensing for rapid MR imaging,” Magn. Reson. Med., vol. 58, no. 6, pp. 1182–1195, Dec. 2007.

[3] D. L. Donoho, “Compressed sensing,” IEEE Trans. Inf. Theory, vol. 52, no. 4, pp. 1289–1306, Apr. 2006.

[4] A. Massa, P. Rocca and G. Oliveri, "Compressive sensing in electromagnetics—A review", IEEE Antennas Propag. Mag., vol. 57, no. 1, pp. 224-238, Feb. 2015.

[5] A. Budillon, A. Evangelista, and G. Schirinzi, “Three-dimensional SAR focusing from multipass signals using compressive sampling,” IEEE Trans. Geosci. Remote Sens., vol. 49, no. 1, pp, 488-499, Jan.2011.

[6] S. Xilong, Y. Anxi, D. Zhen, and L. Diannong, “Three-Dimensional SAR Focusing Via Compressive Sensing: The Case Study of Angel Stadium,” IEEE Geosci Remote Sens Lett, vol. 9, no.4, pp. 759-763, July. 2012.

[7] J. Yang, J. Thompson, X. Huang, T. Jin, and Z. Zhou, “Random-frequency SAR imaging based on compressed sensing,” IEEE. Trans. Geosci. Remote Sens., vol. 51, no. 2, pp. 983-994, Feb.2013.

[8] M. Sacchi, J. Wang and H. Kuehl, "Regularized migration/inversion: New Generation of Seismic Imaging Algorithms,” CSEG Recorder, vol. 31, pp.54 - 59, Dec. 2006.

[9] T. Nemeth, C. Wu, and G. T. Schuster, “Least-squares migration of incomplete reflection data,” Geophysics, vol. 64, no.1, pp. 208-221, Jan. 1999.

[10] M. E. Vardy and T. J. Henstock, “A frequency-approximated approach to Kirchhoff migration,” Geophysics, vol. 75, no. 6, pp. S211–S218, Nov. 2010.

[11] Noreen Jamil, "A Comparison of Direct and Indirect Solvers for Linear Systems of Equations", Int. J. Emerg. Sci., vol. 2, no. 2, pp. 310-321, June 2012, ISSN 2222-4254.

[12] A. Yousefzadeh, and J. C. Bancroft, “Kirchhoff imaging in a matrix form. Part II: least squares Migration,” Expanded Abstracts, GeoCanada 2012.

[13] E. van den Berg and M. P. Friedlander, “Probing the Pareto frontier for basis pursuit solutions,” SIAM J. on Scientific Computing, vol. 31, no.2, pp.890-912, Nov. 2008.

[14] A. Yang, A. Ganesh, Z. Zhou, S. Sastry, and Y. Ma, "Fast ℓ1 minimisation algorithms and an application in robust face recognition: a review," Technical Report UCBIEECS-20iO-13, 2010.

[15] A. Beck and M. Teboulle, "A fast iterative shrinkage-thresholding algorithm for linear inverse problems," SIAM J. Imaging Sciences, vol. 2, no. 1, pp. 183-202, 2009.

[16] S. Kaplan, P. Routh, and M.D. Sacchi, 2010, “Derivation of forward and adjoint operators for least-squares shot-profile split-step migration,” Geophysics, Vol. 75, No.6, pp. s225-s235, 2010.

[17] S. J. Reeves, R. M. Mersereau, "Optimal Regularization Parameter Estimation for Image Restoration", Proc. of SPIE on Image Processing Algorithms and Techniques II, vol. 1452, pp. 127-138, 1991-February.

Chapter 5 Enhancement of SAR imaging result with multi-dimensional pulse compression

5.1 Introduction

In previous chapter I have introduced the least square based methods for near-range SAR processing. The main aim of our methods is to suppress the imaging artifacts caused by the coarse sampling. Although we are solving the linearized problem, we still need to solve the problem by iteration processing which is not practical for real-time processing. In this chapter I will try to solve the imaging problem in a different way. As I mentioned before, the main problem of the imaging artifacts is that we cannot find the inverse matrix for the data inversion because of the complicity of the targets. As the result, the SAR processing results seems to be "blurred" comparing with the accurate shape of the targets. In this case, we can also try to use a specific filter to remove these artifacts and such processing is known as deblurring for imaging processing [1][2][3]. As it concluded in [3], such processing is actually a spatial filter applied to an image or video that depends on different situations, such as the shaking of the camera, coarse sampling or limitation of the hardware.

For signal processing there is also a similar processing that is known as pulse compression or deconvolution [5][6]. The idea is to use the inverse wavelet to design a 1-dimensional filter to compress the wavelet into a pulse. A conventional way to apply the pulse compression is to apply it with the Wiener filter [6]. It is easy to apply in frequency domain and it can somehow compensate the noise components. However, due to the noise or other clutters, the pulse compression always do not have a good performance for real dataset because it is actually trying to find the least square solution [6]. In order to achieve higher resolution I tried to apply $\ell 1$ norm regularized least square method that we used for imaging problem on pulse compression and it gives good result for the real dataset that I acquired with our sparse array system. Similar approach is also introduced in signal processing articles that defined with different names such as sparse deconvolution or spike deconvoluiton [7][8]. The results indicate that pulse compression for near-range imaging is very effective.

The only difference between the imaging deblurring and the pulse compression is that deblurring uses the inverse of the PSF function instead of the inverse wavelet. By using such idea we can also try to solve our problem by the means of image deblurring and in later section I will show that the forward modelling processing is actually "blurring" the accurate reflectivity model.

This idea is not totally new and in [9] Hu already explained the results by deconvolution before or after the migration imaging processing with mathematical formulation and pointed

out that the migration imaging is just “blurred” version of the accurate reflectivity model. And he also suggested to use the 2-dimensonal spatial filter to compensate the blurring effect on migrated images directly so that the resolution can be enhanced. However, for the seismic application this method do not show much difference comparing to the conventional deconvoluted result hence there are not so many research that follows this topic. However, if we consider about the imaging artifacts that caused by the sparse array, I think this approach may have good performance to enhance the imaging results. In later section I will introduce a practical way to apply the deblurring filter on SAR image acquired with the sparse array system to enhance the imaging resolution and reduce the imaging artifacts that I discussed in previous chapters.

5.2 1-dimensional pulse compression with Wiener filter

5.21 pulse compression with Wiener filter

Pulse compression or it is also called deconvolution processing is a popular method that widely used for seismic data processing [10]. The idea is straightforward, if we know the waveform of the transmitted signal, we can just do the inverse processing of the convolution modelling (5.1) where d_w denotes the acquired data with a wavelet convoluted and W is the convolution matrix include a certain wavelet and this is the simple form of (2.3). Now we do not consider about the imaging operator G that we discussed in Chapter 4 and ignore the noise n, so we can simplify the problem to (5.3) which has similar form to SAR processing problem as (5.2). It means we can restore the reflected signal into a pulse so that we can achieve to a better resolution or even super-resolution.

$$d_w = WGm + n \tag{5.1}$$

$$d = Gm \tag{5.2}$$

$$d_w = Wd \tag{5.3}$$

Pulse compression can be treated as an inverse problem and can be solved with the least square methods in both time-domain and frequency domain. [11] introduced more details about the deconvolution processing and it pointed out that the complicated time-domain convolution calculation can be greatly simplified in frequency domain, here we directly give the Wiener inverse filter in frequency domain as (5.4)

$$\mathrm{X}(\omega) = \frac{H^T(\omega)\mathrm{Y}(\omega)}{|H(\omega)|^2 + \beta^2} \tag{5.4}$$

where $Y(\omega)$ is the acquired data in frequency domain, $X(\omega)$ is the deconvoluted signal, $H(\omega)$ is the reference signal in frequency domain and the parameter β can be considered as a regularization parameter.

5.22 Effect of the regularization parameter

The optimal solution is a compromise between the stability and accuracy of pulse compression and it is controlled by the regularization parameter. Stability means the capability of handling the noise with the Wiener filter. And accuracy described the possibility of compressing the waveform. Normally the less is stability the larger is accuracy. [12] introduced a way to estimate the parameter by using (5.5)

$$\beta = \frac{3\delta}{\bar{Y}} \tag{5.5}$$

δ stands for the noise level (square root from noise energy), and $\bar{Y}$ is the mean spectral density of the acquired spectrum. Theoretically it can estimate the optimized parameter quiet well but it still has error, it is because the definition of the noise is hard to define especially when the noise is always mixed with the wavelet signal. Practically this equation can give a relatively good results but we may still need to adjust this parameter.

Figure 5.1 shows an example of compressing a complicated waveform that is generated with a spiral antenna. Figure 5.1(a) is the acquired signal that reflected from a metal plate and we use the acquired signal itself as the reference signal to compress it into a pulse. Figure 5.1(b) shows the compressed result with the parameter equals to 3.2 that calculated with (5.2). As we discussed above we find this value is still too large because the wavelet shape is still remains. Figure 5.1(c) shows the result with parameter equals to 0.1 and we can find that the result is more like a pulse. However, we may also notice that the stability of the result become worse since the signal becomes noisier. If we further decrease the parameter the generated noise will become stronger than the compressed pulse. And this is the balance between the stability and the accuracy that I mentioned above.

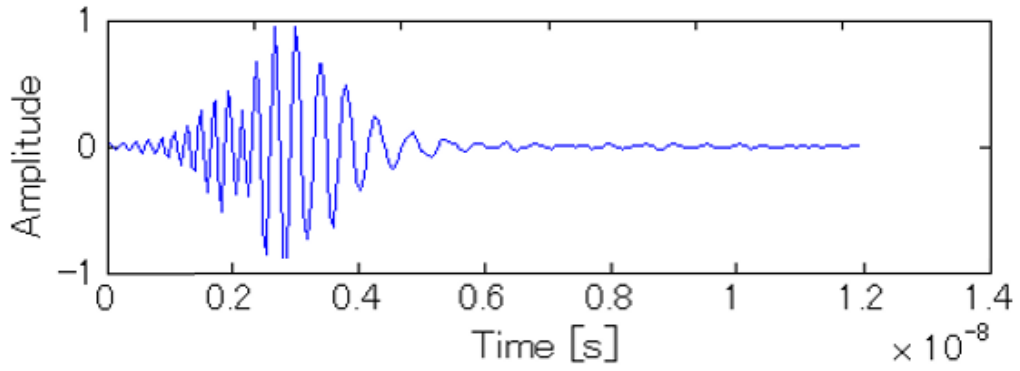

(a)

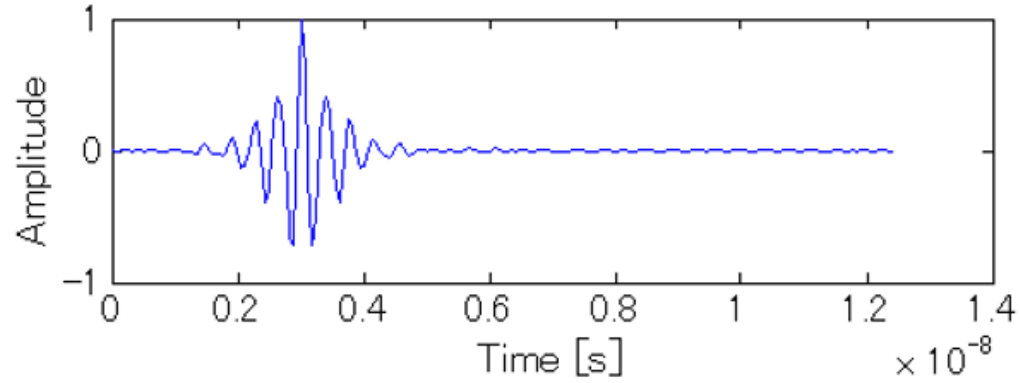

(b)

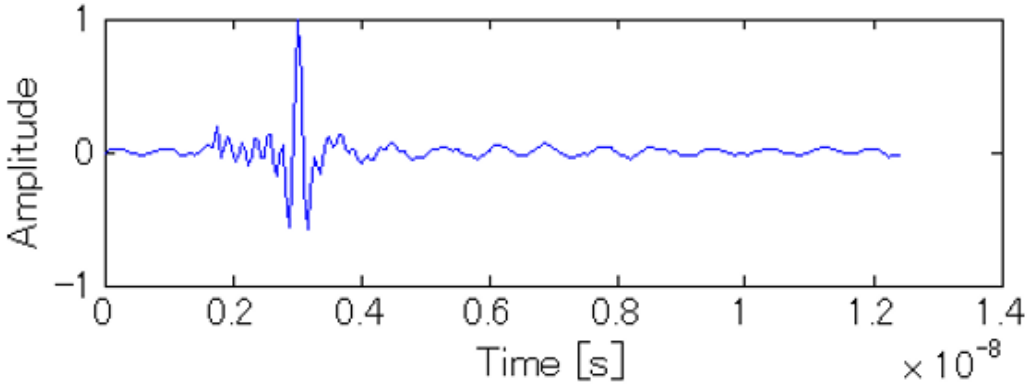

(c)

Figure 5.1 The pulse compression with Wiener filter, (a) raw signal acquired with spiral antenna; (b) after pulse compression with regularization parameter equals to 3.2; (c) after pulse compression with regularization parameter equals to 0.1.

5.23 Effect of the reference signal

Beside the parameter, the reference signal is also a main factor for the pulse compression processing. The deconvoluiton processing is easier to be understand from the view of image matching. What we are actually doing is to find out the reflected signals among a serious of reflected signals which “looks like” the reference signal. However, this is almost impossible to get perfect reference signal because the reflected signal may include noise, multiple reflections and also changes of the frequency components. And this is the reason why we have to use the Wiener filter so that we can somehow compensate the inaccurate reference signal.

On the other hand, [13][14] mentioned the feature of the wavelet shape and pointed out that the minimum-phase signal is much easier for pulse compression. I think it is a similar reason to what we have discussed in Chapter 2 that the simple wavelet is better for the inverse processing from the mathematic point of view.

5.24 ℓ1 norm regularized pulse compression

In previous chapter we introduced that we can use the ℓ1 norm regularization to enhance the sparsity of the SAR processing so that the resolution can be further improved and part of the imaging artifacts can be suppressed. It can be also applied for the pulse compression processing and it is known as the spike deconvoluiton in seismic signal processing [14]. As it introduced in [14], the Weiner filer is just a simple way to find the least square solution of the pulse compression processing under the ℓ2 norm regularization. So the ℓ1 norm regularized pulse compression is also quiet straightforward by solving (5.6)

$$arg\ min\|d\|_1\ s.t.\ \|Wd - d_w\|_2 < \epsilon \tag{5.6}$$

Comparing to the ℓ1 norm regularized SAR method, the only difference is to change the SAR operator G to the convolution matrix W that include a reference wavelet signal. We can also solve it in same way with that we introduced in Chapter 4. For the simplicity here we will not repeat the detail explanation of the method.

We found that the ℓ1 norm regularized pulse compression has better performance than conventional Weiner filter when the acquired data is noisy. However, it is similar to the ℓ1 norm regularized imaging case that when there are multiple targets or distributed targets, this method may not robust as the conventional Weiner filter.

Figure 5.2 shows an example of the real data trace that acquired by the vivalid antenna and the target is a metal sphere located at 0.5 m away. Due to the noise level, Weiner filter cannot give a good result even after I tried to adjust the parameter carefully. We can find that the wavelet is slightly compressed but the noise level is start rising already. In Figure 5.2(c) we can find that the proposed method gives much better result and the target

reflection is compressed into a pulse and only a few noise components are remind as weaker response.

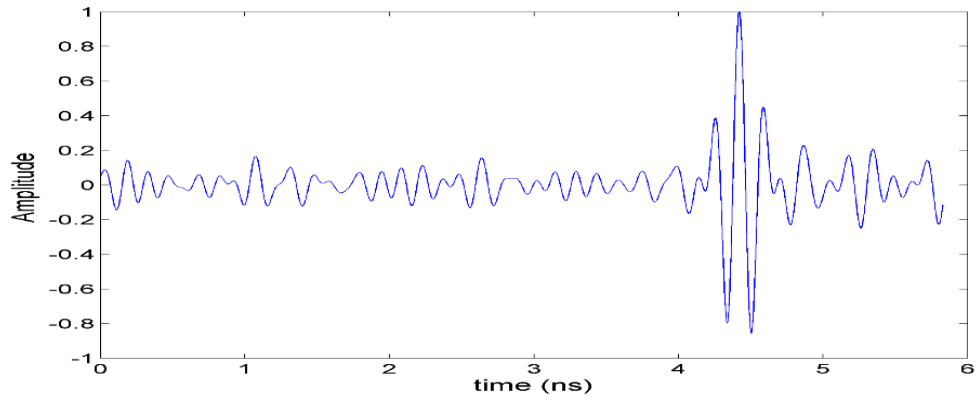

(a)

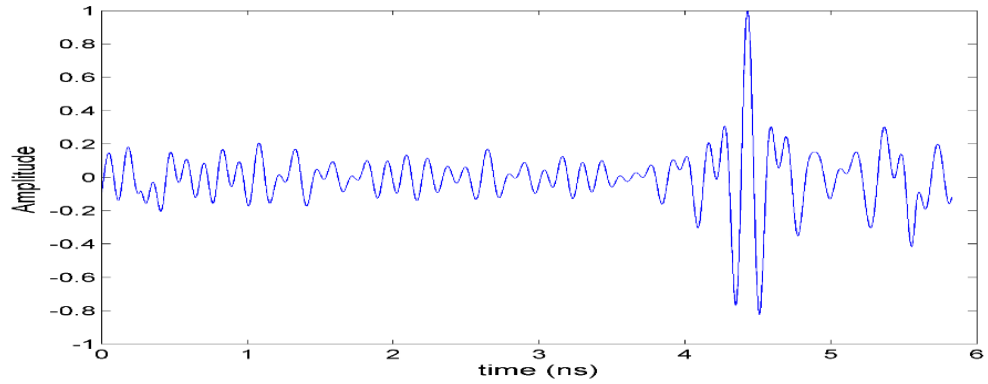

(b)

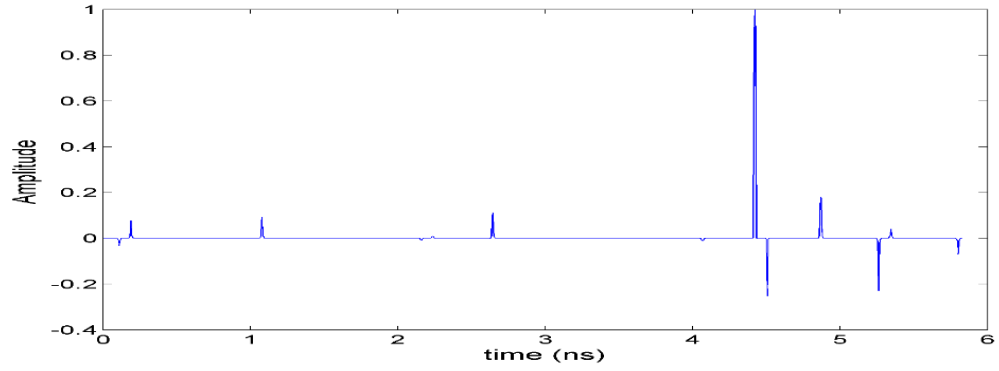

(c)

Figure 5.2 Comparison of Wiener filter and ℓ1 norm regularized method, (a) raw signal acquired with vivalid antenna; (b) pulse compression with Wiener filter; (c) pulse compression with ℓ1 norm regularized method.

5.25 Pulse compression and SAR imaging

Now if we go back to previous discussions on SAR algorithm, it is clear that actually SAR processing is under the assumption that the waveform of the transmitted signal is just a pulse. Obviously it is not true for near-range SAR imaging and it somehow explained why the simple waveform is better for least square imaging methods. Since we did not consider the waveform within the least square iterations, the algorithm will recognize the waveform as multi targets at different distance and it cause problem for imaging. It delights that we may need to apply pulse compression before the SAR processing especially for our sparse array applications.

Here we show a real dataset example for pulse compression and SAR processing. The dataset is acquired with the linear sparse 1-dimensional array that we have introduced in Chapter 2. Also eight transmitter and eight receiver antennas are used for the array system, the antenna configuration is shown in Figure 2.10. The frequency ranged from 4 to 8 GHz and the target is a metal sphere located at 0.5 m away. In Figure 5.2 we actually used one of the trace from this dataset and we show that $\ell 1$ norm regularized pulse compression gives a good result. Figure 5.3 shows the acquired 64 channel dataset before/after pulse compression processing. We can observe that after the pulse compression processing the time resolution is greatly improved. However it also introduces problem for simple SAR processing because there is almost no negative value and artifacts cannot be canceled well as it is shown in Figure 5.4(b). In Figure 5.4(c) I tried the semblance weighted SAR method that we introduced in Chapter 3. As the result we can get high resolution reconstruction result.

Here we should delight that $\ell 1$ norm regularized SAR processing that we introduced in Chapter 4 can get quiet similar result as we shown in Figure 5.4. But the physical meaning is slightly different, as I mentioned before SAR processing does not consider about the wavelet information and it is same to $\ell 1$ norm regularized method. However, with $\ell 1$ norm regularization some of the sidelobes in time-domain may treated as noise and thresholded while minimizing the $\ell 1$ norm, which means the pulse compression is also partially included although there is no pulse compression processing included. While the $\ell 1$ norm regularized pulse compression is physically more accurate and we expect it has better accuracy. From this point of view, a good way for processing should include $\ell 1$ norm regularized pulse compression and then apply $\ell 1$ norm regularized SAR processing. However, this processing is extremely time consuming but not improving so much comparing the processing we use for Figure 5.4. However, it inspired us the possibility of combing the pulse compression and SAR processing together.

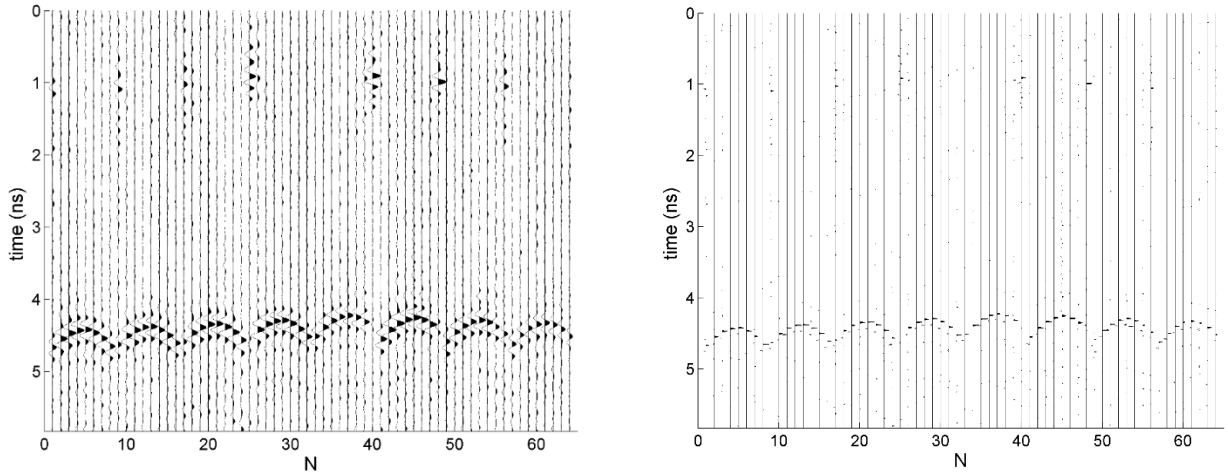

(a) (b)

Figure 5.3 1-dimensional array dataset with ℓ1 norm regularized pulse compression, (a) radar signal of all channels before pulse compression; (b) after pulse compression.

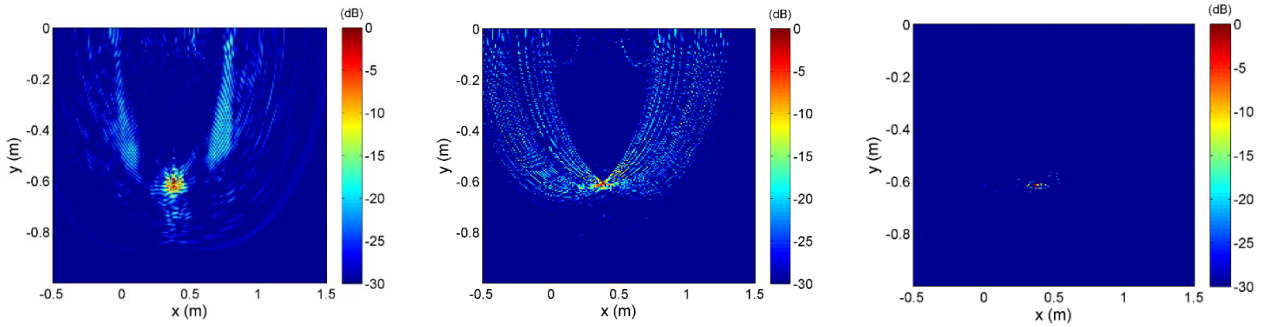

(a) (b) (c)

Figure 5.4 SAR processing results with pulse compression, (a) conventional SAR processing result; (b) conventional SAR processing result after pulse compression; (c) Semblance weighted SAR processing result after pulse compression.

5.3 Multi-dimensional pulse compression of SAR imaging result with the deblurring filter

5.31 Methodology

An idea that use multi-dimensional pulse compression processing on focused optical imaging is introduced in [15] to further enhance the spatial resolution. The core idea is to

compensate the artifacts that caused by the observation system which is very similar to our case that imaging with a certain sparse array. This idea to seismic processing as a multi-dimensional deconvoluiton technique and shows it can somehow improve the imaging quality [9]. I think it is a good approach to deal with sparse array artifacts since these artifacts are spatially variant as we discussed in previous sections.

From (5.1) we can combine the convolution matrix and SAR operator together as a operator L, hence we can have (5.7)

$$d_w = Lm \tag{5.7}$$

The blurred result can be acquired with (5.8)

$$\widehat{m} = L^T d_w \tag{5.8}$$

Also we can get the relation between model and the blurred result in (5.9)

$$m = (L^H L)^{-1} \widetilde{m} \tag{5.9}$$

It indicates that we may further improve the migrated results with an inverse filter $(L^T L)^{-1}$. Actually, this is known as the deblurring processing for imaging problem. This deblurring filter is still very difficult to solve for the whole imaging area, but we can use the local filters at different position instead of a whole filter. It is much easier to explain this with mathematics. For a given matrix, if there is only one non-zero value exists, the inverse matrix can be uniformly determined. And this is exactly same that in a local window there is only a scatterer exists. The inverse matrix may not uniformly determined when there are many non-zero values, which is just the reason why it is difficult to find the inverse of the whole imaging area.

In order to realize this method, a dictionary needs to be reconstructed correspond to the antenna configuration and the background velocity first. At each local window we put a point scatter in the middle and calculate the forward modelling result and the migrated result of this local window. Then the local deblurring filter can be uniformly determined. After we construct this dictionary for a certain survey area, we can apply the filters to the acquired dataset. Since the local deblurring filter is just the inverse PSF function of the simulated data of the point scatterer, we need to apply the filter as the matched filter. For simplicity we directly applied it as the Weiner filter. In order to improve the imaging quality, the filters at different local windows should be overlapped properly. In general, we can propose the flow chart of the deblurring method in Figure 5.5.

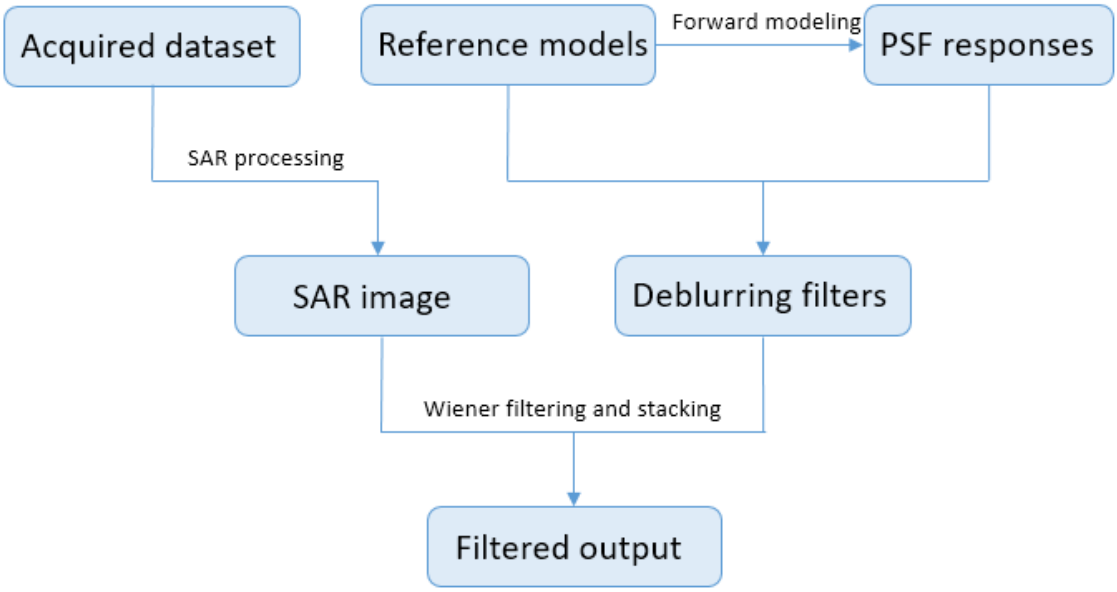

Figure 5.5 Flow chart of applying the deblurring filter method on conventional SAR processing results.

5.32 Simulation tests for a single scatterer deblurring

In previous section we have introduced the basic idea of the deblurring imaging method. Here we start with the simplest example that apply the deblurring filter on a single scatterer itself. Figure 5.6 shows the monostatic simulation example and the target is a scatterer located at the middle of the imaging area. And the wavelet is still the Gaussian wavelet with 4-8 GHz bandwidth. The transceivers are distributed on a 1.2 m survey line and there are only five traces remind so that we can observe strong artifacts after SAR processing.

In this simple test, we can directly use this dataset as the dictionary by using a rectangular window with the scatterer in the center as indicated as a re rectangular in Figure 5.6(b). Then we can acquire the deblurring filter by dividing the windowed dataset with the model which include only a non-zero value in the center. After that we can apply this filter to other part of the SAR imaging result. If we directly apply this filter to the red rectangular area which is just the filter response itself, we can get perfect reconstruction result in Figure 5.7(b) as we can expect. All the imaging artifacts are removed and also the wavelet is further compressed. In Figure 5.7(c) we show the case that apply this filter to the blue rectangular area. Although the reference does not fit the blue rectangular area perfectly, we can still get good deblurring result with the Wiener filter processing. As we explained in previous section, deblurring filter actually includes two steps: a conventional 1-dimensional pulse compression processing that can compress the waveform and also 2-dimensional deblurring processing that suppress the artifacts that created by the distributed antenna array.

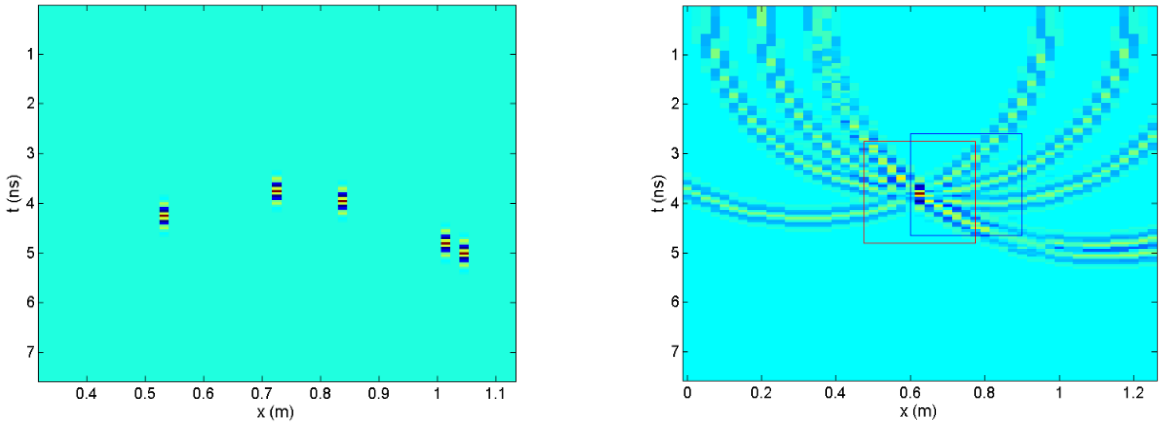

(a) (b)

Figure 5.6 A simulated data of a point scartterer; (a) Simulated radar profile after coarse resample; (b) conventional SAR imaging result of (a). The data within the red rectangular is used for generating the deblurring filter.

Figure 5.8 also shows another case that we do not include the wavelet while generating the dictionary. We can find that in this case the point response does not compressed but the artifacts still can be suppressed. In this case the processing is very similar to the ℓ2 norm regularized least square method for SAR processing. As we explained before, these kind of imaging artifacts may not fully eliminated with ℓ2 norm regularization.

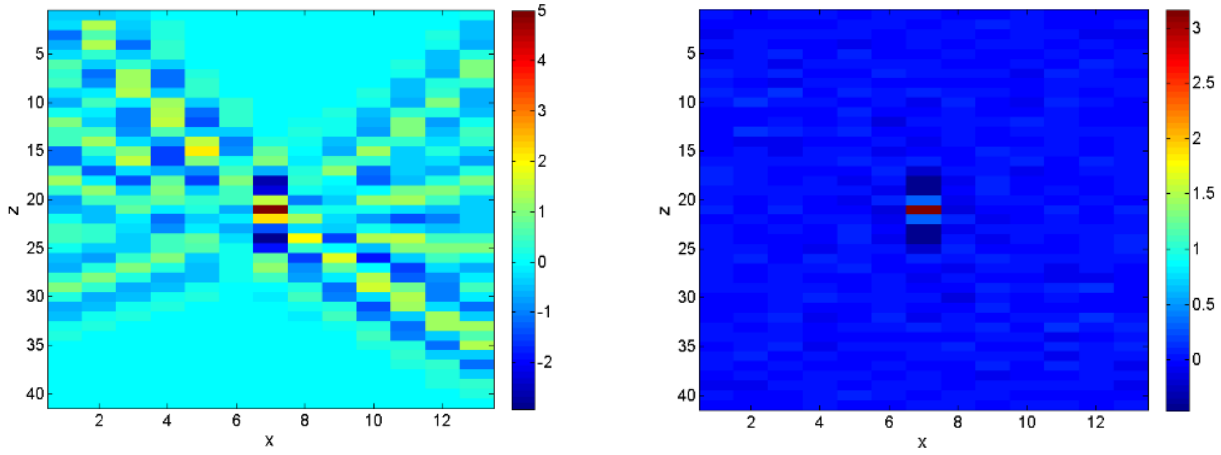

(a) (b)

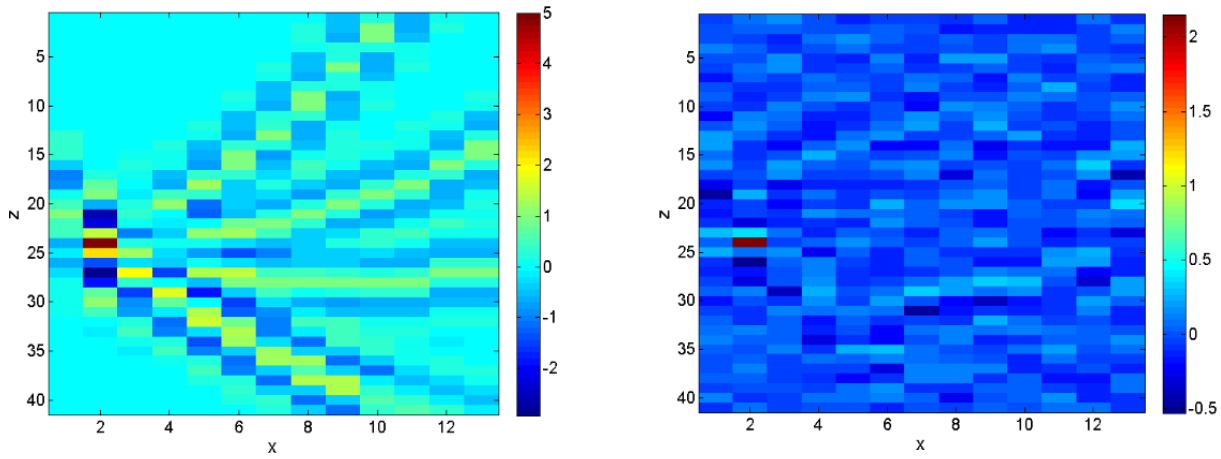

(c) (d)

Figure 5.7 results of deblurring filter applied to the sub-windows, (a) sub-window data indicated with red rectangular in Figure 5.6; (b) after applying deblurring filter; (c) sub-window data indicated with blue rectangular in Figure 5.6; (d) after applying debluring filter.

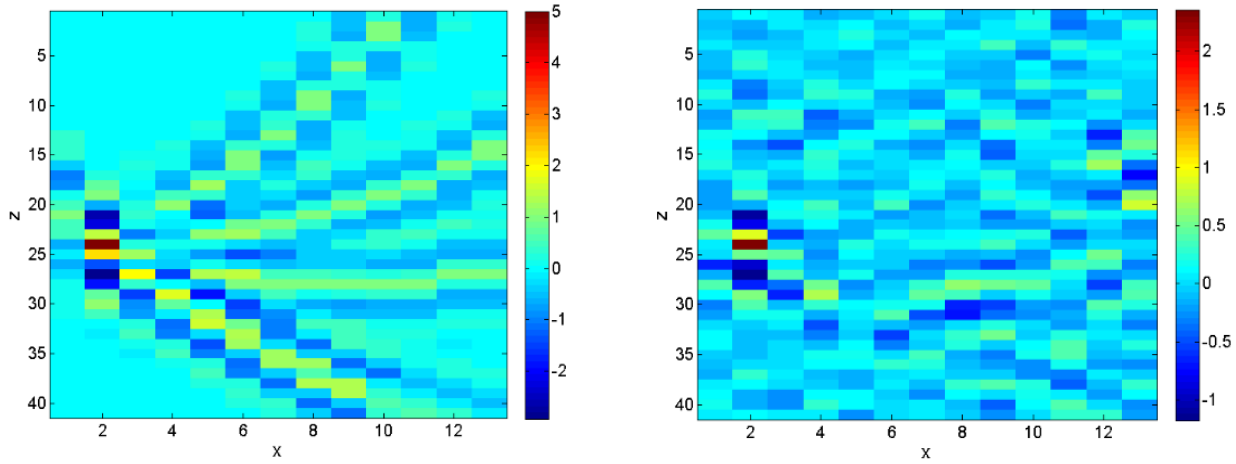

(a) (b)

Figure 5.8 results of deblurring filter that generated without known wavelet; (a) before applying the deblurring filter; (b) after applying the deblurring filter.

It is obvious that when the position of the scatterer in dictionary is coincident overlap with the scatterer in acquired dataset we can get the best matched deblurring result. And it seems to be that if we can create a dictionary that includes the deblurring filters of all the possible position then we can get a good result. However for real application it is not really helpful

because in most of the cases the dictionary created by simulation is not totally matched with the acquired dataset due to the noise or the change of the wavelet (or we can understand the change of the frequency component), also the real targets may include the distributed targets that is not exist in our scatterer dictionary. This is a general problem for all the deblurring processing and [9] pointed out that it can be somehow overcome by proper stacking of the filtered windows. As we can already observe in Figure 5.7. If we simply stack the Figure 5.7 (b) and (d), the scatterer can be further enhanced and the surrounded artifacts caused by the filtering can be suppressed. It delights that it is important to choose the proper window size and the stacking interval of different windows. It is not really possible to give a deterministic solution so we may need to analyze it with the experience.

5.33 Factors for applying deblurring filter method

In previous sections we have introduced an imaging method that based on deblurring filter. Theoretically it can generate the least square migration result based on a conventional migration result without iteration processing. Here we will make more accurate explanation of this method, and extend it to the current sparse array system.

The fundamental idea of this method is using the reference model, which include only point scatterers and their PSF function to design the 2-dimensonal pulse compression filters at different regions of the imaging area. Mathematically, when there is only a non-zero value within a window which is just the case that there is only one point target in the middle of the window, the inverse matrix can be determined uniquely. Then we apply this filter with Weiner filter method because the reference model is always different with real data practically. Some more detailed explanations are given in presentation.

In this case, the main factors of this method includes the accuracy of the reference signal and the size of the filter. As I mentioned before, this deblurring filter is actually the 2-dimensional pulse compression that applied to the migration results. Hence it is similar to the 1-dimensional pulse compression that the accurate wavelet reference is very important. For our case, we can acquire the wavelet from the acquired dataset since it is quiet stable. Another problem is more significant that the assumed position of the scatterers. Ideally, we should make as many possible scatterers as possible but it is not practical in real application. Firstly, no matter how dense scatterers reference model we make, it always not really work for distributed target. Even if we have only one scatterer reference model, somehow we still can use it to suppress the artifacts. Secondary, If the scatterers are distributed too dense in imaging area, it will cause problem to the size of the filter near the boundary of the imaging area.

On the other hand, since this method is more like an imaging method, the effect of the filter size is more significant because larger filter size provide more information to ‘recognize’ the point target. We found that practically only a few scatterers reference model is already quiet enough. But it is much better if we know the about distance of our target.

5.34 Simulation and experimental results with sparse array system

Here we will demonstrate the proposed method with both sparse array system that we have introduced in Chapter 2. We use the same antenna configuration and use 4-8 GHz Gaussian wavelet to generate the ray tracing simulation results. Here we should notice that the proposed method is applied base on the conventional SAR imaging results.

In Figure 5.9 we use 1-dimensional linear array configuration for the simulation test. The model include a linear reflector at 0.8 m away and a point scatterer at 0.5 m away. Figure 5.9(a) shows the imaging result with conventional SAR processing. Basically both targets can be imaged well but the hyperbola artifacts appears due to the sparse sampling. With this antenna configuration we assumed 9 point scatterers that distributed uniformly in the imaging area for the reference model and generated 9 deblurring filters at different position of the imaging area. After the deblurring processing we can find that the linear reflector and the point scatterer is further focused. Also the hyperbola artifacts are greatly reduced. It proved the possibility of the proposed method. However, here we should point out that in this example the proposed method has good performance is mainly because that both the accuracy of the wavelet and the position of the reference model are designed to fit with this dataset. For the real application the situation will be much complicated as we already discussed in previous section.

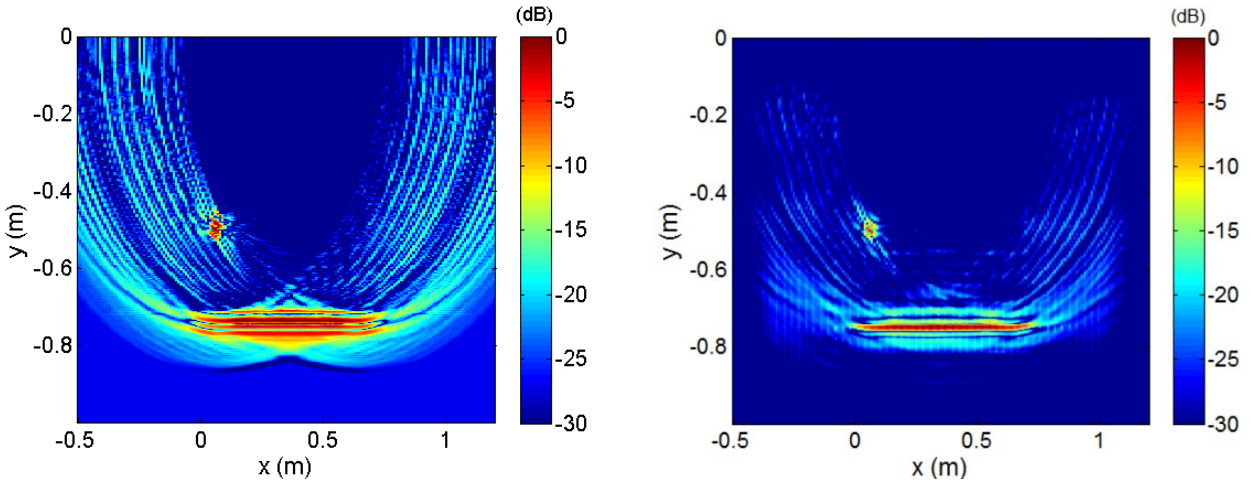

Figure 5.9 results of deblurring fillter applied to 1-dimesional sparse array simulated data, (a) conventional SAR processing result; (b) after applying the deblurring filter to (a).

Figure 5.10 shows the proposed method that applied to the real data acquired by the 1-dimensional linear sparse array. The target is a metal sphere and we extracted the reference wavelet from the acquired dataset and we also generated 9 deblurring filters that distributed

uniformly within the imaging area. However, the performance of the method is not good as the simulation example that we show in Figure 5.9. We can find the imaging artifacts are well suppressed but the target itself did not focused well. As we introduced in section 5.2, I tried to adjust the parameter of the Wiener filter to improve the quality. However, we find that with a smaller parameter the imaging result will be destroyed by the noise since the conventional SAR imaging result in Figure 5.10(a) is already quiet noisy.

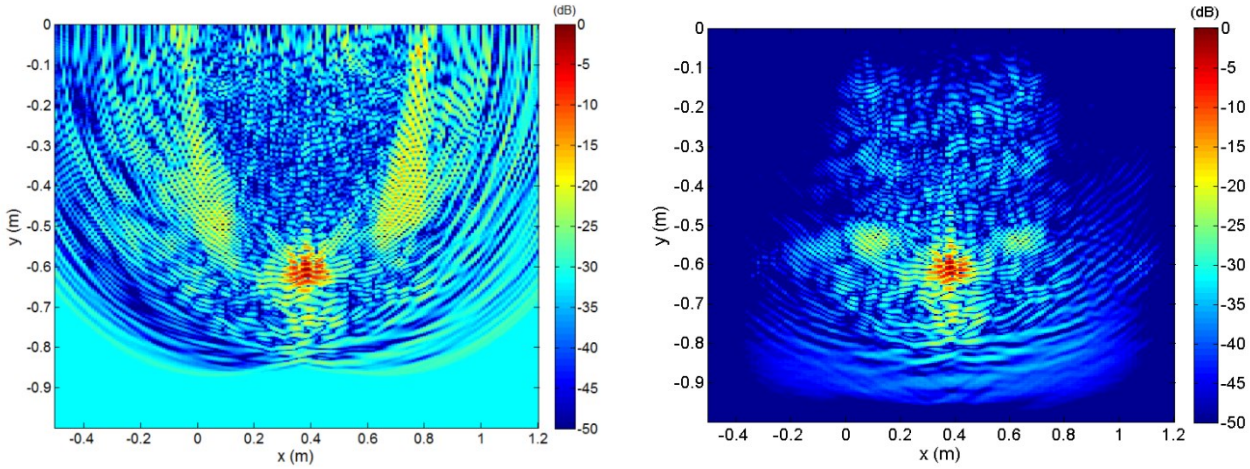

(a) (b)

Figure 5.10 results of deblurring fillter applied to 1-dimesional sparse array experimental data acquired for a metal sphere target, (a) conventional SAR processing result; (b) after applying the deblurring filter to (a).

With Figure 5.11 we show another experimental dataset that acquired with 1-dimensional linear array system. Here we change the metal sphere to a metal pipe located at 0.65 m away. Same with the previous example we extract the reflection from the metal pipe as the reference wavelet and generated 9 deblurring filters. In this case we used smaller value of the Wiener filter parameter to show another kind of imaging result from the previous example. In Figure 5.11(b) we can find that the reflection from the target is further focused into the pulse, while the imaging artifacts still remain strong comparing with the conventional SAR imaging result. Here we did not show too much processing results with different parameters because this method is still quiet practical and target dependent. Although the calculation is much simple comparing with the iteration algorithm that we introduced in Chapter 4, the optimization of the regularization parameter is still tricky for the real dataset that include complicated reflections and noise.

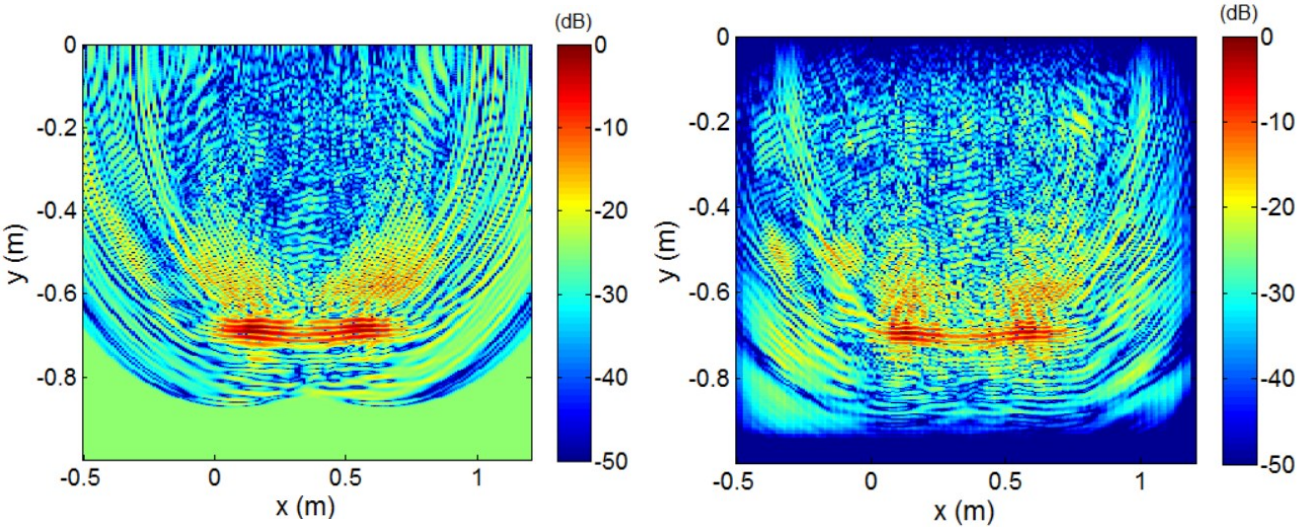

Figure 5.11 Figure 5.10 results of deblurring fillter applied to 1-dimesional sparse array experimental data acquired for a metal pipe, (a) conventional SAR processing result; (b) after applying the deblurring filter to (a).

5.35 Simulation and experimental results with sparse array system

In order to apply the proposed method to 2-dimensional sparse array. We need to extend the 2-dimensional filtering to 3-dimensinal filtering. There is not so much difference comparing with the previous processing and we only need to use 3-dimensional Fourier transform instead of the 2-dimensional Fourier transform and make the 3-dimensional deblurring filters. However, we found the deblurring processing for 3-dimensional data cube is not that predictable as 2-dimensional case and the results with real 2-diemensional sparse array data are not good.

Here we show some result with simulated dataset that using the 2-dimensional array configuration to demonstrate the performance of the proposed method. Figure 5.12 shows the simulated SAR imaging with a scatterer in the center of the imaging area. We are still using the 9 deblurring filters that are uniformly distributed in the imaging area. As we can see, after the proposed method the artifacts are removed and the scatterer is further focused. However, in Figure 5.12(e) and (f) we can observe that the artifacts are turned into different distribution and become stronger. Similar problem also happens to other simple model that we did not shown here and this problem still need to be further discussed.

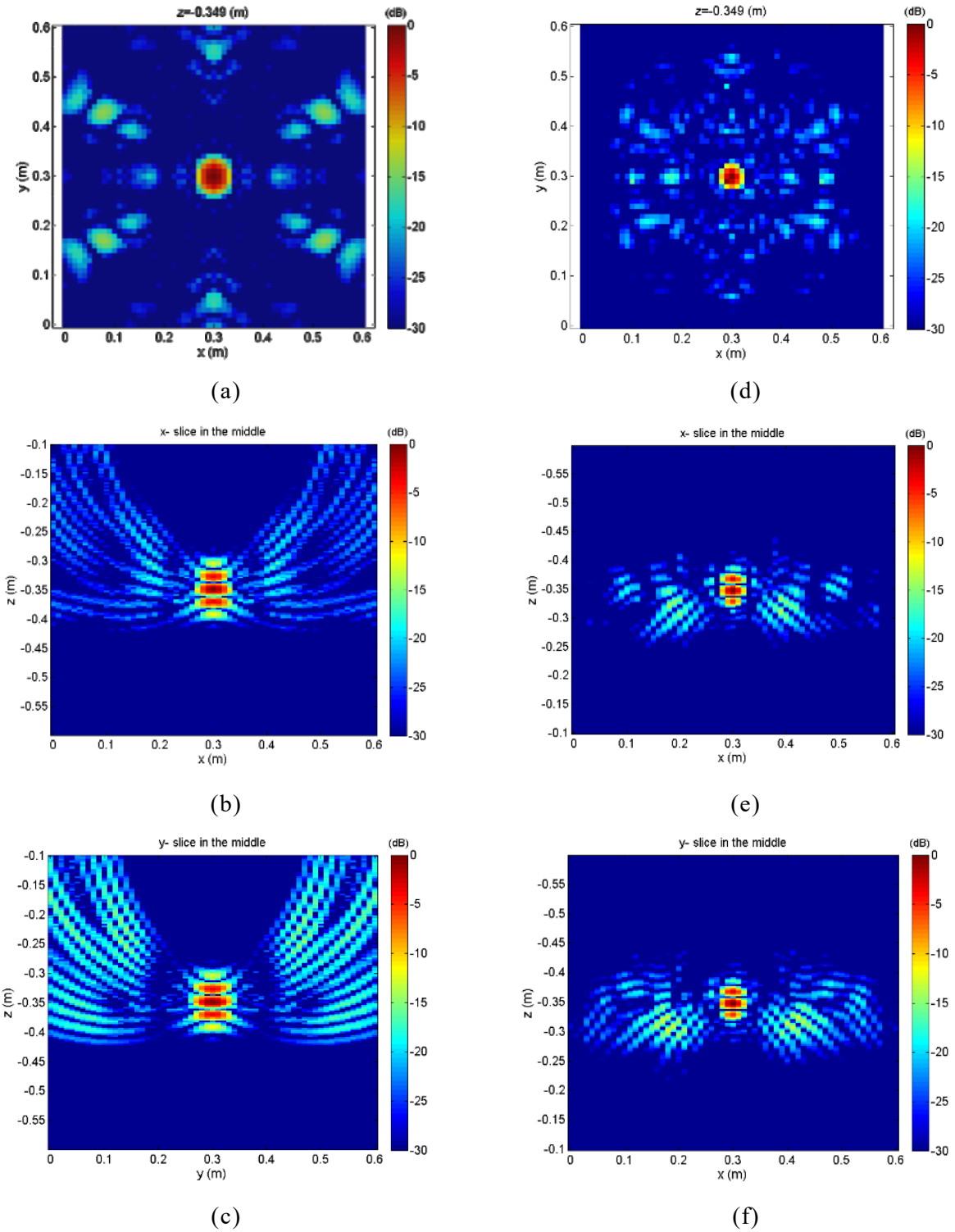

Figure 5.12 results of deblurring fillter applied to 2-dimesional sparse array simulated data acquired for a point target, (a)(d) horizontal slice before/after applying the deblurring filter; (b)(d) vertical slice in x- direction before/after applying the deblurring filter; (c)(f) vertical slice in y- direction before/after applying the deblurring filter;

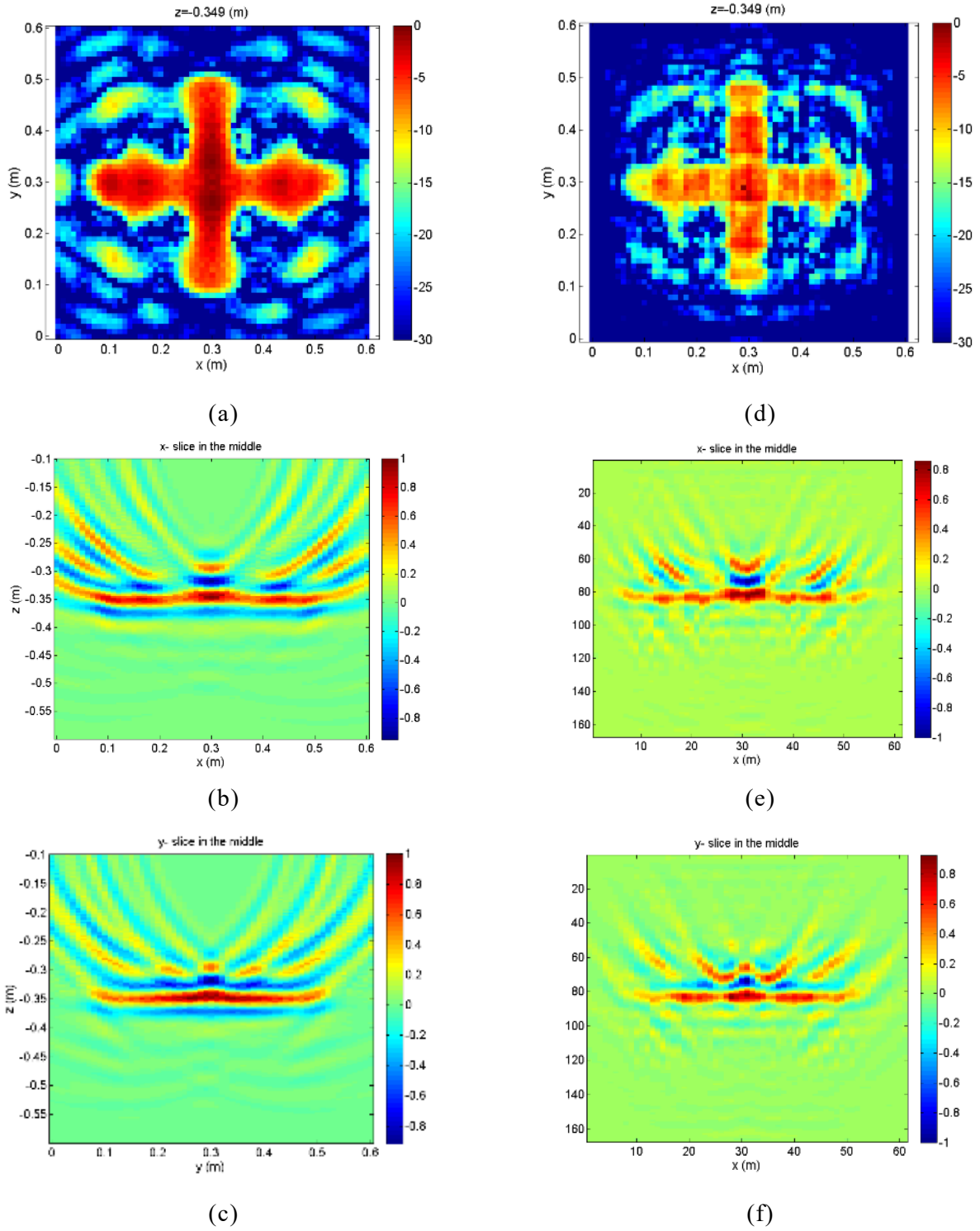

Figure 5.13 results of deblurring fillter applied to 2-dimesional sparse array simulated data acquired for a point target, (a)(d) horizontal slice before/after applying the deblurring filter; (b)(d) vertical slice in x- direction before/after applying the deblurring filter; (c)(f) vertical slice in y- direction before/after applying the deblurring filter;

In Figure 5.13 we also tried the cross-shape target that we always use in previous chapters. When we compare the horizontal slice we can find that the shape of the target become more sharp and accurate due to the deblurring process. However in this result the target looks not continuous and we cannot observe clear improvement from the vertical slices. Also the result changes a lot with different parameters and we find it is much difficult to select a proper parameter for 2-dimensional sparse array case.

5.4 Summary

As I introduced in previous chapters that SAR processing is not considering about the wavelet shape which lead to the appearance of the artifacts after imaging processing. In this case, I think the pulse compression processing is important especially for the near-field imaging since the duration of the wavelet is relatively large comparing with the imaging area. I reviewed the conventional Wiener filter and applied $\ell 1$ norm regularized least square method to achieve better results. It is shown that the $\ell 1$ norm regularized pulse compression can restore the signal into the pulse and it has better performance against noise than Wiener filter. AS the drawback it also require iterative calculation although it is much faster than $\ell 1$ norm regularized SAR processing method. Also it is similar to $\ell 1$ norm regularized SAR processing, the setting of the regularization parameter has strong effect to the results.

Based on the idea of the spatial filtering, I proposed to use the deblurring filter technique to remove the imaging artifacts caused by the sparse array. Mathematically we can obtain similar result with the least square SAR processing method. And since we are applying the deblurring filter as a spatial variant local filter, the calculation is simplified and we do not need to use iterative algorithm which can be a great benefit comparing with the least square SAR processing technique. With the simulated experiment and experimental dataset acquired with the 1-dimensional linear array system I demonstrated the possibility of the purposed method. I also extended this method to 3-dimensional spatial filtering method and applied to the 2-dimesional sparse array configuration. However, this method is very practical and the result is strongly dependent on the reference scatterer model that we created. Due to the uncertainty and the noise of real dataset, I still do not obtain idea result from the 2-dimensional sparse array system.

5.5 References

[1] R. Fergus, B. Singh, A. Hertzmann, S. T. Roweis, and W. T. Freeman, “Removing camera shake from a single photograph,” ACM Transactions on Graphics (TOG), vol. 25, no. 3, pp. 787–794, 2006.

[2] I. Aizenberg, D. V. Paliy, J. M. Zurada, and J. T. Astola, “Blur iden-tification by multilayer neural network based on multivalued neurons,” Neural Networks, IEEE Transactions on, vol. 19, no. 5, pp. 883–898, 2008.

[3] L. Xu, X. Tao, and J. Jia, “Inverse kernels for fast spatial deconvolution,” in Computer Vision-ECCV 2014. Springer 2014, pp. 33–48.

[4] T. Taxt and G. V. Frolova, "Noise robust one-dimensional blind deconvolution of medical ultrasound images," IEEE Trans. Ultrason., I'ermelect., Freq. Contr., vol, 46, no. 2, pp. 291-299, 1999.

[5] T. Taxt and G. V. Frolova, "Noise robust one-dimensional blind deconvolution of medical ultrasound images," IEEE Trans. Ultrason., I'ermelect., Freq. Contr., vol, 46, no. 2, pp. 291-299, 1999.

[6] P. E. Blankenship, E. M. Hofstetter, "Digital Pulse compression via fast convolution", IEEE Trans. On Acoustics Speech and Signal Processing, vol. ASSP-23, pp. 189-222, April 1975.

[7] E. Candes, C. Fernandez-Granda, "Super-resolution from noisy data", Journal of Fourier Analysis and Applications, vol. 19, no. 6, pp. 1229-1254, 2013.

[8] V. Duval, G. Peyré, "Exact support recovery for sparse spikes deconvolution", Found. Comput. Math., vol. 15, no. 5, pp. 1315-1355, 2015.

[9] J., X., Hu, and G., T., Schuster, “Migration deconvolution: Mathematical Methods,” SPIE Proceedings, vol.3453, pp. 118–124, 1998.

[10] Y. Wang, "Inverse Q-filter for seismic resolution enhancement", Geophysics, vol. 71, pp. 51-60, 2006.

[11] J. Wang, "The determination of optimal gate lengths for time-varying Wiener filtering", Geophysics, vol. 34, no. 5, pp. 683-695.

[12] T.G. Savelyev, L. van Kempen and H. Sahli, “GPR anti-personnel landmine detection: improved deconvolution and time-frequency feature extraction”, in Nondestructive Evaluation and Health Monitoring of Aerospace Materials and Composites II, Andrew L. Gyekenyesi, Peter J. Shul, eds., Proc. SPIE 5046, pp. 232-241, 2003.

[13] H. W. Engl, M. Hanke, and A. Neubauer, Regularization of Inverse Problems, Kluwer Academic, Dordrecht, 1996.

[14] O. Yilmaz, “Deconvolution,” in O. Yilmaz, Seismic Data Processing, Tulsa, Society of Exploration Geophysicists, 1987.

[15] [Xiang Zhu, Peyman Milanfar, "Removing Atmospheric Turbulance via Space invariant Deconvolution", IEEE Transactions on Pattern Analysis and Machine Intellingence, vol. 35, 2013.

Chapter 6 Subsurface velocity estimation methods with array radar system

6.1 introduction

In previous chapters I discussed about the near-range imaging problems of sparse array radar system. While in this chapter I will mainly discuss on how we can use the flexibility of the array system for velocity estimation of the medium. This special application is mainly related to the GPR technique, it is a powerful tool that is used for subsurface exploration. It is a non-destructive method and can provide the highest resolution among all methods of subsurface imaging. In previous researches, it has been shown that the GPR technique has many advantages, which leads to its wide use in different fields [1][2][3].

Currently we are conduction a research project on monitoring of pavement at airport runway by using ground-based SAR and array-type GPR. In this research project, we are developing radar technologies to detect the defects or anomalies which occurred inside the pavement of the surface of the pavement of the runway and taxiway or park apron in airports. In this project, I mainly focus on estimating the slight velocity changes within the single layer reflections such as the inspection of the pavement. Under such simple condition we are aiming at using limited number of antennas for precise velocity estimation.

I first introduce the theory that uses the CMP dataset to estimate the velocity of electromagnetic wave propagation in subsurface [4]. In previous work we applied this method with a bistatic GPR system to acquire the CMP dataset [5]. However, the data acquisition is very complicated for a CMP dataset at one fixed position. In most cases we have to use the limited information, for example, we have to decide only a few CMP points based on the knowledge of hydrology to estimate the subsurface properties in a relatively large area [6]. In order to improve the efficiency of the data acquisition, we are also considering to use multistatic system for CMP data acquisition instead of the biastatic system. In previous chapters it was already shown that the resolution of the SAR technique is mainly related to the maximum aperture and it is similar for CMP velocity estimation. However, artifacts may introduced if there are only a few antenna combinations exist within this distance [7]. The artifacts make it difficult to pick the velocity automatically. In this case, I introduced a method to enhance the estimated results by removing the aliasing components caused by the coarse sampling and then interpolating the CMP dataset, so that the velocity can be picked automatically at every position. I also show how the velocity estimation can be enhanced with the real data acquired at a sand dune. The result also indicates that the velocity of multiple layers can be acquired for the hydrology research.

On the other hand, due to the similarity of the CMP velocity estimation and the SAR

imaging, I also try to apply the ℓ1 norm regularized least square method for precise velocity estimation. It shows that few millimeter per nano second velocity changes can be detected and the result is much easier for automatic velocity picking [8].

In the end, for the special application case I proposed a practical way for single layer pavement inspection method based on interference of two different CMP dataset [9]. The core idea of this approach is based on the time lapse monitoring technique that is widely used in different domains [10]. The main advantage of this method is that we can distinguish the velocity and/or thickness change of the single layer structure with only few antenna pairs.

6.2 velocity estimation with CMP dataset

6.21 Common-mid-point (CMP) velocity analysis with Bistatic GPR

CMP data is a unique dataset that can be acquired by the bistatic GPR system. The vertical root mean square (RMS) velocity of electromagnetic wave propagation in subsurface layers can be estimated from a CMP dataset. Its successful applications have been demonstrated for example for hydraulic property estimation [3].

For the CMP analysis at a fixed position, reflected signals need to be measured at both sides of the middle point with different antenna distances as Figure 6.1 shows. If the subsurface is homogeneous and horizontally layered, the two-way travel time of the reflection signal can be given with (6.1).

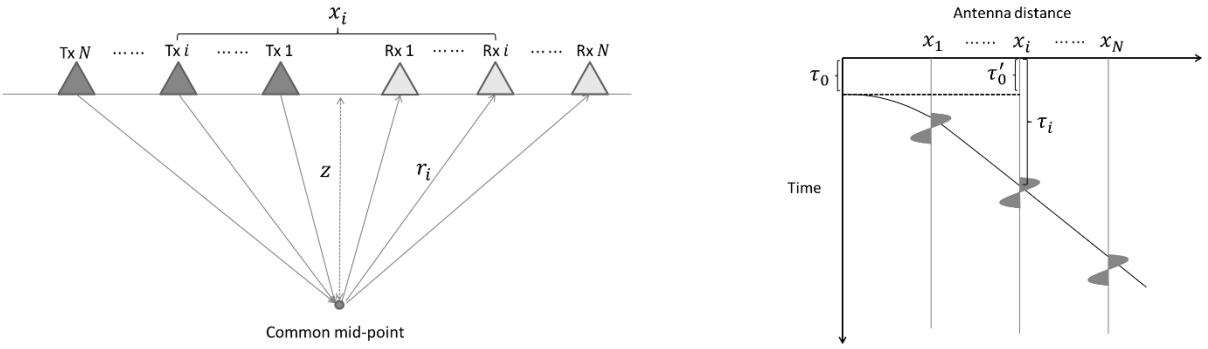

(a) (b)

Figure 6.1 Configuration of a CMP dataset; (a) data acquisition; (b) corresponding CMP data.

$$\tau_i(v,z) = \sqrt{\frac{4z^2 + x_i^2}{v^2}} \tag{6.1}$$

$$P(v,z) = \sum_{i=1}^{N} d(\tau_i(v,z), x_i) \tag{6.2}$$

Where z is the depth of the horizontal reflector, x_i is the distance between the antenna pair i, v is the trial velocity, N is the number of the traces and d is the CMP data. After a CMP dataset is acquired, we can apply the velocity analysis to obtain the velocity spectrum P with (6.2). Velocity spectrum shows the stacked amplitude of the signals at different positions along the hyperbolic curves given by (6.1). When a trial velocity is close to the real velocity, the stacked energy will be enhanced. Hence we can pick the estimated velocity at the maximum energy point. Figure 6.2 shows a simple simulated CMP dataset and its velocity spectrum. Here we assume that there is only one reflector located at 0.5 m depth with 0.12 m/ns subsurface velocity. We can find that due to the different distance between the antenna pairs the reflected signal forms into a hyperbolic curve as it shown in Figure 6.2(a). The direct coupling is also included that is shown as a straight line. After the velocity analysis we can acquire the velocity spectrum as shown in Figure 6.2 (b). We can find that the energy is well focused at the position where the velocity is equals to 0.12 m/ns. The quality of the velocity spectrum is related to the length of a CMP survey line which is decided by the largest distance of an antenna pair for multistatic system, the wavelength of the signal, signal to noise ratio (SNR) and the update step of the trial velocity. Also the artifacts may be introduced when the data is very coarse as I mentioned before. More details on CMP analysis can be found in [4][5].

On the velocity spectrum we can pick the depth and also the velocity of the upper layers. Here we should notice that the picked velocity is RMS velocity which indicates the average velocity of a layer as

$$v_{rms} = \sqrt{\frac{\sum v_1 d_1 + v_2 d_2 + \cdots}{\sum \frac{d_1}{v_1} + \frac{d_2}{v_2} + \cdots}} \tag{6.3}$$

Here d and v represents the thickness and the velocity of different layers. The quality of the velocity spectrum depends on the effective length of a CMP survey line, the pulse width of the signal, trial velocity update step, depth of layer and noise [4]. From Equation (6.1) we can see that the velocity analysis processing is very similar to SAR processing; therefore, many features of SAR processing also apply. As it is shown in Figure 6.2, the velocity analysis transforms the CMP dataset to velocity-depth domain. This explains well that the small velocity update step gives better resolution in velocity spectrum. The effect of the pulse width and the CMP survey length is same as that in the SAR processing, as a shorter pulse and longer effective survey line give better resolution. The effective CMP survey length means the maximum offset that can observe the hyperbolic reflections from a layer.

It is related to the antenna radiation pattern and the depth of the layer. The observation length of a CMP dataset limited the resolution of the velocity spectrum. The coarse sampling does not reduce the resolution, however, it may introduce the imaging artifacts that distort the velocity spectrum. Noise can be a problem to almost all the signal processing methods. The best way is to suppress the noise while acquiring the data, and it may be reduced further with de-noising algorithms that we also mention in later part.

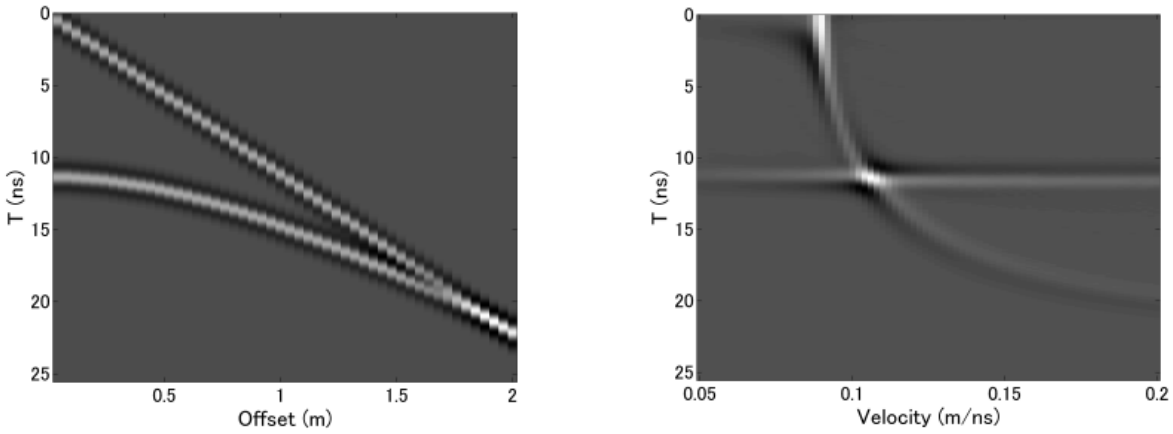

(a) (b)

Figure 6.2 The simulated CMP dataset (a) and its velocity spectrum (b).

6.22 Fast CMP velocity analysis with multistatic array radar system

For CMP data acquisition the bistatic GPR system is necessary. And the spatial sampling interval should be less than half wavelength to prevent the data from generating artifacts as we pointed out in previous chapters. In this case, we need to move the antennas step by step, and it can be very time consuming for single CMP dataset. On the other hand, for the geological application or the pavement inspection, the velocity information in single position is not enough. It is much better if we can acquire the velocity information along a survey line or even the distributed 2-dimensional area which is very difficult for bistatic system. It is similar to the SAR system problem that we discussed in previous chapter, we may also solve this problem with the multistatic system. In 2012, we developed a multistatic array GPR system named YAKUMO [11], the details of the system will be introduced in next chapter. With this antenna configuration, it is also possible to acquire the CMP data at a fixed position as Figure 6.3 shows. Due to the size of antennas, each trace of the CMP data is not placed on a line. Comparing to the configurations of the common CMP measurements, the CMP data acquisition of YAKUMO system is very fast and convenient. As the trade off, the CMP data acquired by YAKUMO system includes only eight traces

and the spatial interval of the antenna distances between the different antenna pairs are not unique. As I mentioned in previous section, the coarse CMP data generates artifacts in velocity spectrum and it makes the automatic velocity picking much difficult. In this case, some special processing techniques are required for the coarsely acquired CMP dataset.

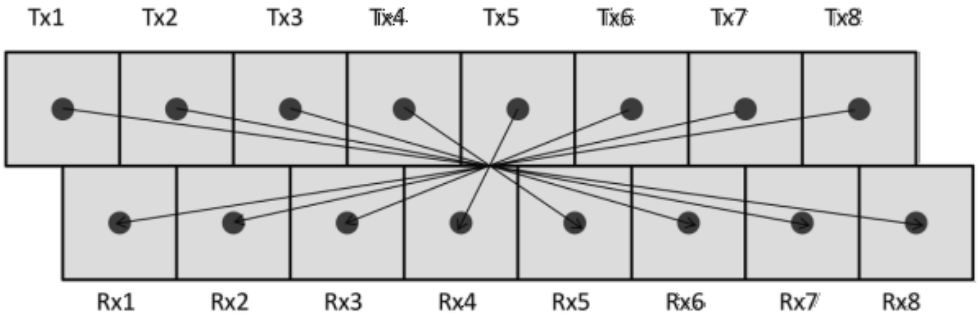

Figure 6.3 Antenna configuration of YAKUMO system.

6.3 Interpolation of YAKUMO CMP dataset

From the view of imaging processing, the aliasing are generated by the tilted linear objects which are not well sampled. Here we try to use a trial velocity to regularize the antenna pairs with different distance to zero distance. It can be calculated for each antenna pair by geometry with (6.4).

$$\tau_0 = \sqrt{\tau_i^2 - \frac{x_i^2}{v^2}} \tag{6.4}$$

Where τ_i is the two-way travel time with different antenna distance x_i and τ_0 is the estimated two-way travel time when the distance between the antenna pair is zero. Here we should notice that the trail velocity v is unknown so the τ_0 is not equals to τ_0. As I mentioned above, the travel time with different antenna pairs are shown as a hyperbolic curve in CMP dataset which can include strong aliasing when it is not well sampled. If we know the accurate velocity, the hyperbolic can be then flattened to a horizontal reflection by using the time delay acquired by (6.4). Here the trial velocity can be seen as an initial value that is used for accurate velocity estimation. Hence we can use a trial velocity that is estimated within the current survey area when the subsurface velocity does not change dramatically. After the aliasing removal, we applied an interpolation method that can handle the irregular data to reconstruct the CMP dataset [12]. And at the end we do the inverse correction to remove the time shift we acquired by (6.4). Figure 6.4 shows the processing

schedule of the proposed method. Figure 6.4(a) shows a simple simulated CMP dataset that includes a direct coupling and a layer reflection with 0.12 m/ns subsurface velocity at 0.5 m depth. We show the similar configuration to YAKUMO system that there are only eight traces available while the antenna offset reach to two meter. Figure 6.4(b) shows the flattened reflect signals with an inaccurate velocity 0.15 m/ns. As it shows, the reflected signal is not flattened perfectly but goes slightly upward, and the direct coupling is not a hyperbolic curve so it is not flattened correctly. However, as the interpolated result shows, the reflected signal are interpolated correctly because it is still much flattened by the aliasing removal. But the direct coupling cannot be interpolated well because of the aliasing problem we discussed above. Here we should point out that in most cases the direct coupling can be ignored or muted before the velocity analysis, but the direct coupling may overlap to the reflected signal when reflect layer is too shallow.

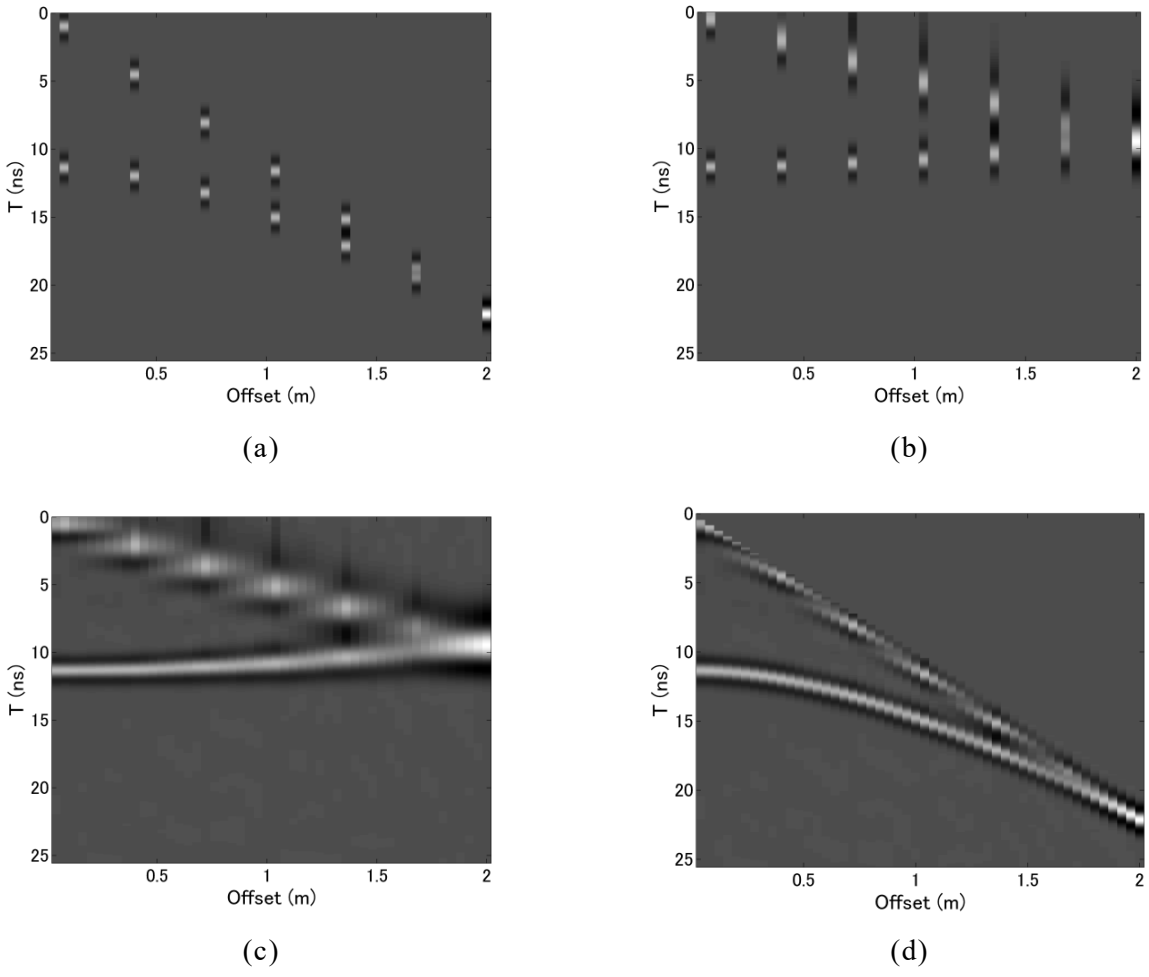

Figure 6.4. The processing schedule of a simulated CMP dataset with the proposed method; (a) Raw data; (b) After the aliasing removal by forward transform; (c) After the interpolation; (d)After the inverse transform.

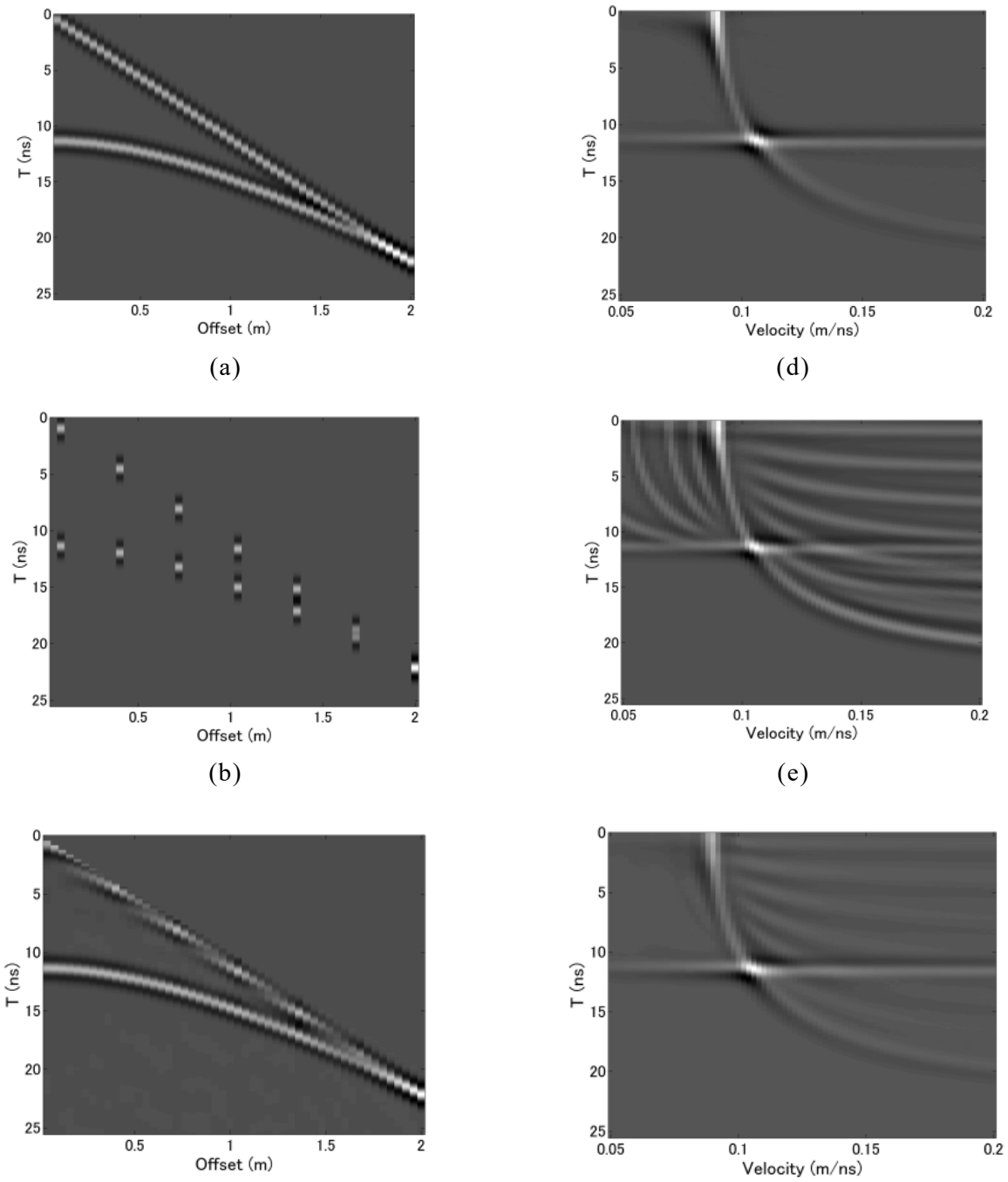

Figure 6.5 The velocity analysis of simulated datasets; (a)(d) original CMP dataset and its velocity spectrum; (b)(e) the CMP dataset after resample with 0.3 m spatial interval and its velocity spectrum; (c)(f) interpolated CMP dataset after the proposed method and its velocity spectrum.

Figure 6.5 shows a velocity analysis example with the coarse simulated data. As we discussed above, the sparse CMP dataset will introduce strong artifacts which will damage the results as it shows in Figure 6.5(e). In this example there is only one reflection so the artifacts are not so strong and we still can distinguish the focused energy well. With the

proposed method, the artifacts in the velocity spectrum are well eliminated. We also tested the method with the real CMP datasets acquired from YAKUMO system, in most cases the velocity can be automatically picked at different depth.

Figure 6.6 shows a vertical slice data acquired with YAKUMO system. It was acquired at a sand dune near the seashore. We can observe multiple layer reflections in this dataset which are caused by the interaction of the wind and the trends at different time periods. Figure 6.7 shows one of the YAKUMO CMP dataset that was acquired within this survey line at eight meter. As I mentioned above this CMP dataset includes several reflect layers and it is more complicated than the simulated case. In Figure 6.7(a) we can find strong artifacts appear at low velocity and most of them are as strong as the focused energy of the hyperbolic curve, which will make the automatic velocity picking become difficult. After the proposed method, these artifacts are well eliminated and the velocity spectrum becomes much clean. The velocity profile can be then generated automatically from the velocity spectrum at different positions. In Figure 6.7(d) the energy are well focused at 6 ns, 10ns and 12 ns, and the result shows that the subsurface velocity is decreasing at each layer. It is also another application of the CMP velocity analysis which we can provide the velocity at each layer directly related to the soil moistures so that the geologist can use this information. If we can acquire this information at every position and then we can generate a velocity profile, it can be used for the initial model for the further processing including migration or tomography. On the other hand, we expect that the velocity profile can also be used to detect a slight velocity change within a survey area when the reflected wave caused by the damaged pavement is hard to identify. These velocity changes may indicate the slight changes of the physical properties which related to our interest.

However, the velocity picking at each position is still not a simple task. Ideally, the slight velocity change or thickness change can be detected directly with the velocity spectrum; when the focused energy shifts in vertical direction, it indicates the thickness changes; while it shifts in horizontal directions, it indicates the velocity changes. Due to the limitation of the velocity analysis, the real value of the velocity is still difficult to pick. As shown in Figure 6.5, the focused energy still cannot be focused into a point even with this ideal simulated dataset. When the dataset is more complicated, the slight changes are even more difficult to pick.

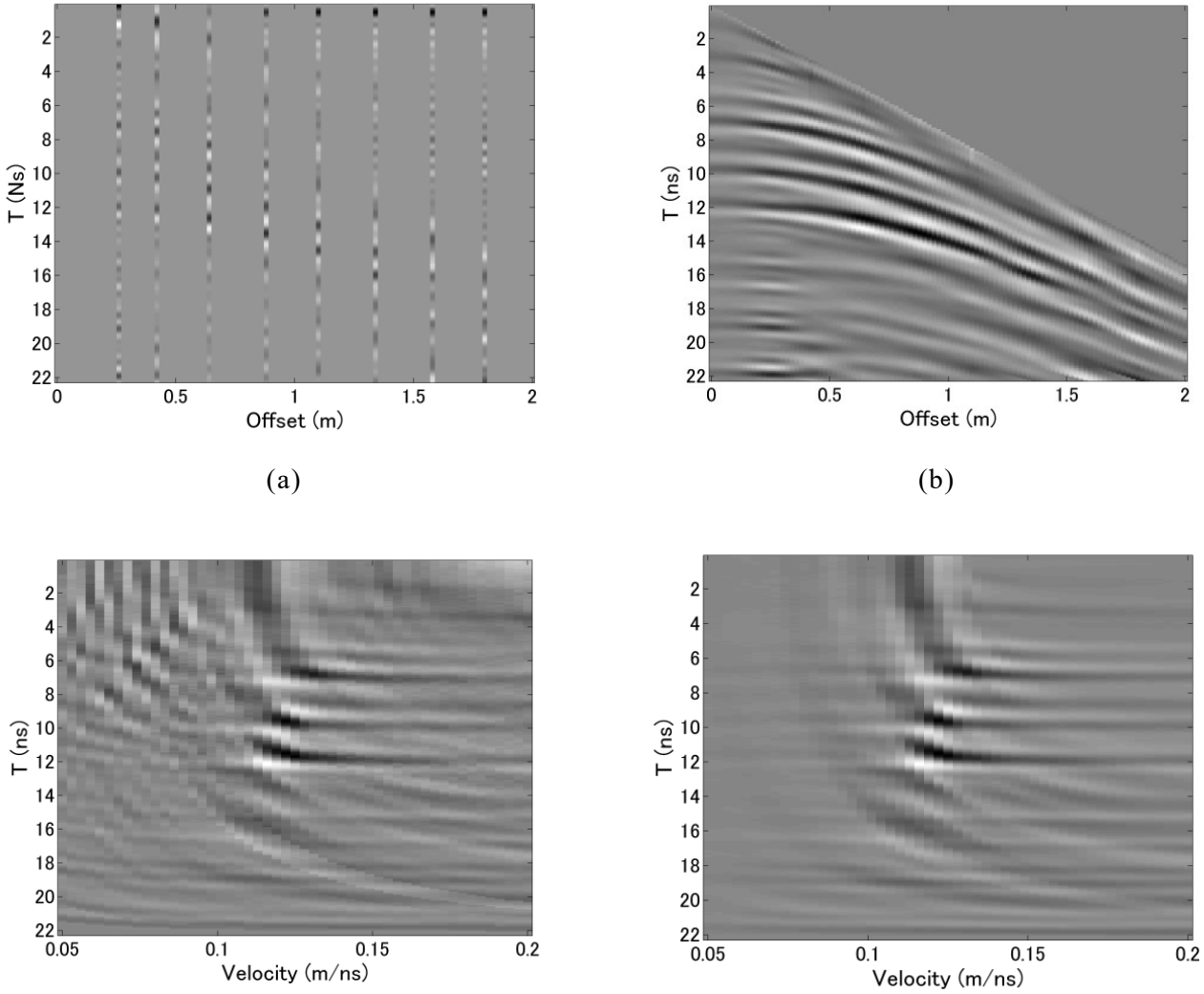

Figure 6.7 Velocity analysis results of CMP dataset acquired by YAKUMO; (a)(c)the original CMP dataset and its velocity spectrum; (b)(d) the processed CMP dataset with proposed method and its velocity spectrum.

6.4 ℓ1 norm regularized CMP velocity analysis for high accuracy velocity estimation

As we described above, velocity analysis is very similar to the SAR processing, while SAR processing transforms signals to the spatial domain and velocity analysis transforms signals to velocity-time-domain. It is shown in previous chapter that such approach can be seen as a linear transformation and expressed in matrix form. The forward modelling can be written in matrix form as

$$d = Gm \tag{6.5}$$

The measured dataset d can be uniquely determined by a forward operator G. The operator G can be generated by using (6.1), and the model m will be the exact velocity spectrum each point corresponding to the reflected layer and the RMS velocity above it.

$$arg\ min\|m\|_1\ s.t.\ \|Gm - d\|_2 < \epsilon \tag{6.6}$$

The problem can be solved with (6.6). Comparing with the problem that we solved in Chapter 4, the only difference is that the operator G is velocity estimation operator instead of SAR processing operator. The general idea of using ℓ1 norm regularized least square problem is already well discussed as well in Chapter 4 and the details of constructing the operator can be referred to [13]. The main aim of this approach is to get a further focused imaging result of the velocity spectrum so that the slight change of the velocity can be distinguished and the focused result is easier for automatic picking.

In Figure 6.8 we show a simple simulation test of the proposed method. Here we should notice that until this chapter we used simple ray tracing for the simulation test, it is because that we are focusing on the imaging algorithm. Our algorithm is designed under the ray tracing theory so the complicated simulation will introduce error that is not belongs to the algorithm. However, for velocity estimation we have to consider it in a more realistic case. We need to evaluate if the velocity estimation algorithm can deal with some real problems that violated the assumptions. For example, the wavelet changes caused by the increasing antenna offset or the attenuation within the medium, and also the semblance problem that we discussed in the end of the section 6.21. Hence we chose FDTD simulation for the velocity estimation examples for the practical evaluation of the proposed algorithms [14].

In this example, the model is very simple that only included a layer reflection and the upper part is 15 cm thick asphalt layer with velocity assumed to be 0.1 m/ns, also we have 1 cm air layer at the top of the model because for real application the antenna may not attached on the surface perfectly. We can find that the proposed method can provide much higher resolution in velocity spectrum. However, we may notice that the estimated velocity is slightly higher than the real value. There are mainly two reasons for this issue, and the first reason is the 1 cm air layer at the top of the model. It can be seen as another layer with higher velocity, since the velocity estimation is estimating the RMS velocity of all the layers beyond the base soil, the air layer will increase the RMS velocity as the result. The second reason is the wavelet change, we may notice from Figure 6.8(b) that the wavelet shape at different antenna offset changes a lot due to the strong attenuation of the medium and the dramatic change of the incident angle. Since the velocity estimation is just evaluation the stacked energy, such phase change will also affect the final result. It is also the main reason why I mentioned that stacking method is better for GPR application but not semblance in seismic velocity analysis application. This problem indicates us that GPR

velocity estimation has some limitation on precise velocity estimation as it pointed out in previous researches. We cannot expect a very precise value of the real velocity of within the subsurface layer, however, we can use the high resolution result to detect the velocity difference at different position. I think these velocity differences may more reliable, and it can be used for inspection applications, more details on this topic will be given in next chapter.

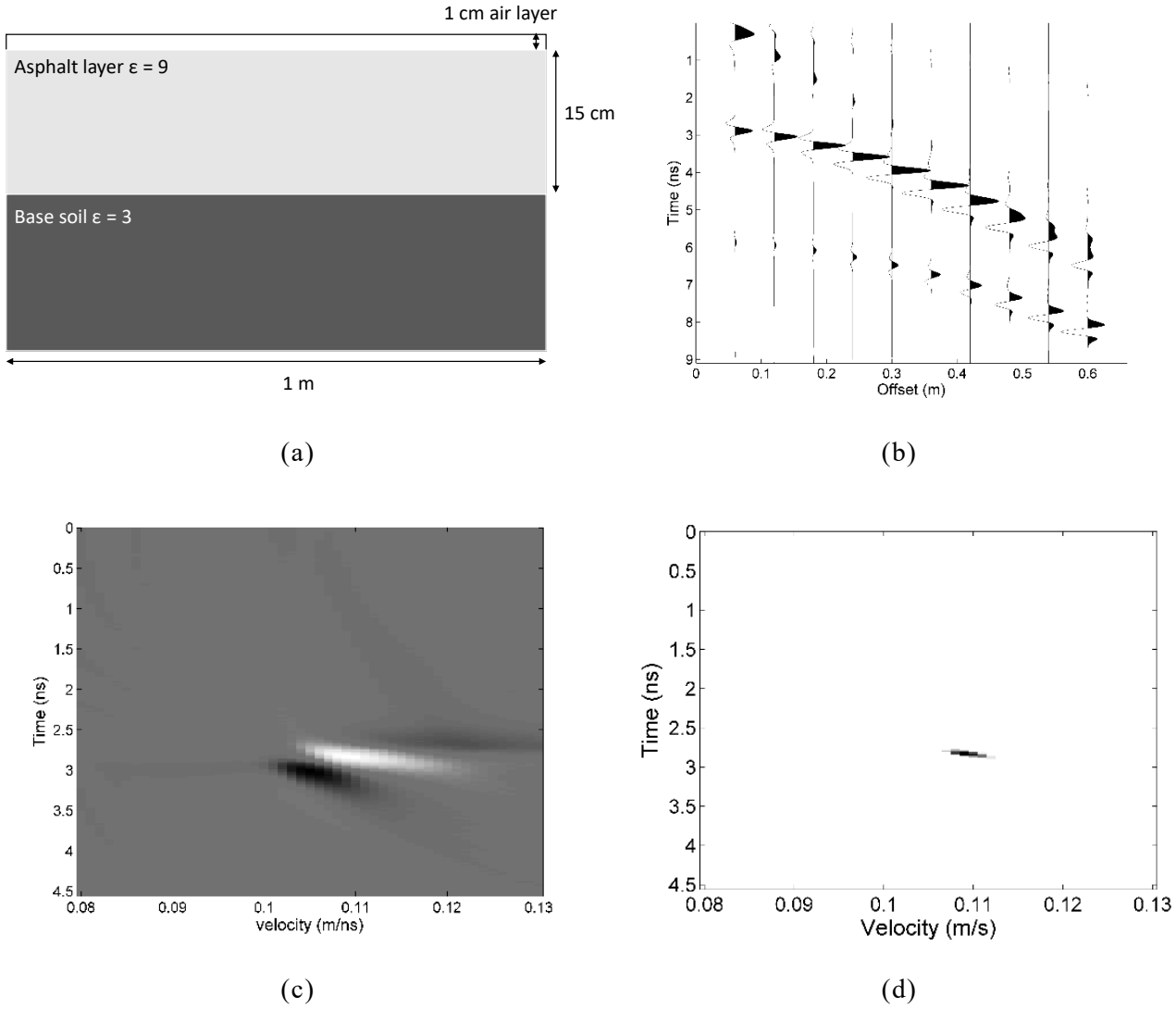

Figure 6.8 Simulated test of the ℓ1 norm regularized velocity estimation method; (a) FDTD model; (b) the simulated CMP dataset in the middle; (c) the velocity spectrum acquired with conventional velocity analysis; (d) the velocity spectrum acquired with the proposed method.

Another problem of using this method is calculation itself, as I mentioned in Chapter 4 we still have to using the iteration algorithm for ℓ1 norm solution. However, for large scale inspection application this problem can be greatly simplified. Since the thickness and the velocity will not change that much, the calculation area can be greatly reduced. For example, in Figure 6.8 we know the reflect layer is at 15 cm and velocity is around 0.11 m/ns. When

we want to detect the slight change, we can reduce the velocity estimation range from 0.08-0.13 m/ns to 0.1 to 0.12 m/ns, and the depth can be also reduced from 0 to 4.5 ns to 2.5 to 3.5 ns. In this case, not only the calculation area can be greatly reduced, but also the noise or other clutters can be reduced. Hence, the parameter for the ℓ1 norm calculation will be easier to define.

6.5 Simultaneous Estimation of Velocity and Thickness of Stratified Material

As I mentioned above, it is possible to estimate the velocity and thickness with the velocity spectrum. A straightforward way is to evaluate the shifts of the focused energy in velocity spectrum to estimate the velocity and thickness changes. For example, if the focused energy from the same reflector shifts in horizontal direction, it indicates the velocity changes; while it shifts in vertical directions, it indicates the thickness changes. However, the resolution of the velocity spectrum is limited by many different factors as I mentioned above.

In order to improve the accuracy of the estimated results, the key issue is to improve the resolution of the signals. For example, if the reflected signal is only a pulse and there is no noise, the energy in velocity spectrum can focused into a point. Hence the slight velocity/thickness changes can be easily detected. However, such ideal case is not exists. Another way is to improve the quality of CMP dataset to enhance the resolution of the velocity spectrum. In previous work we used the interpolation method to improve the quality of the CMP dataset and the artifacts in the velocity spectrum are well suppressed. With that approach can find out some velocity/thickness anomalies automatically. But it is still difficult to quantify the differences and distinguish the velocity and thickness changes simultaneously [4].

Since the accurate travel time of the reflected signal is difficult to be measured accurately, we have to find other ways. The interferometry technique is widely used in SAR applications. Here we can also borrow this idea to measure the accurate time delay differences of two CMP datasets by cross-correlation [15][16] .

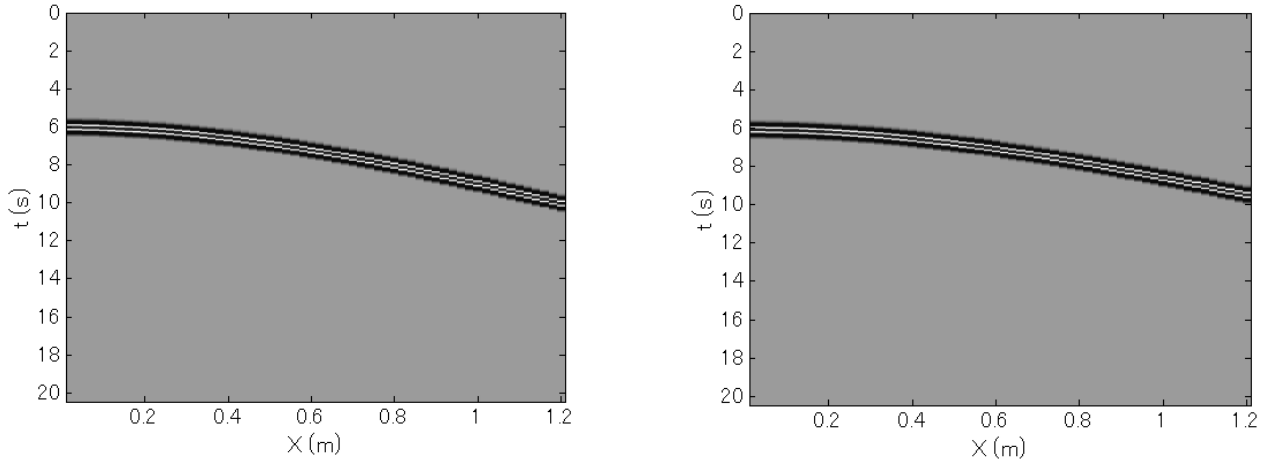

(a) (b)

Figure 6.9 Simulated CMP datasets with only one layer; (a) Base dataset, z=0.35 m, v=0.15 m/ns; (b) Monitor dataset,z=0.37 m, v=0.17 m/ns;

If the time delay can be determined accurately, we can use it to find out the changes on velocity or thickness. With the simple cross-correlation algorithm, we can pick the high accurate time delay information. Figure 6.9 shows a simple simulated dataset that only include one layer reflection. The velocity of the base data is assumed as 0.15 m/ns and the thickness is 0.35 m. While the velocity of the monitor data is assumed as 0.17 m/ns and the thickness is 0.31 m;

As shown in Figure 6.9, the two CMP dataset are very similar. However, with the cross-correlation, we can extract the time delay difference at different offsets as shown in Figure 6.10. We also show the theory results with the known velocity and thickness of monitor data. The measured results agree well with the theory.

After the time delay was acquired, we assume there are slight changes in velocity and the reflector depth.

$$\frac{\Delta z}{z}, \frac{\Delta v}{v} \ll 1 \tag{6.7}$$

With this assumption we can derive the first order differential of the arrival time with (6.8)

$$\Delta\tau(x) = \Delta\left(\frac{1}{v}\sqrt{4z^2 + x^2}\right) = \frac{4z}{v}(\sqrt{4z^2 + x^2})^{-1}\Delta z - \frac{1}{v^2}\sqrt{4z^2 + x^2}\Delta v \tag{6.8}$$

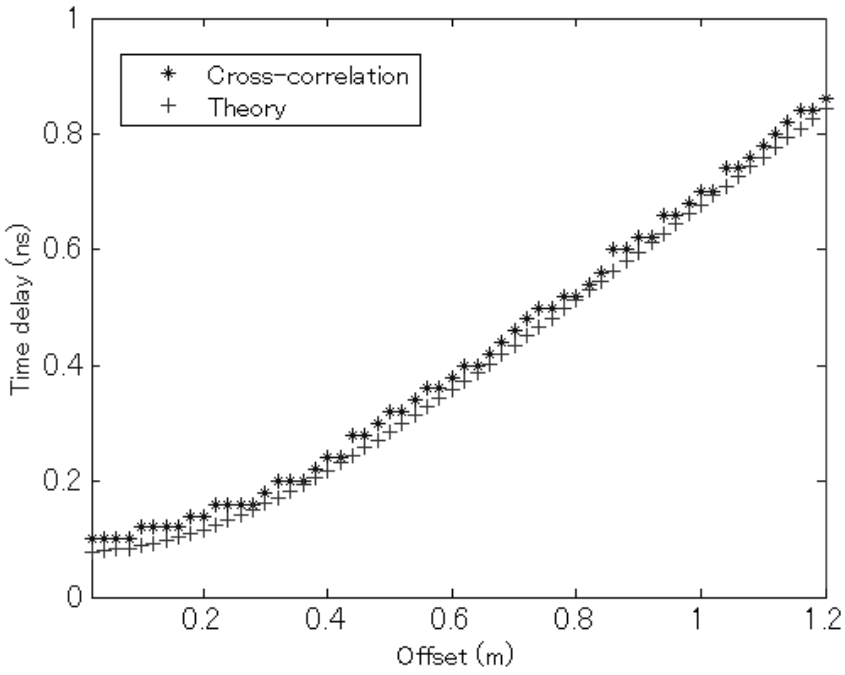

Figure 6.10. The time delays at different offsets;

It indicates that if we have the known velocity v and the reflector depth z at a known point which we define it as the base dataset, we can calculate the slight velocity change dv and thickness change dz with time delays difference $\Delta\tau$ of base dataset and another interested position which we define it as monitoring dataset. In order to solve (6.8) we need at least two different antenna pairs with different offset x, and we can also solve this over determined problem by finding the least square solution with more antenna paris. The accuracy will be better if we chose two offsets that are far away to each other, the details will be discussed in later section. Figure 6.11 shows the estimated velocity and thickness changes with the time delay differences at 0.1 m offset and other offsets. As the result shows, when there are slight changes on velocity and thickness, the value can be estimated accurately by the proposed method. Here we should delight that the base information can be estimated by the velocity spectrum. As I mentioned above, the accurate value of the thickness and velocity maybe difficult to determine. The inaccurate base information will lead some errors to the estimated velocity/thickness changes. As we have tried out, in most cases the error can be ignored because we did not use the higher order in (6.7).

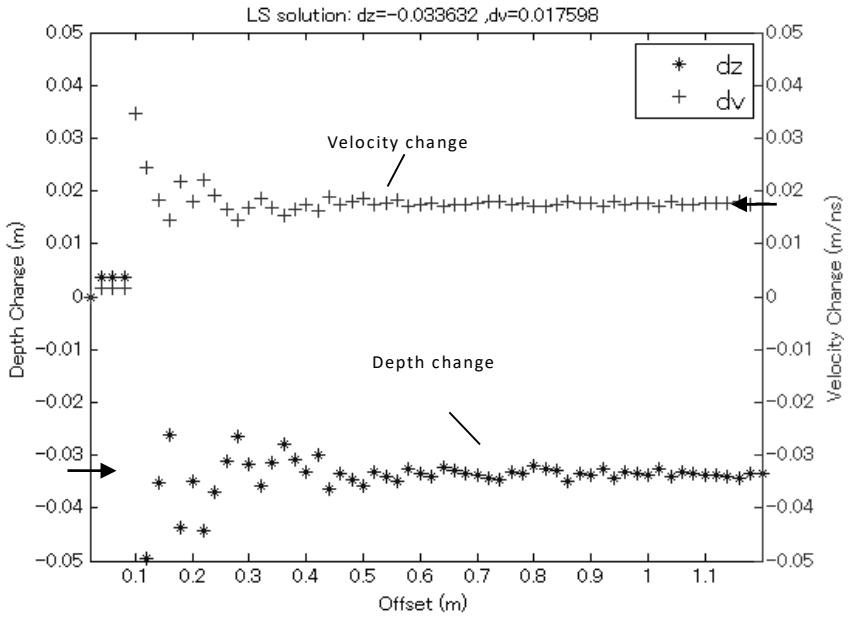

Figure 6.11 Estimated velocity/thickness changes with the proposed method. The arrow indicated the real value of the velocity change 0.018 m/ns and the real value of the thickness change 0.033 m. The least square solution is shown in the title of the figure.

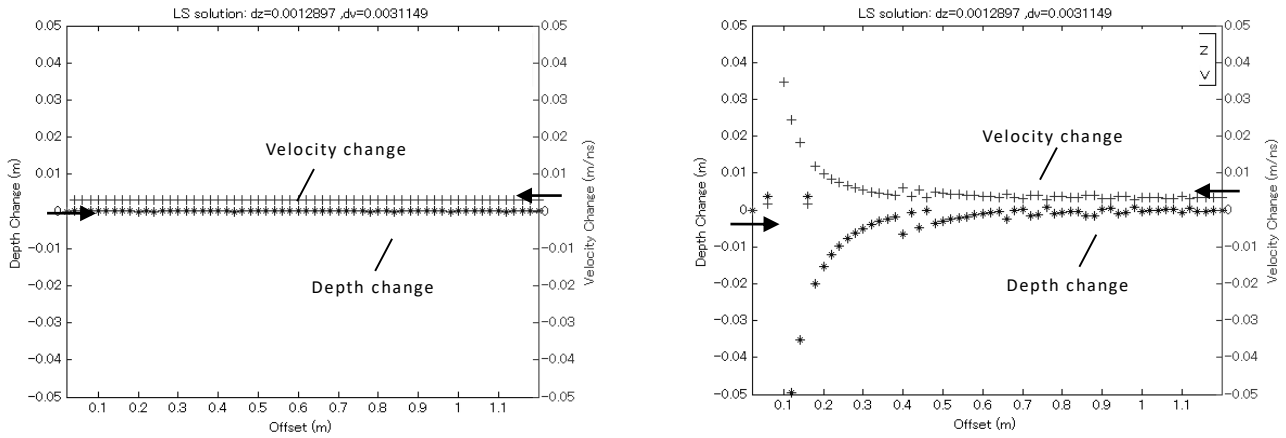

(a) (b)

Fig 6.12 Simulated results with single layer, the velocity changes is 0.003 m/ns that indicated with the arrow, (a) Calculated with the theory time delay; (b) Calculated with the time delay estimated by the cross-correlation.

The proposed method is still not complete now. As it shows in Figure 6.11, we found that the estimated results are not correct when the offset is small. I think it is caused by the

error in time delay estimation. When the offsets are getting smaller, the accuracy of the cross-correlation results will become worse. Fig 6.12(a) shows the results that calculated with the theory time delay calculated by the known parameters. In this case we set 0.003 m/ns velocity changes in monitor data. When the time delays are accurate, we can estimate accurate velocity estimation with each pair of the time delay information. However, if we use the time delays estimated by the cross-correlation in Fig 6.12(b), the estimated results with small offset are incorrect as we expected. I think more advanced cross-correlation algorithm need to be considered.

Another issue that we may concern is the accuracy of the estimated parameters. As I mentioned above, if we want to estimate the true value of the changed Velocity and thickness, the given parameter of the base dataset must be accurate. However, the base information is unknown or inaccurate in most of the cases and we have to deal with this problem. Figure 6.13 shows a simple example when we use inaccurate base information. Here we still use the same parameter as shown in Figure 6.11. The velocity of the base dataset is 0.15 m/ns and thickness is 0.35 m with 0.02 m/ns velocity change together with 0.04 m thickness change. However, here we assume that we get inaccurate base information that the velocity of the base dataset is 0.2 m/ns and the thickness is 0.2 m. As the result, we can still detect the velocity and thickness changes and the error is acceptable. Also I tried the cases with only velocity or thickness is changed and we found in this case even the base information is not accurate. The constant velocity or thickness is always not change. It means that the proposed method has a relatively robust result when the base information is not accurate.

Figure 6.14 show a FDTD simulated dataset includes the CMP datasets on a survey line. It shows more realistic situation that includes some multiple reflections and dispersion effects. In the middle part of this survey line there is a 2 cm thickness change as it indicated in Figure 6.14(a). If we acquired such dataset, we can find that there are some anomalies appear in the middle part as it shows in Figure 6.14(b). However, both the deeper reflection and lower velocity can cause the same results as shown in Figure 6.14(b). After we processed this dataset with the proposed method, we found that the quality of the time delay estimation is not good. The near offset traces show incorrect time delay because of the strong direct couplings. Figure 6.15(a) and 6.15(b) shows the estimated time delay and the estimated thickness/velocity changes and the results are not correct because of the wrong time delay estimations of near offset traces. Here we simply do not use the near offset traces. And then we can get much better estimation results as shown in 6.15(c) and 6.15(d). This is just a simple approach to improve the quality of the cross-correlation results. More advanced methods are still under investigation. This example indicates that the near offset traces are difficult to estimate the correct time delays. So, when use the time delays at two different offsets, we should avoid using the pairs that close to each other. For the YAKUMO system that includes only eight CMP traces, we can estimate 64 different results. In this

case, we need to select the useable pairs of the different offsets.

On the other hand, this method is specific for the one layer structure, but we can apply it to complicated structures by assuming the upper part of a layer reflector is homogeneous. For example, there is always a 5 cm air layer between YAKUMO system and the ground surface and we can just ignore this 5 cm air space and combine its effect together with the near surface medium. It may lead some errors to the values we estimated, but the slight changes on a specific layer still can be determined.

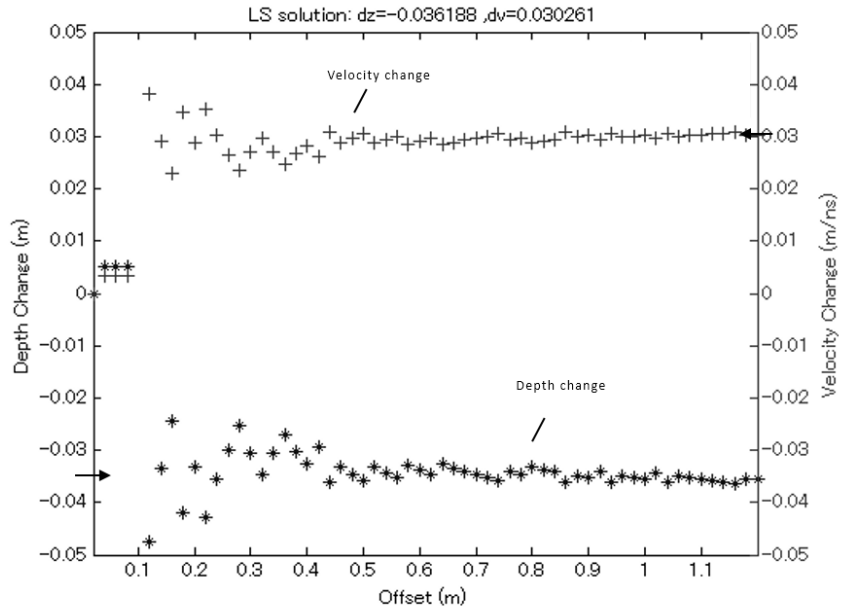

Figure 6.13. Estimated velocity/thickness changes with inaccurate base information.

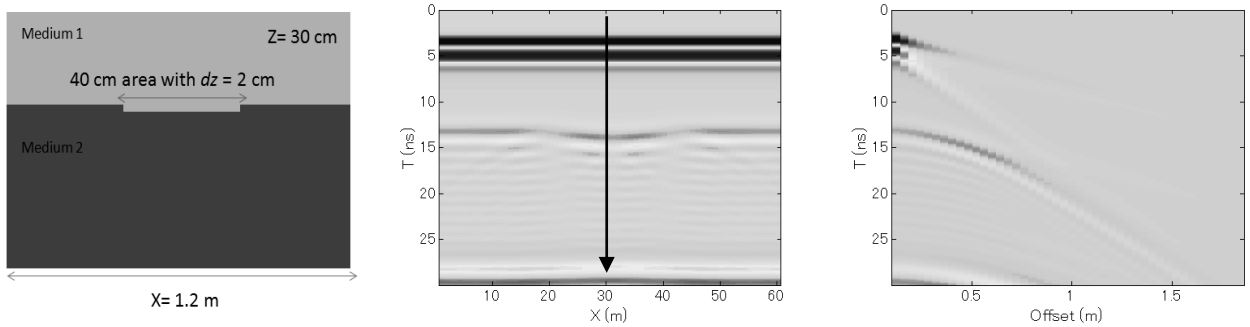

(a) (b) (c)

Figure 6.14. FDTD simulated single layer data and CMP gather. There is a 2 cm thickness change in middle part of the data. (a) Model (b) Vertical slice of the simulated area; (c) Simulated CMP gather in the middle part of the survey line (The arrow in Figure 9(b) indicated the position of the CMP gather).

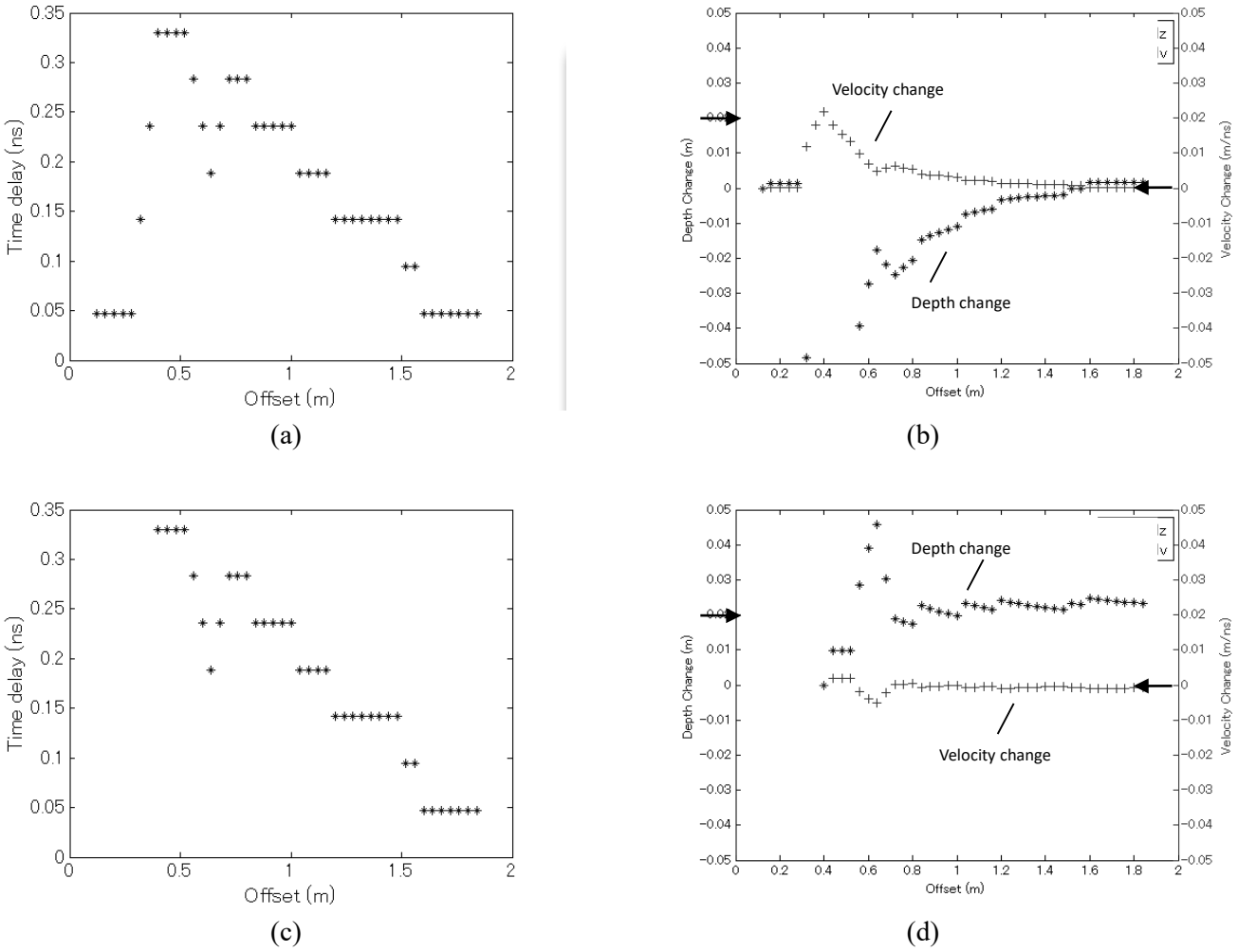

Figure 6.15. Estimated time delay and velocity/thickness changes of the FDTD simulated dataset, there is a 2 cm thickness changes in monitor data. The arrow indicated the 0.02 m thickness change. (a) Estimated time delay with the cross-correlation; (b) Estimated velocity/thickness changes; (c) Estimated time delay without near offset traces; (d) Estimated velocity/thickness changes without near offset traces.

6.6 Summary

In this chapter I discussed about another topic of using the sparse array radar system. It is demonstrated that we can arrange the sparse array system for CMP data acquisition instead of using the bistatic radar system. And the electromagnetic wave propagation velocity within the layer mediums can be estimated with CMP dataset. Also I pointed out that the velocity estimation with the CMP dataset is very similar to the SAR processing that I have discussed in previous chapters. Hence the artifacts may introduced to the velocity estimation result and make it difficult to pick the correct velocity of a certain reflect layer. In this case, I introduced three different ways to improve the velocity estimation result acquired with limited antenna elements.

The interpolation of the CMP dataset is the most straightforward approach. Comparing with the monostatic radar profile with unknown reflection, the CMP dataset is easier to be interpolated from the imaging processing point of view. I demonstrated that we can flatten the reflected signal with the estimated velocity to improve the interpolation result. In most of the cases we can reconstruct the CMP dataset with coarse sampled CMP data that far beyond the Nyquist sampling criterion has defined.

The ℓ1 norm regularized velocity estimation method can be achieved due to the similarity of velocity estimation processing and SAR processing. It can greatly improve the resolution of the velocity estimation result. Comparing to its application on SAR imaging, the required calculation area is much smaller since the subsurface velocity usually only change in a relatively small range, hence the iterative algorithm can also done fast. However here I should delight that although the velocity estimation result can be focused, due to the effect of the wavelet we cannot confirm the focused velocity is just the real velocity value. It is better to apply this approach for slight velocity change detection.

The last method is a practical method that can be done with only few antenna elements. It can estimate the slight velocity/thickness change simultaneously. However the limitation of this method is much tighter, it can only be applied to single layer reflection, or it can be done when there is no clear reflection from other reflection layers. And these changes should be relatively small. The key point is to detect the time delay of two different CMP dataset, however, for the real dataset the reflected waveform may different when the medium is significantly different and the phase center of a certain waveform maybe will changed. I think the phase center of the waveform still need to be further analyzed in order to reach higher accuracy for the velocity estimation. It is a practical way to distinguish the distortion of the reflected signal from a layer reflection and I expect that this method can be applied for pavement inspection applications.

6.7 Reference

[1] D. Goodman, "Ground-penetrating radar simulation in engineering and archaeology," Geophysics, vol. 59, pp. 224-232, 1994.

[2] D. J. Daniels, "A review of GPR for landmine detection," Sensing and Imaging: An International Journal, vol. 7, pp. 90-123, 2006.

[3] R. J. Yelf, "Application of Ground Penetrating Radar to Civil and Geotechnical Engineering," Electromagnetic Phenomena, vol. 7, p. 18, 2007.

[4] O. Yilmaz, “velocity analysis and Statics Corrections,” in O. Yilmaz, Seismic Data Processing, Tulsa, Society of Exploration Geophysicists, 1987.

[5] H. Liu, X. Xie, and M. Sato, "Accurate Thickness Estimation of a Backfill Grouting Layer behind Shield Tunnel Lining by CMP Measurement using GPR," in 14th International Conference on Ground

Penetrating Radar, Shanghai, China, 2012, pp. 142-147.

[6] Q. Lu and M. Sato, “Estimation of Hydraulic Property of an Unconfined Aquifer by GPR,” Sens. Imaging An Int. J., vol. 8, no. 2, pp. 83–99, Sep. 2007.

[7] Li Yi, Kazunori Takahashi, and Motoyuki Sato, “Large scale subsurface velocity estimation with array GPR system YAKUMO,” accepted by the radio science bulletin.

[8] Li Yi, Kazunori Takahashi, and Motoyuki Sato, “Application of ℓ1 norm approach to data acquired by the array GPR Yakumo”, in proc. the 10th European Conference on Antennas and Propagation (EUCAP2016), 10 - 15 April, Davos, Switzerland, 2016.

[9] Li Yi, Kazunori Takahashi, and Motoyuki Sato,” Simultaneous Estimation of Velocity and Thickness of Stratified Material with Array GPR System YAKUMO”, IEICE Technical Report, 2015, pp. 19-24.

[10] S. Kuroda, H. Jang, and H. Kim, "Time-lapse borehole radar monitoring of an infiltration experiment in the vadose zone," Journal of Applied Geophysics, vol. 67, pp. 361-366, 2009.

[11] M. Sato "Array GPR “Yakumo” and its application to archaeological survey and environmental studies," In Proc. of General Assembly and Scientific Symposium (URSI GASS), Beijing, China, pp.1-2, Aug 2014.

[12] Li Yi, Kazunori Takahashi, and Motoyuki Sato, “A Fast Iterative Interpolation Method in f-k Domain for 3-D Irregularly Sampled GPR Data,” IEEE Journal of Selected Topics in Applied Earth Observations and Remote Sensing, Vol.9, no.1, pp. 9-17,January 2016.

[13] W. A. Burnett, “A reversible transform for seismic data processing,” CREWES, Calgary, Canada, vol. 20, 1-17, 2008.

[14] T. Bergmann, J. O. Robertsson, K. Holliger, "Finite-difference modeling of electromagnetic wave propagation in dispersive and attenuating media", Geophysics, vol. 63, no. 3, pp. 856-867, 1998.

[15] Z. Peng, Q. Sun, "The real-time monitoring tool states based on cross-correlation detection", Proc. Int. CMSP, vol. 1, pp. 232-236, 2011-May-14–15.

[16] Consolatina Liguori, Vincenzo Paciello, Alfredo Paolillo, Antonio Pietrosanto, "Real-Time Detection of Low-Frequency Components", Instrumentation and Measurement IEEE Transactions on, vol. 62, pp. 1118-1129, 2013, ISSN 0018-9456.

Chapter 7 Case study: applications of array GPR system

7.1 Introduction

In this chapter I will mainly focus on the application of the array GPR system YAKUMO that I have already mentioned in Chapter 6. Currently there are several groups are investigating the array type GPR system for the engineering applications or archaeological applications. [1] [2] [3]. Comparing with the other system, one of the main advantage of our YAKUMO system is the fast data acquisition of the multistatic dataset. We can acquire the 64 channels dataset in real-time while moving the system along the survey line. As I have already discussed in Chapter 2 that the multistatic data coverage has much advantages than monostatic for sparse array imaging. An archeological field experiment with YAKUMO system will be introduced in later section. The performance of the YAKUMO system for 3-dimensional GPR data acquisition will be demonstrated.

On the other hand, In our previous research work for the large scale subsurface velocity estimation, the data acquisition is always a problem for its long term operation which limited the quantity of the information that we can acquired in each field experiment [4][5]. In this case, with YAKUMO system we can fully use the special configuration for the continuous CMP data acquisition. The CMP dataset along a survey line can be acquired continuously and these information can be used to generate a velocity profile which can provide much more information [6]. Although the CMP dataset is coarse and it may cause some problems, we can overcome these problems with the methods that I have introduced in Chapter 6.

Besides of the archeological application, GPR system is also widely used for engineering application such as pavement inspection. There are already many researches on this topic [7][8][9]. In previous researches, most of the inspection processing are analyzing the reflected signal form the damaged part and focusing on relatively large target such as the holes generated in meters depth. However, one of our project request us to investigate a way to inspect the pavement of the airport taxi-way which is very different from the previous cases. The targets are the thin cracks with millimeter thickness that distributed within the 15 cm thick asphalt layer just above the surface. It is already proved to be a difficult task if we want to use the reflected signal to detect these thin cracks in previous researches [10] [11][12]. Here I tried to use the slight velocity changes to detect these thin cracks with velocity estimation techniques. With the high-resolution velocity estimation obtained by $\ell 1$ norm regularized least square solution, I show the possibility of detecting the slight velocity changes. Both simulation and field experiment are used to analyze the proposed method.

7.2 Array GPR system yakumo

7.21 Array GPR system YAKUMO

Yakumo is a SFCW multistatic GPR system, it operated from 50MHz to 1.5GHz. It has 8 transmitting and 8 receiving antennas, having the swath width of 2m. The main purpose of YAKUMO system is for large scale GPR surveys, because we can get totally 64 channels at each position that covers the 2 m width. For large scale survey we can operate the system on a single survey line and then we can acquire the 3-dimensional data cube with SAR processing. The sampling interval along the survey direction is 1 cm which satisfied the sampling criterion well, but the spatial interval along the perpendicular direction is much coarse if we think about the mid-point assumption that I mentioned in Chapter 2. The size of each antenna element is 24 cm so we can assume that there are 16 traces that have 12 cm spatial interval. It means that there may be some imaging problems happen with conventional SAR processing and I will discuss more about it in later sections. Currently we have operated our system for the survey of tsunami victims in sand beach in East Japan, and archaeological surveys [13]. More recently, we also use it for nondestructive inspection of airport taxi-way pavement.

Another advantage of YAKUMO system is that it can be used for estimating the subsurface velocity of EM wave propagation. One of the main difference of the GPR system with the sparse array system I mentioned in previous Chapter is that the velocity of the EM wave is not constant anymore. In order to do the imaging processing we need to know the subsurface velocity distribution to prevent the wrong imaging result. Also, the subsurface velocity is also an important information for environmental studies [14].

The antenna distribution is shown in Figure 7.2. Here we should notice that the original idea of the YAKUMO array distribution is different from the sparse array design that we discussed in previous chapters. If we assume the middle point of each transmitting and receiving antenna pair as the monostatic transceiver, we can find that there are only 16 virtue transceiver along the 2 m width and each of the position is overlapped several times. There are mainly two purpose of using the overlapping virtue transceiver: the first reason comes from seismic exploration that the subsurface environment is much complicated than it in air. There are many scatterers such as small stones, wooden pieces, or sudden change of the dielectric constant due to the ground water so the imaging result will suffer from these unwanted scatters. Although the virtue transceiver is overlapped, each of the antenna pair has different observation angle and they are actually “looking” different scatterers except the main target. Hence by stacking them together it is possible to preserve the unwanted scatterers; another reason is that by using this configuration, we can get CMP dataset at each position for the continuous velocity estimation.

Figure 7.1 Operation of array GPR system YAKUMO

7.22 Effect of the Antenna polarization

Yakumo is equipped with bowtie antennas so the radiation pattern of the antenna element is strongly related to the antenna polarization direction [15]. We arranged the antenna orientation in two ways as shown in Figure 7.2. The antenna polarization in the antenna arrangement #1, shown in Figure 7.2 (a) is parallel to the direction of the survey line. In this case, antenna coupling are strong, even for the antenna pairs which located at the other end of the array. It means that with such antenna configuration the far-offset antenna pair can work well so it has more advantages especially for the CMP data acquisition. However, the near-offset antenna pairs have weak coupling and their vertical profiles may have poor performance. On the other and, in the antenna arrangement #2 shown in Figure 7.2 (b), antenna coupling is strong only among nearby antenna pairs, but relatively weak for a pair at long antenna offset. And vice versa, the near-offset vertical profile can have much better performance.

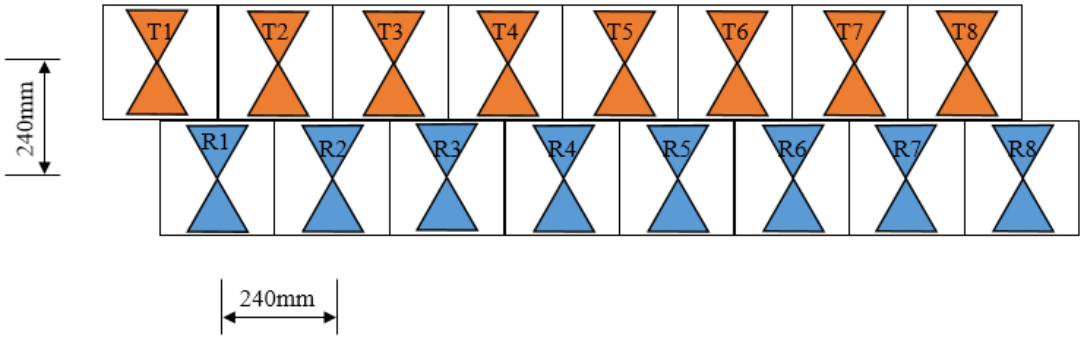

(a)

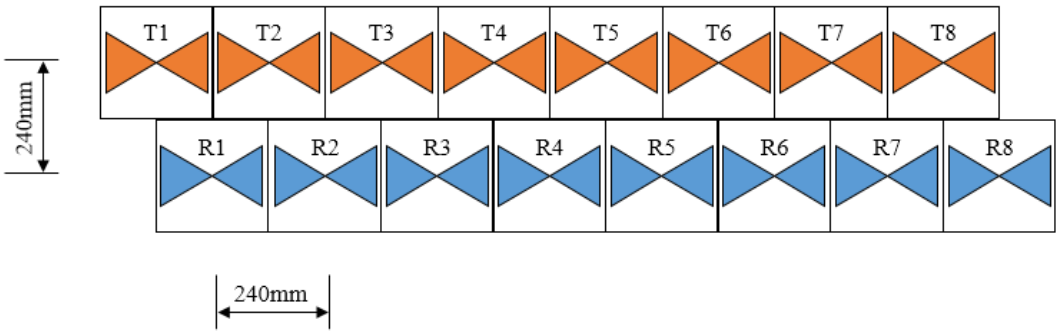

(b)

Figure 7.2 Antenna configuration of YAKUMO system, (a) antenna arrangement #1; (b) antenna arrangement #2.

We also did experiment before/after rotating the antenna at the same location. In Figure 7.3 we show a vertical profile that acquired in same location with different antenna pairs. We compared three different pairs as T4 to R4, T3 to R5 and T2 to R6. They correspond to near, middle and far offset antenna pairs. As we described in the beginning, antenna arrangement #1 have better performance than #2 with far offset. However, if we only compare the near offset profiles with Figure 7.3(a) and Figure 7.3(d) we can find that antenna arrangement #2 has better performance and the details can be seen more clearly.

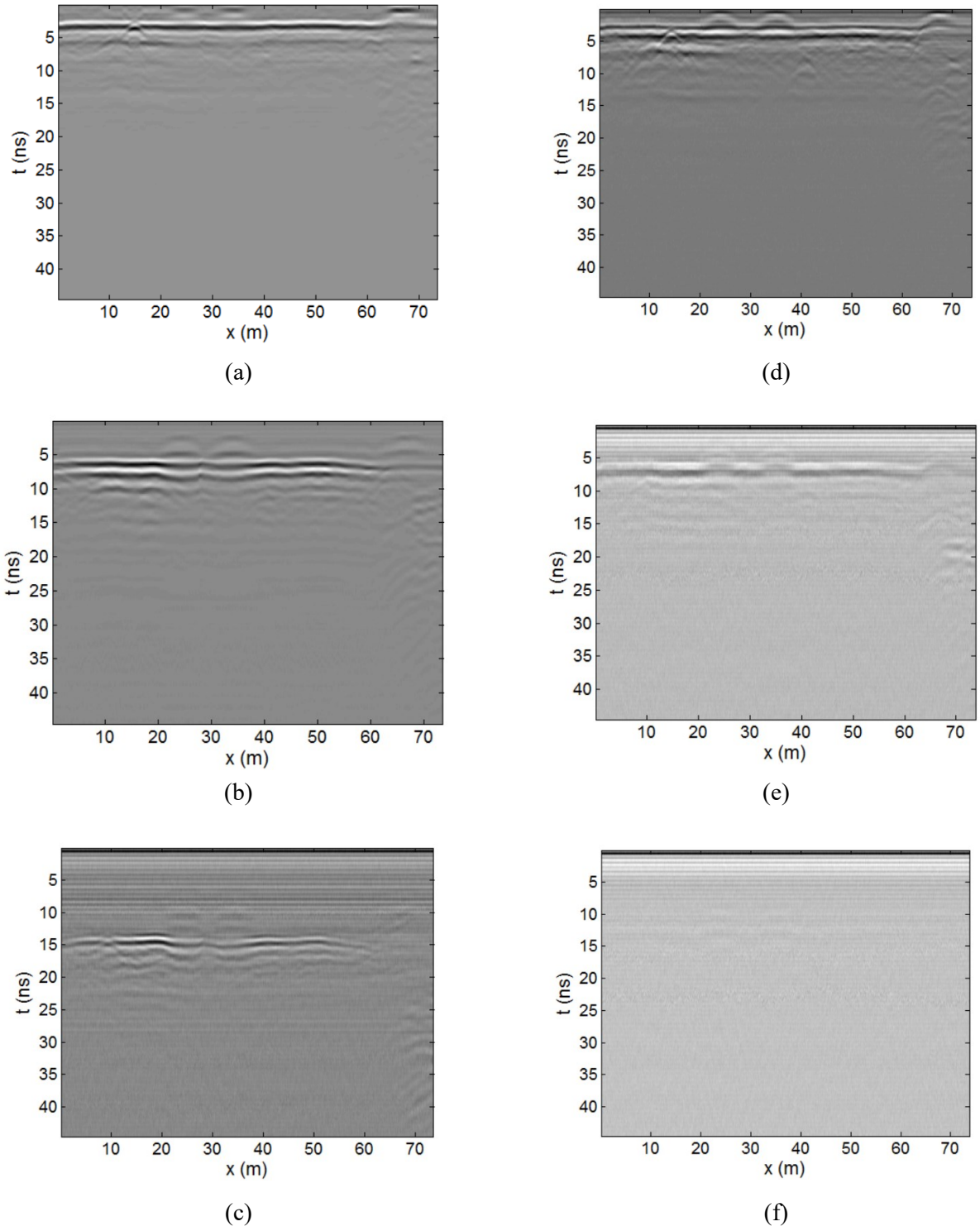

Figure 7.3 Comparison of the antenna arrangement #1 and #2 with different antenna offset, (a)-(c) are acquired with antenna arrangement #1 and (d)-(f) are acquired with antenna arrangement #2; (a)(d) are acquired with nearest antenna offset; (b)(e) are acquired with medium antenna offset; (c)(f) are acquired with far antenna offset.

In Figure 7.4 we compared the CMP dataset with both antenna configuration at the middle position of the profile that we show in Figure 7.3. Also as we predicted, antenna arrangement #1 has better performance for CMP dataset because the reflected signal still can be seen with the far offset antennas, which means we can have higher resolution in velocity spectrum. Also we may notice that the wavelet shape is also changed due to the change of the polarization direction. This is also a problem that affect the accuracy of the velocity estimation as we discussed in Chapter 6. By comparing this two cases, we may notice that there is a balance of the current YAKUMO system, when we want to have better velocity profile with near offset antennas, we will lose affective observation length in CMP dataset. In order to solve this problem, we have to improve from the hardware design. Now we are considering to use cross-bowtie antenna or change part of the antenna orientation to optimize both vertical profile and the CMP dataset.

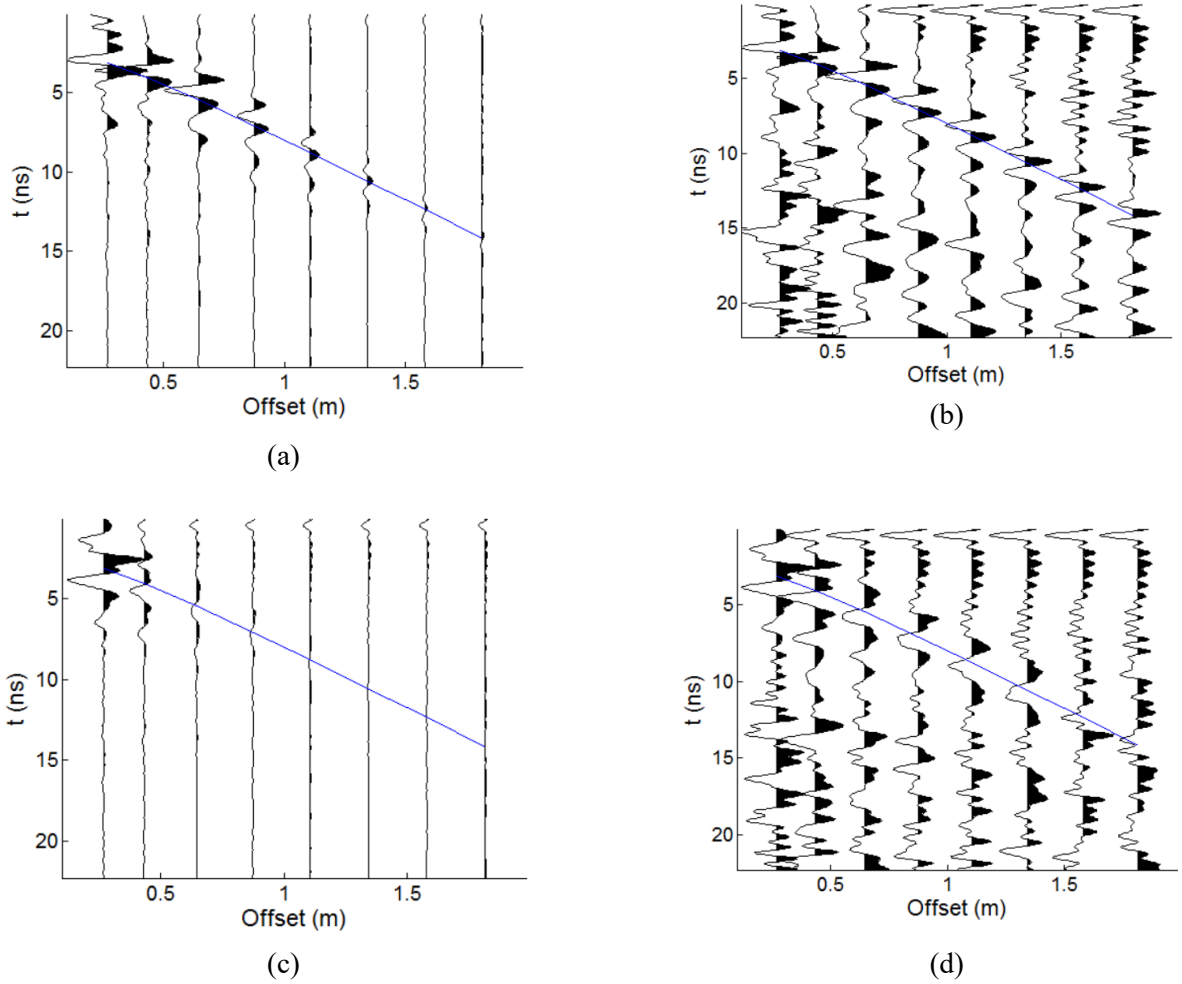

Figure 7.4 CMP dataset with two antenna arrangements, (a)(b) antenna arrangement #1 before/after gain and trace balance; (c)(d) antenna arrangement #2 before/after gain and trace balance;

7.23 An example of archaeological survey at Kunohe

(a) (b)

Figure 7.5 Experimental site at Kunohe, (a) sketch map of survey area; (b) geometry of experimental site.

As we introduced in the beginning, one of the main purpose of developing YAKUMO system is large scale archeological survey. In this section we will introduce a field experiment to demonstrate the performance of YAKUMO system.

The site is located in Kunohe district, Iwate prefecture of Japan. There is a historical remaining of the Kunohe castle that already destroyed hundred years ago. And the local government want to find some remained structures that may located at few meter depth within this area. The indicated survey area is about 50 m by 35 m as we marked in Figure 7.5(a). It is a huge survey area and can be extremely time consuming to acquire the 3-dimensional data with the conventional monostatic GPR system since each survey line should be acquired very dense. However, we can acquire a 2 meter wide 3-diemensional data cube with YAKUMO system by a single survey line. It can greatly improve the data acquisition time and we took only two hours to acquire the whole dataset that covered this area.

In Figure 7.6 we show two vertical slices at around 6 m and 12 m in Y- direction. The data is processed with gain function hence we can still see the reflected signals at 2 meter. We find it is very difficult to intemperate this area with only vertical slice because there are too much clutters that comes from small stones and they stacked with each other and the subsurface layers. In general, we can see several tilted boundary reflectors that goes up to the X- direction.

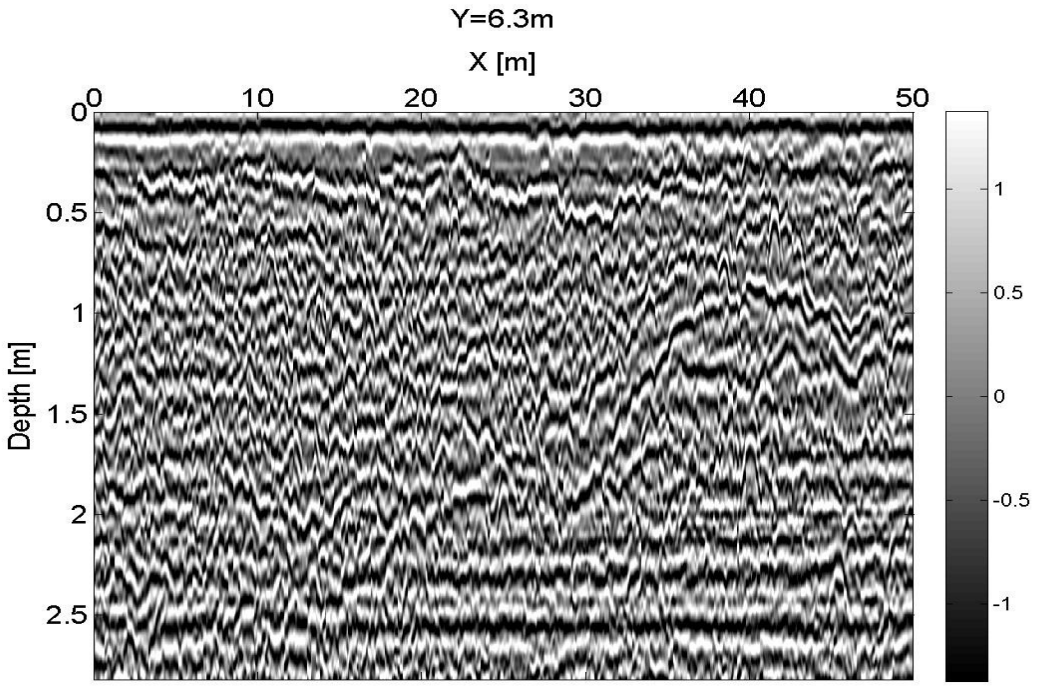

(a)

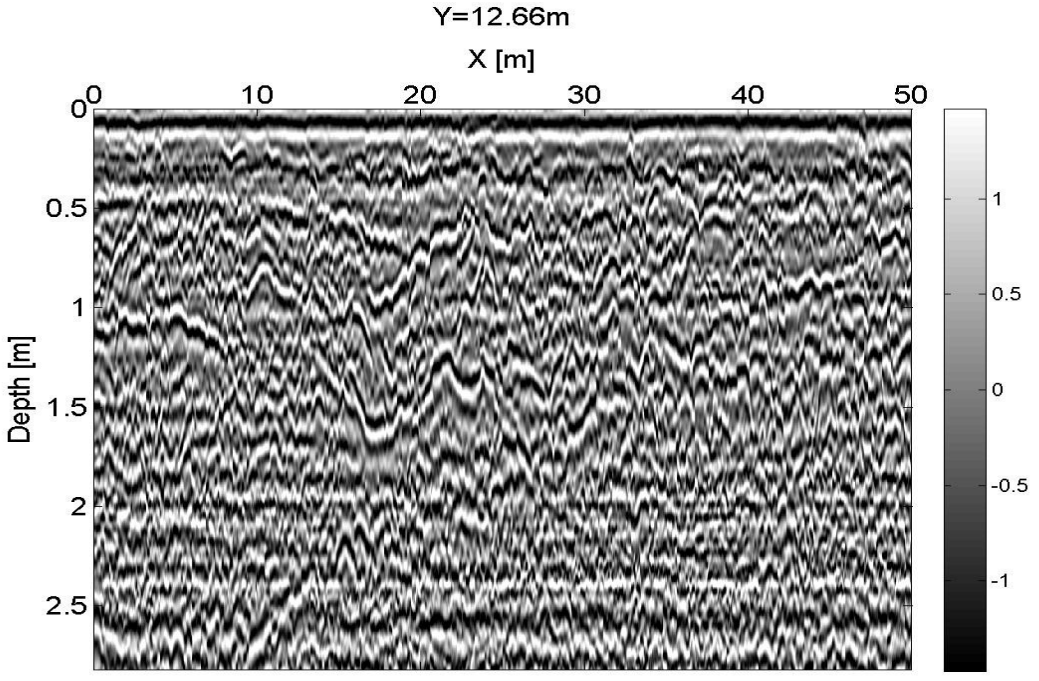

(b)

Figure 7.6 Vertical profiles at x- direction (survey direction); (a) Y=6.3 m; (b) Y= 12.66 m.

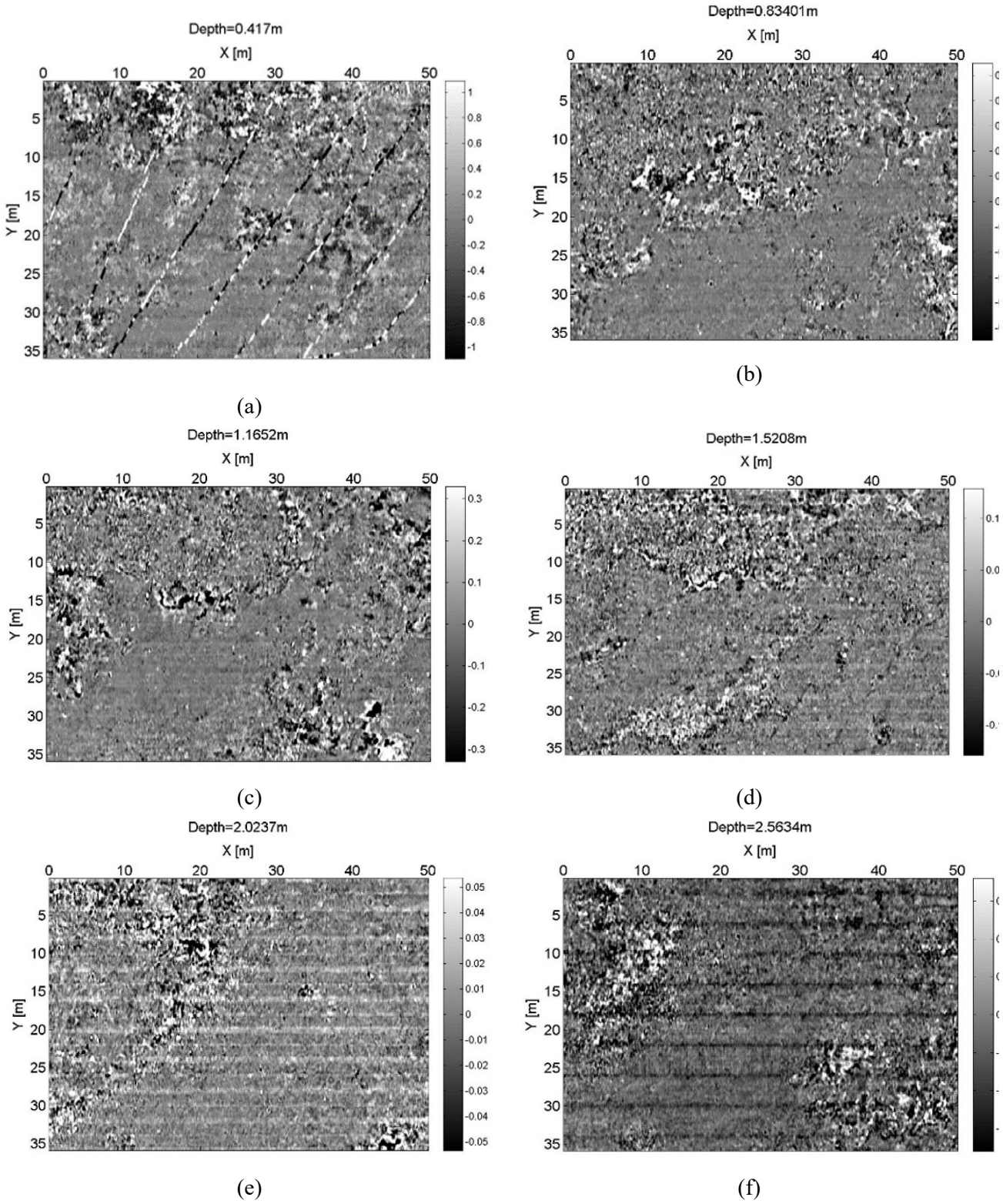

Figure 7.7 The depth slice of the survey site at different depth, the velocity is estimated as 0.9 m/ns; (a) depth slice at 0.41 m; (b) depth slice at 0.83 m; (c) depth slice at 1.16 m; (d) depth slice at 1.52 m; (e) depth slice at 2.02 m; (f) depth slice at 2.56 m.

In Figure 7.7 we show the horizontal slices at different depth. In Figure 7.7(a) we can see many linear structures in shallow depth and we found that these are the abandoned wires buried in recent years. Then we can see some distributed shape in Figure 7.7(b) and (c) that is located around 1 m depth. I think it maybe the old layer structure that indicates the previous geometry of this area. And this layer can be also seen clearly in vertical slices that are shown in Figure 7.6. From 1 meter depth to 2.5 meter, we can always observe some reflections from around the right-bottom of the imaging area. I think these reflections maybe caused by larger stone structures which can be the target that we want to find out. Later the archaeologists also mentioned that the remains of the old city can be located near that area. Currently the further investigation of this area is still undergoing.

We also applied the SAR processing technique with this dataset however we find the processed result lost many detail information and the performance is not that good. It is a common problem of applying the SAR technique to the GPR dataset especially for the complicated reflections. While in some special case SAR processing give better results as we introduced in [16] [17]. Archaeological survey is a special application of radar technique and it require experience, sometimes we cannot simply apply all the processing techniques to the dataset for the sake of losing important information.

7.3 Pavement inspection application for airport taxi-way with YAKUMO system

7.31 Pavement inspection at near-surface

As I mentioned in the beginning of this chapter, one of our goal is to apply the velocity estimation technique for airport taxi-way's pavement inspection. In this section we will further discuss on how we can apply the velocity technique for pavement inspection.

Pavements of airport taxi way usually consists of a few layers. The asphalt layer on the top of the pavement is about 15 cm and the health condition of this layer is our main interest. One of the problems is delamination that is caused by water intruded from surface cracks due to the daily use which expand the space between layers. By temperature and/or pressure changes, the space between layers would be further expanded. When cracks appear in the asphalt layer, the most straightforward way to detect them is to observe reflected signals from the cracks. The reflected signals from the crack are directly related to the pulse-width of the GPR system. The relation between the amplitude of the reflected signal and the crack aperture or antenna band-width are shown in [18]. It shows that when aperture is less than 1 cm, it is very difficult to see the reflection directly with about 1 GHz center frequency. When a higher frequency is used, reflected signals from other scatterers can also be observed and it is difficult to determine the source of the reflected signals. Since the asphalt layer is always a constant layer structure and has strong homogeneity, we may also use some other parameters such as the RMS

velocity to detect the partially damaged pavement. For example, if the pavement is partially damaged, there may be some cracks or change of the density and the permittivity of this part of the asphalt layer may also be different to the healthy part. If we can detect these slight changes in RMS velocity by the CMP analysis, this information can be used as another parameter to evaluate the pavement.

In the case of pavement inspection, the reflector is very shallow. So the cracks within the pavement and the distance from antenna to the surface are both significant issues to the estimated velocity. For example, if there is a 1 cm gap between antenna and the surface, it can be seen that there is another air layer since it is thick enough compared to the 15 cm thick asphalt. From (6.3) we can also derive another form for this case as it shown in (7.1), here d is total thickness of asphalt layer and s is the crack aperture. We can calculate that with 1 cm air layer the RMS velocity of the asphalt layer increases about 0.05 m/ns. Also from this equation we can find that the RMS velocity of the asphalt layer is only related to the total thickness of the air layer. And when there are several cracks exist at different depth, the RMS velocity will not change. It indicates the possibility of the crack detection with the velocity change of the asphalt layer.

$$v_{rms} = \sqrt{\frac{v_1(d-s)+v_2 s}{\frac{d-s}{v_1}+\frac{s}{v_2}}} \tag{7.1}$$

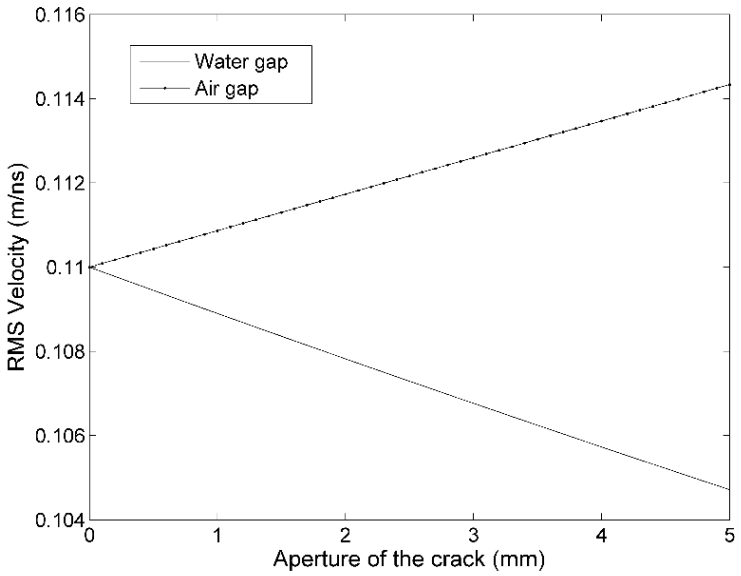

Figure 7.8 aperture of the crack with the RMS velocity with water/air filled inside.

As we calculated from the equation (6.7), the relation between the crack thickness and the RMS velocity of asphalt layers are shown in Figure 7.8 with the asphalt velocity assumed to be 0.11 m/ns. In both cases that the space filled with air and water, it shows the nearly linear relation between the delaminated space and the RMS velocity.

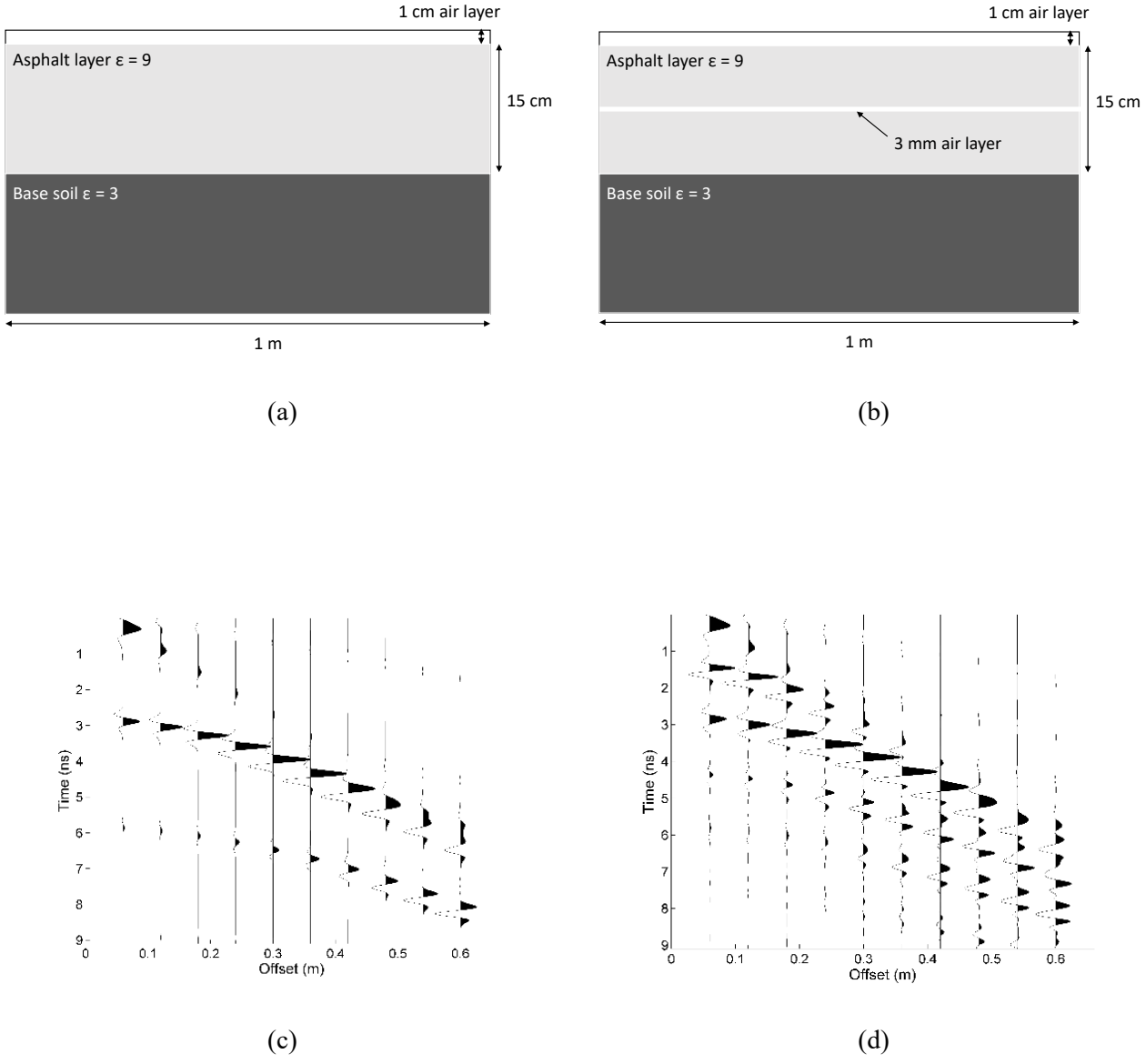

Figure 7.9 Simulated CMP datasets with/without crack filled with air; (a) model without air layer (b) model with 3 mm air layer within the asphalt layer; (c) Simulated CMP dataset of (a); (d) Simulated CMP dataset of (b).

Figure 7.9 shows the FDTD simulated CMP dataset of the asphalt layer with/without the crack. The thickness of the asphalt layer is assumed to be 0.15 m, and the velocity is 0.1 m/ns. The wavelet is 1.5 GHz Ricker wavelet and the pulse width is about 1 ns. The antenna is set 1 cm above the surface. We

should notice that due to this 1 cm air layer, the estimated RMS velocity become higher than the real value. Hence we should get about 0.11 m/ns estimated RMS velocity as we can calculate with (4). It is also pointed in (1) that the far-offset traces are very sensitive to the slight change of the velocity, but they also suffer from the attenuation during the wave propagation. The pulse width become wider when the antenna offset is large so the far-offset trace may introduce error. We can observe such phenomenon with Figure 7.9(c) and (d). For real application we may need some processing such as gain or trace balance to enhance the far-offset trace but please notice that they still include error for velocity analysis.

The air filled crack is located in the middle of the asphalt layer which is at about 10 cm depth from the surface and the aperture is 3 mm. In this simple simulation we can see the multiple reflections with small antenna offset as it is shown in Figure 7.9, but we usually cannot see it in the real dataset because the crack may not distributed totally flat with few millimeter aperture. This is also the reason why we mainly focus on analysis the reflection from the bottom layer of the asphalt. Due to the incident angle change the reflection from the crack reduced quickly with the increased antenna offset as it is shown in Figure 7.9(b). It reminds us that we should use small antenna offset to receive the reflected signal from the near surface cracks; however, due to the limited size of the antenna element the received signal can be very weak. For our YAKUMO system case, the antenna element is about 24 by 24 cm, which means the minimum antenna offset is already 24 cm, comparing with the simulated result in Figure 7.9(b), it is predictable that the reflected signal from the crack is very difficult to be observed.

Figure 7.10 shows the results with the conventional velocity analysis method and the proposed method. As we introduced before, the proposed method can greatly increase the resolution of the velocity spectrum and reduce the artifacts caused by the coarse sampling. Figure 7.10 (a) shows the results of the conventional velocity analysis. The depth and the velocity of the reflected layer can be picked roughly due to the limited resolution as we described in previous part. Figure 7.10 (b) shows the results of the proposed method, we can find that the RMS velocity above the reflected layer is clearly indicated and there is about 0.02 m/ns velocity difference caused by the 3 mm air layer. Due to the property of the ℓ-1 norm regularized least square method, the resolution of the velocity spectrum with this FDTD simulated data can be extremely high. Here we need to delight that during the velocity analysis processing we did not consider about the effect of the wavelet and phase. Actually ℓ-1 norm regularized least square method is trying to find a best curve to fit with the reflected signals at different antenna offset to retrieve the high resolution. It may include some errors due to the phase change of the wavelet, however our main aim is to enhance the resolution so that the slight velocity changes can be observed better so that it can be automatically picked.

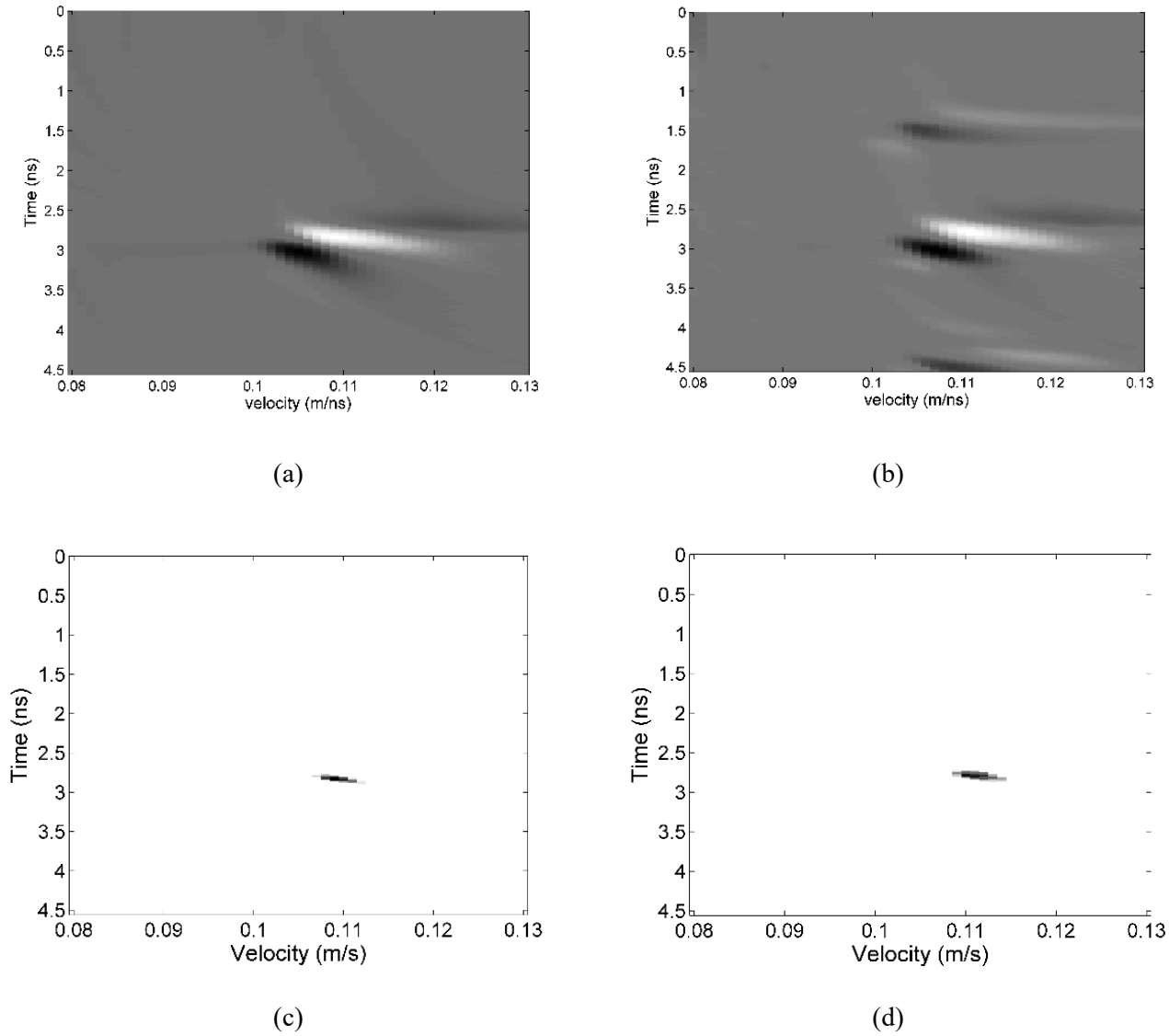

Figure 7.10 Comparison of velocity spectrum acquired by different methods; (a) velocity spectrum acquired by convention method without air layer (b) velocity spectrum acquired by convention method with air layer; (c) velocity spectrum acquired by proposed method without air layer; (d) velocity spectrum acquired by proposed method with air layer

Another model is same with the air filled crack but we changed the air to water. It is more similar to the real case because there is always water remind in the cracks. Since the difference of the permittivity is much larger, we can expect that the thin crack filled with water is easier to be detected. However, we should notice that this is just ideal case and in real situation we may still cannot observe the reflection from the water layer directly which we will show in the later part. Figure 7.10 shows the CMP dataset and the result of the analysis with ℓ-1 norm regularization. We can find that the reflected signal from the water layer is much stronger than the previous case as we expected, but it is too ideal and I think we should ignore this reflected signal and still use the reflected signal from the bottom of

the asphalt layer. Due to the attenuation effect of the water layer the waveform is more complicated than it through the air filled crack, hence the energy cannot be focused well. With the proposed method we can find that the velocity is about 0.03 m/ns lower than it in Figure 7.10(c) due to the water layer. This is not so accurate comparing to the theoretical results we calculated from Figure 7.9 due to the complicated phase changes while the signal propagate through the water layer. But it can still indicate the existence of the anomalies.

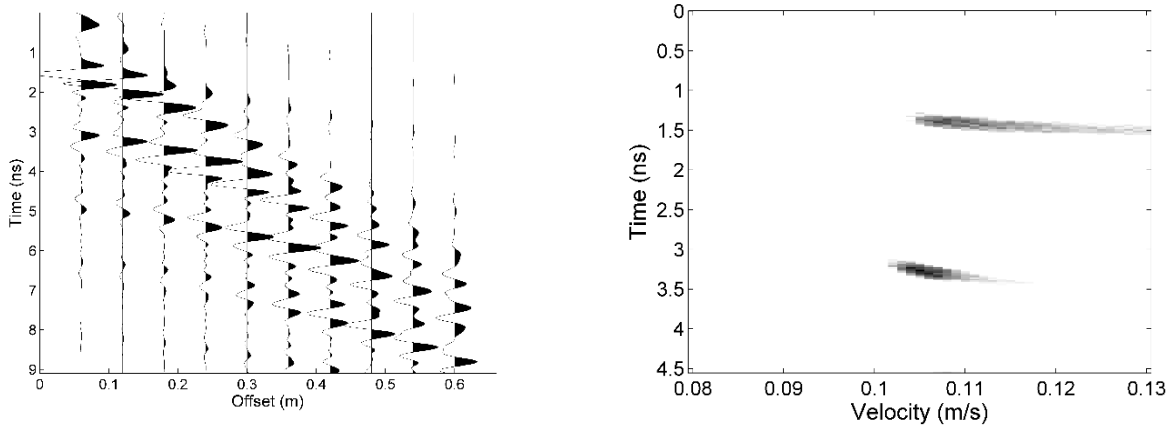

(a) (b)

Figure 7.11 Simulation for water filled crack; (a) Simulated CMP dataset; (b) Velocity spectrum acquired by proposed method.

7.32 Application to field data

Here we show an example that uses the velocity information in damaged pavement inspection. The data was acquired at an airport runway model in Port and Airport Research Institute located in Nobi, Kanagawa Prefecture, Japan. The experiment site is shown in Figure 9 and we selected a part of it as the inspection area. This area is a 15 m by 7 m rectangular area and the sketch is shown in Figure 7.13. We defined the 15 m side as the x-direction and the other side as y-direction. There are two man-made cracks simulated by embedding nonwoven fabrics in between 5 cm thick asphalt layers. Then the water is injected into the asphalt layers. Both cracks are located at around 0.1 m depth along the y-direction, however, the aperture between the asphalt layers is not clear due to the construction process. And they are located at x=4 m and x=9 m respectively. Due to the 24 cm offset of the YAKUMO antenna pair, in most profiles the reflected signals from the crack is very weak and difficult to be distinguished. Figure 11 shows the vertical profile at y=2 m, in this profile we can see that the first void is clearly imaged at 4 m but the other one at 9 m is not clear when we use the smallest offset. However, it is interesting that with the far offset vertical profile we can observe the arrival time differences at the reflect layer. It indicates the position of the cracks, however, it is not possible to

analysis the reason of this time difference only with this vertical profile because it may also be caused by the change of the thickness but not velocity.

Figure 7.12 Data acquisition with YAKUMO on the airport runway model in Nobi experiment site.

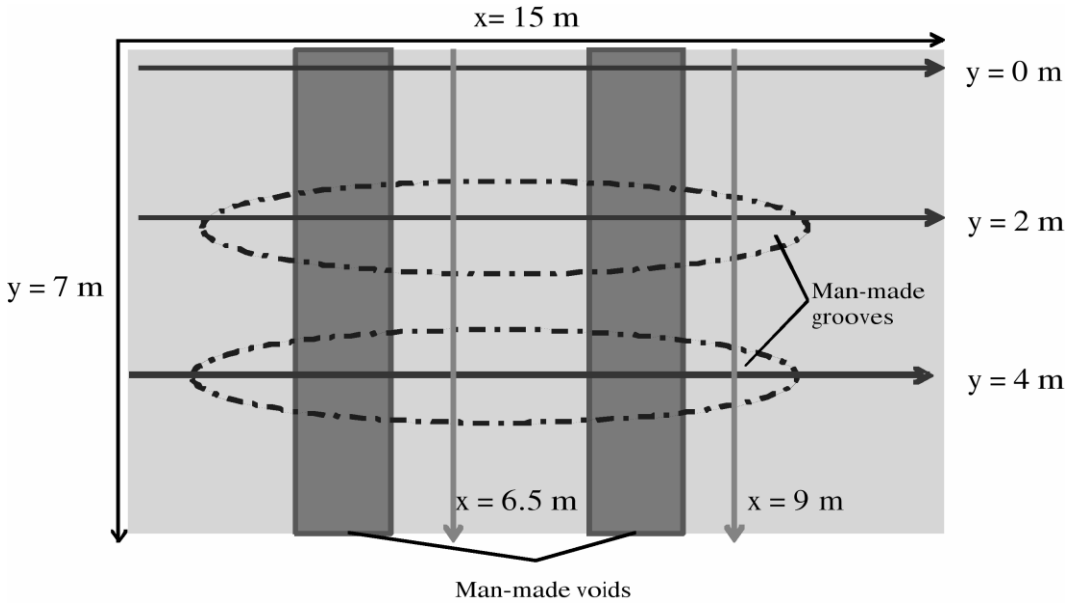

Figure 7.13. The sketch of the survey site, the man-made voids are indicated by dark rectangles and the dash circles indicate the location of a man-made rut.

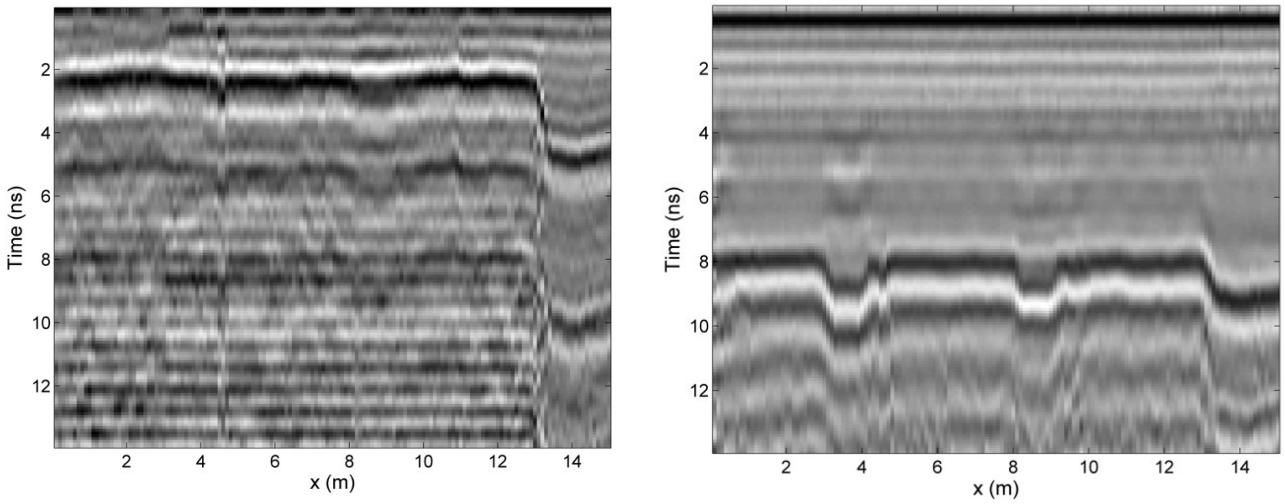

(a) (b)

Figure 7.14 A vertical slice extracted from YAKUMO dataset at y=2 m, (a) near-offset antenna combination (0.2 m offset); (b) far-offset antenna combination (1 m offset).

Figure 7.15 shows the results of the conventional velocity analysis method and the proposed method. The three CMP positions are indicate at Figure 7.14(a). We can find that the resolution of the velocity spectra by the proposed method is much increased and most artifacts are suppressed. In this case we did not compensate the effect of the wavelet hence we can see the positive value and negative value in the result. We can just pick one of them although there is slight difference between them. And this is the remained problem that we mentioned in above that the proposed method can provide better imaging resolution, while it does not means that the accuracy of the estimated velocity is enhanced. The proposed method make it easier to extract the slight velocity changes of different dataset, but it may not increase the accuracy of a certain CMP position. The data shown in Figure 7.15(a) and Figure 7.15. (c) are acquired at the crack positions and Figure 7.15(b) is away from the crack. We can find that there is about 0.04 m/ns velocity decrease at the position of the crack. Comparing with the simulated results we may judge that there is water inside the cracks and the thickness is around 3 mm.

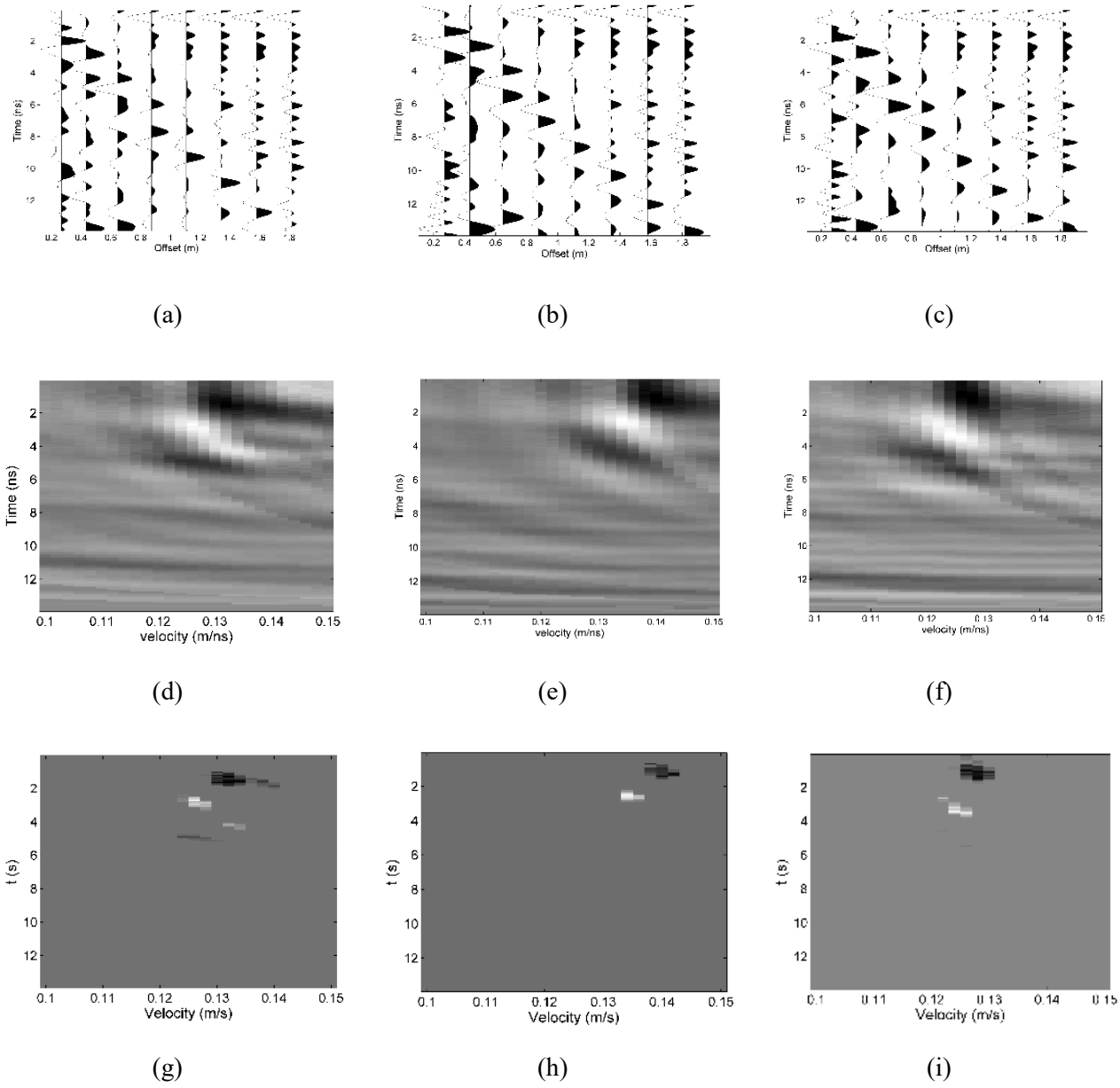

Figure 7.15 Comparison of conventional velocity analysis and proposed method with YAKUMO dataste, (a)-(c) are acquired CMP datasets, (d)-(f) show the velocity spectrum acquired with conventional method, (g)-(i) show the velocity spectrum acuired with ℓ1 norm regularized velocity estimation method. (a)(d)(g) are acquired at x=3.8 m, (b)(e)(h) are acquired on the healthy pavement at x=6.5 m and the rests are acquired at x=8 m.

Figure 7.15 shows the results of the conventional velocity analysis method and the proposed method. The three CMP positions are indicate at Figure 7.14(a). We can find that the resolution of the velocity spectra by the proposed method is much increased and most artifacts are suppressed. In this case we did not compensate the effect of the wavelet hence we can see the positive value and negative value in the result. We can just pick one of them although there is slight difference between them. The data

shown in Figure 7.15(a) and Figure 7.15. (c) are acquired at the crack positions and Figure 7.15(b) is away from the crack. We can find that there is about 0.04 m/ns velocity decrease at the position of the crack. Comparing with the simulated results we may judge that there is water inside the cracks and the thickness is around 3 mm.

In previous results we set relatively large imaging area for velocity analysis. Once we know the depth of interest in the survey area, we can further reduce the imaging area of the velocity spectrum since the ℓ1 norm regularized analysis employs an iterative algorithm. When the imaging area is small and the CMP dataset is sparse, the velocity estimation can be done in real time. Fig. shows the velocity profile of the survey line and the color legend indicates the RMS velocity. From the result we can see that the crack positions are clearly indicated with the low RMS velocity.

The velocity profiles at x-direction are shown in Figure 7.16. First of all, we can find the man-made voids imaged much clearly than is in vertical profile that shown in Figure 7.14. Both of the voids are imaged accurately with lower velocity. It is because that these voids have some reflections in shallow depth and the velocity profiles include the information from the different antenna combinations that enhanced the imaging results. Also we can find that the profile at y=2 m and y=4 m shown in Figure 7.16(b) and 7.16(c) which are located near the man-made groove shows lower velocity than the another velocity profile and I think it may caused by the man-made grooves. This velocity change is further proofed with the velocity profiles at y-directions that shown in Figure 7.17. We can always see two low velocity areas in the middle part of the velocity profile. With this information we can find the location of the low velocity area matches well with the position where the man-made grooves exist. I think the lower velocity is caused by the denser pavement. The pavement near the groove has higher density because of the compaction by a truck. Hence the air spaces inside the pavement are reduced which reduce the velocity of the wave propagation.

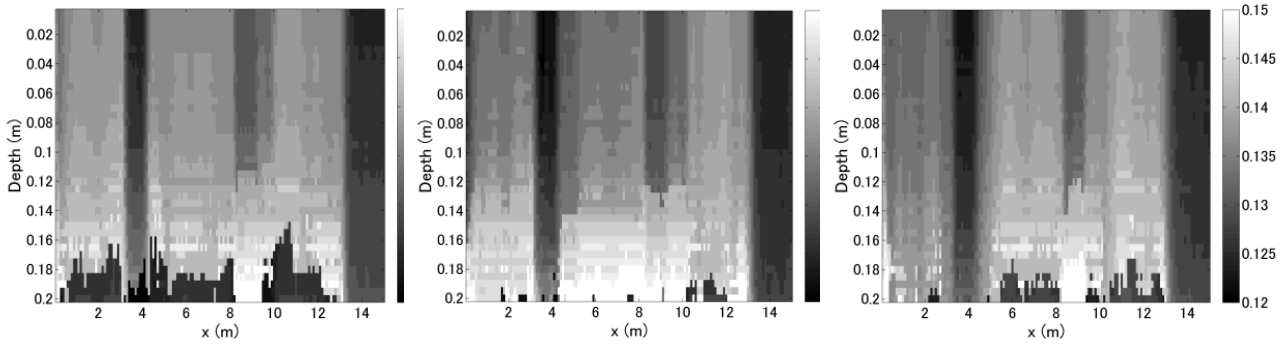

(a) (b) (c)

Figure 7.16 The velocity profiles at x- direction; (a) y= 0m; (b) y=2 m; (c) y=4 m.

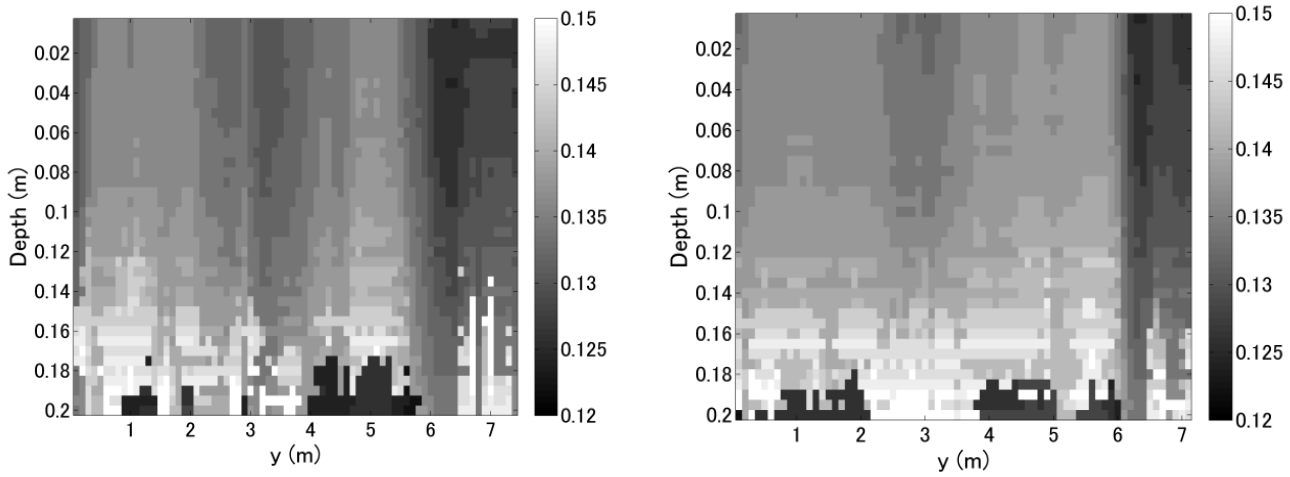

(a) (b)

Figure 7.17 The velocity profiles at y-direction; (a) x= 6.5 m; (b) x=9 m.

7.4 Summary

In this chapter I introduced the YAKUMO array GPR system and its application cases on archeological and engineering applications. The performance of the system for both 3-dimensional data acquisition and CMP data acquisition are well discussed with different antenna arrangement. I concluded that due to the polarization effect of the bowtie antenna, the performance of scan dataset and CMP dataset need to be balanced.

An archaeological survey example at Kunohe city is introduced. Large scale 3-dimensional dataset can be acquired conveniently with YAKUMO system, and some interpolations are given together with the imaging results of this area. Some stones structures can be found and the location is matched with the expectation of the archaeologist.

I mainly introduced the pavement inspection application at the airport taxi-way with YAKUMO system. Since it is difficult to find the reflection from the thin layer, I proposed an approach that use the slight velocity changes to identify the damaged pavements with thin cracks inside. I use FDTD simulation to analysis the possibility of detecting the thin cracks with slight velocity change and I applied the $\ell 1$ norm regularized velocity estimation method to detect the precise velocity changes with few centimeters per nanosecond. Here we need to emphasis the conclusion that is given in previous chapter that the proposed method can only increase the imaging resolution of the velocity spectrum so that the slight velocity changes at different CMP location can be detected. While it is similar to the least square method for imaging, the proposed method is somehow trying to find the peak value within the

waveform with the mathematical approach, in this case the high resolution result may not correspond to the real phase center of the waveform. Hence even when we can pick the unique value within the velocity spectrum, it may not match perfectly with the real velocity of the medium. But the method that I proposed is focus on detecting the slight velocity changes at different positions which can be achieved by the proposed method. With both the simulation experiment and the YAKUMO dataset at the experimental field I show that it is possible to detect the damaged pavement with the velocity estimation methods. Velocity profiles at the experimental site is also generated with YAKUMO system and the damaged part can be detected easier than using the reflected signal only.

7.5 References

[1] N. Linford, P. Linford, L. Martin, A. Payne, "Stepped frequencyground-penetrating radar survey with a multi-element array antenna: Results from field application on archaeological sites", Archaeol. Prospect., vol. 17, pp. 187-198, 2010.

[2] H. Liu, J. Zhao, M. Sato, "A Hybrid Dual-Polarization GPR System for Detection of Linear Objects" in IEEE Antennas Wirel. Propag. Lett., vol. 14, no. 99, pp. 1-4, 2014.

[3] R. Persico, M. Ciminale, L. Matera, "A new reconfigurable stepped frequency GPR system possibilities and issues; applications to two different Cultural Heritage Resources", Near Surface Geophysics, vol. 12, no. 6, pp. 793-801, December 2014.

[4] Q. Lu, M. Sato, "Estimation of Hydraulic Property of an Unconfined Aquifer by GPR", Sens. Imaging An Int. J., vol. 8, no. 2, pp. 83-99, Sep. 2007.

[5] H. Liu, X. Xie, K. Takahashi, M. Sato, "Groundwater Level Monitoring for Hydraulic Characterization of an Unconfined Aquifer by Common Mid-point Measurements using GPR", J. Environ. Eng. Geophys., vol. 19, no. 4, pp. 259-268, 2014.

[6] L. Yi, K. Takahashi, M. Sato, "Large scale subsurface velocity estimation with array GPR system YAKUMO", Radio Science Bulletin, Mar 2016.

[7] A. Benedetto, F. Benedetto, "Optimal algorithm for the ground penetrating radar signals processing in road pavement analysis and monitoring", Proc. Int. Conf. Appl. Adv. Technol. Transp. Eng., pp. 370-377, 2002.

[8] A. Benedetto, G. Manacorda, A. Simi, F. Tosti, "Novel perspectives in bridge inspections using GPR", Nondestruct. Test. Eva., vol. 27, no. 3, pp. 239-251, 2012.

[9] V. Rampa, U. Spagnolini, "Multi-layer detection/tracking for monostatic ground penetrating radar", Proc. Int. Geosci. Rem. Sens. Sympos., vol. 4, pp. 2038-2040, 1996.

[10] N. Ahmad, H. Lorenzl, M. Wistuba, "2011. Crack detection in asphalt pavements how useful is GPR? 6th Int", Workshop on Advanced Ground Penetrating Radar (IWAGPR), June 22–24, 2011.

[11] S.R. Pennock, C.H.J. Jenks, "Road surface and pavement condition assessment by high frequency GPR diffraction", Ground Penetrating Radar (GPR) 2014 15th International Conference on, pp. 881-886, 2014.

[12] J. Liu, D.G. Zollinger, and R.L. Lytton, "Detection of Delamination in Concrete Pavements Using Ground-Coupled Ground-Penetrating Radar Technique", Journal of Transportation Research Board, National Research Council, Washington, DC, Transportation Research Record, Vol. 2087, pp. 68-77, 2008.

[13] M. Sato, K. Takahashi, "Array GPR system “Yakumo” for Natural Disaster Mitigation", the International Workshop on Advanced Ground Penetrating Radar 2015 (IWAGPR), 2015.

[14] R. J. Greaves, D. P. Lesmes, "Velocity Variations and Water Content Estimated from muti-offset ground-penertrating radar", Geophysics, vol. 61, no. 3, pp. 683-695, May-June 1996.

[15] G. Chen, R. C. Liu, A. Zhang, "Design and implement of an UWB bow-tie antenna with back-covity of ground penetrating radar", Chinese journal of radio science, vol. 25, no. 2, pp. 221-226, Apr. 2010.

[16] I. Trinks, B. Johansson, J. Gustafsson, J. Emilsson, J. Friborg, C. Gustafsson, J. Nissen, A. Hinterleitner, "Efficient large-scale archaeological prospection using true three-dimensional GPR Array System", Archaeological Prospection, vol. 17, pp. 175-186, 2010.

[17] L. B. Conyers, "Analysis and interpretation of GPR datasets for integrated archaeological mapping", Near Surface Geophysics, vol. 13, pp. 645-651, 2015.

[18] Z. Deng and M. Sato, “GPR reflection signal from a thin layer,” In Proc. of the SEG-J Conference 134th , Tokyo, Japan, pp. 47-50, 2016

Chapter 8 Conclusions and recommendation

8.1 Conclusions

The near-range microwave imaging with the sparse array system is still relatively new topic for the radar engineering. The existing techniques and the theory are mostly applied with the far-field SAR imaging technique directly, or borrow the methods from the similar research such as ultrasound imaging or seismic imaging. In this work I focused on the imaging artifacts that caused by the coarse sampling during the SAR processing. In general, similar problem happens in different domain such as seismic imaging or imaging processing and radar signal processing. And there are different assumptions or theories that are trying to interoperate the reason of generating the imaging artifacts. For example, in radar science researchers are mainly considering the artifacts as the sidelobe that generated by improper beam-forming; for imaging processing applications the artifacts are presented as the distortion of the imaging and the artifacts is discussed as aliasing effect; similarly for seismic imaging it is common to discuss the aliasing that is caused by the coarse sampling which is similar to the sparse array case in our discussion. Each of these research direction indicates some of the truth of the problem and many methodologies are investigated to overcome the problem, while it is still a difficult question to conclude the source of the imaging artifacts.

In our work, I suggested to analyze the time-domain signal and most of our methods are proposed in time-domain. The idea is that since the time-domain signal is closely related to the physical model of the targets, we can somehow “observe” the generating of the artifacts during the signal processing. In Chapter 3 I presented several different weighting factors within the conventional SAR processing is mostly based on the observation of the artifacts. In a specific case, I conclude that the semblance method that I introduced in this chapter may work only for the point-like targets. This conclusion can be directly observed by analyze the semblance factor in time-domain signal and I think this may be a simplest way to determine this fact.

In Chapter 4 I introduced a mathematical based method for artifacts removal. The relation between the least square method and the CS approach is well described in this chapter. The CS approach have been introduced and applied for SAR imaging techniques for few years. While the sensing matrix of most SAR system is not satisfied with the random sampling condition, the good results can still be achieved in previous research. One of our interpretation is that the $\ell 1$ norm regularization term promoted the sparsity of the solution and I think although the random sampling is difficult to achieve with the array system, $\ell 1$ norm regularized least square method is still a good way to remove the imaging artifacts and enhance the imaging resolution. It is an interesting trial that I tried to apply the weighting factors into the iterative algorithm. The results become not stable due to the violation on the mathematic

criterion, however in some certain cases the results can really be improved. Some more discussions will be given in later sections.

In the rest part of the thesis I mainly focus on the velocity estimation technique with the limited number of antenna elements. It is delighted that the velocity estimation with the CMP dataset is similar with the conventional SAR processing, hence many similar problems happen to velocity estimation with coarse data acquisition and on the other hand, many similar methods can also be applied to solve this problem which are introduced in Chapter 6. In most of the cases the precise velocity estimation is not necessary such as for the ground water level detection or use the estimated velocity for the SAR processing. The conventional velocity estimation technique can already satisfy such requirements. While one of our key point is to apply the velocity estimation technique for the large scale velocity estimation or inspection which can only be realized with the array radar system such as YAKUMO. In order to generate the velocity profile, the automatic velocity picking become important, the artifacts removal and the point picking can both be done with the $\ell 1$ norm regularized velocity estimation method. And comparing with its application on SAR imaging, the calculation cost is much reduced. On the other hand, with the proposed methods the slight velocity changes which is few millimeter per nanosecond can be detected. Although the value may not fit with the real velocity perfectly, the enhancement of the resolution can be used to distinguish the velocity changes at different positions. In Chapter 7 I introduced that such small velocity changes can be used for the pavement inspection, a serious experimental examine and real data analysis are done with YAKUMO multistatic array GPR system.

8.2 Results and novelties of this research

Within the framework of this thesis, the following novel results have been achieved and presented:

1. The SAR imaging algorithm is well discussed in both time-domain and frequency domain. It is pointed out that the time-domain algorithm is much accurate and the physical meaning is clearer because frequency domain algorithm include some mathematical simplification for the sake of the high speed calculation with FFT. Although time-domain algorithm requires much larger calculation especially for the 3-dimensional imaging, it will not introduce numerical problem while doing the FFT especially for the irregularly sampled dataset.

2. In order to deal with the irregularly sampled dataset, an iterative interpolation algorithm that based on f-k domain transformation is proposed in early research. The proposed method can deal with the 3-dimensional irregularly acquired dataset and it is designed specifically for the radar signal interpolation. A journal paper is published with the proposed method and the proposed method is also applied to some other applications such as the reconstruction of the CMP dataset.

3. The main factors that generating the imaging artifacts during the SAR processing is summarized form the view of the time-domain imaging processing. It is shown that the SAR imaging results for near-range imaging is affected by the sparsity of the spatial sampling, waveform or frequency bandwidth of the received signal and the imaging algorithm itself. The first two factors are determined with the designed sparse array system, I discussed this issue together with the experimental equipment that is used in this research. And the artifacts removal with the advanced signal processing technique is mainly discussed in this thesis, three different types of the improved SAR imaging algorithms are introduced.

4. The first type of the SAR imaging method is designed by adding a weighting factor or filter within the conventional SAR algorithm. Three sub methods are introduced in Chapter 3. The main advantages of these methods is that they can partially remove the imaging artifacts without too much extra calculation. However, these methods are designed specifically for some certain conditions, for example, the semblance method mainly works for the point-like targets and the rest methods will sacrifice the imaging resolution while reducing the imaging artifacts. Another important feature of these methods is that they can be applied together with other advanced imaging techniques.

5. The second type of the methods is based on solving the least square problem of SAR imaging. The general idea of solving least square solution of SAR processing with different regularization terms is mainly discussed in Chapter 4. It is shown that the CS based SAR imaging method is a special case of the $\ell 1$ norm regularized least square method. Comparing with the $\ell 2$ norm regularized least square imaging method, the $\ell 1$ norm regularized method has better performance for both simulated data and the real data of 2-dimensional sparse array system. I think it is mainly because that during the promotion of the sparsity of the imaging result, the waveform is compressed with the algorithm hence the imaging resolution can be enhanced. At the same time, due to the soft-threshold within the algorithm the weaker clutters and the noise can be well suppressed hence the imaging artifacts can be reduced.

6. Different approaches for improving the least square methods are discussed. The weighting factors are combined with the least square method but the performance is not robust, mathematical explanation is still required. The hard threshold is applied with the $\ell 2$ norm regularized least square method and it shows good performance for better solution and much less iteration. However, I found similar approach is proved to be the solution of $\ell 1$ norm regularized least square method in mathematical research.

7. The pulse compression of UWB signal is reviewed and I think it is important for improving the imaging quality of the sparse array system. The $\ell 1$ norm regularized least square method is applied to the pulse compression problem and it shows good result for real data that include some noise.

8. The third type of the imaging method is investigated for an estimated solution of the least square methods to get rid of the huge calculation. By combing the idea of pulse compression and imaging deblurring, an imaging based method is proposed to enhance the SAR imaging results with the 2-dimensional spatial deblurring filter. The method is demonstrated with the simulated data and it shows good performance with real-time processing ability. However, it is similar to the pulse compression that the method is difficult to apply for the real data because the waveform of real data is not so stable comparing with the simulated data. This method still need to improve for the real application.

9. The velocity estimation with the bistatic radar system is reviewed. It is shown that the velocity estimation with the CMP deataset has many similarities with the SAR imaging algorithm. Although the coarse CMP sampling will not affect the resolution of the velocity spectrum, imaging artifacts will be generated and it may reduce the imaging resolution and make the automatic velocity picking become more difficult. Several methods are proposed for accurate velocity estimation with limited number of the antenna elements.

10. The CMP interpolation is demonstrated. It is shown that the interpolation of CMP dataset is much easier than radar profile because the target is not unpredictable. A trial velocity can be used for assisting the interpolation of the CMP dataset, although it will not enhance the accuracy of the velocity estimation, the imaging artifacts can be well suppressed with this method.

11. The $\ell 1$ norm regularized least square method is also applied for velocity estimation and it shows good performance for this application. Due to the simplicity of the imaging target which is just the focused energy of the reflected layer, this method can greatly improve the imaging resolution and remove the imaging artifacts of the velocity spectrum. Although the high accuracy velocity estimation result may not match with the real value perfectly due to the waveform, this method can be used for precise detection of the velocity changes.

12. By using the cross-correlation of two CMP dataset, the time delays of two CMP dataset can be used for simultaneous estimation of velocity and thickness change of a single layer structure. This method shows good performance and it can be applied with minimum two antenna pairs. However, this method is very practical and can be only used for the limited cases.

13. The multistatic array GPR system YAKUMO is introduced. The performance of the system with different antenna polarization is discussed. A case study of pavement inspection by large-scale velocity estimation with YAKUMO system is mainly discussed in Chapter 7. The response of the thin cracks within the pavement for velocity estimation with $\ell 1$ norm regularized least square method is analyzed with FDTD simulation and I think it is possible to detect these thin cracks by detecting the slight velocity changes. Both simulated data and real data acquired with YAKUMO system show that the slight velocity changes can be detected and it shows the possibility of using

the proposed method for pavement inspection.

8.3 Recommendations

In this section I summarized some interesting problems and idea that I have mentioned in this thesis. A list of the new directions is given in below, the further study and investigation may be required to solve these problems:

1. During the study of this work, I found that the idea of time-domain imaging is very important for the near-range imaging applications. The main reason is that the effect of the waveform and the distributed target are difficult to be analyzed in frequency domain. In most of the far-field SAR research the pulse is commonly used for the simulation or analysis, which is totally different for near-field imaging cases. A complicated waveform will not only introduce imaging artifacts with coarsely sampled data, but also introduce numerical problem for the pulse compression or solving least square problem. However, the definition of the "complicate" for a waveform is still not clear in near-range imaging, and I think better results can be achieved by considering the waveform effect for the near-range imaging. From the view of the frequency domain analysis, which is also means the phase information should be considered for the near-range imaging.

2. In this work I am only focus on the diffraction stacking and some simple extensions with the filter or weighting function. The main reason is that during the previous research work on GPR, I found that the complicated algorithm such as Kirchhoff migration do not have significant advantages for the near-range microwave imaging. In Chapter 2 I have a short introduction on the Kirchhoff migration and I found from the equation it is not clear how it can improve the imaging quality. Because the original idea of Kirchhoff equation indicates that it only has clear physical meaning when I can observe the target from all the directions but not part of it. Since in most of the cases we only use the observation data from one or two dimensional scan at one side of the target, the Kirchhoff migration terms may not working properly for the imaging result. In this case, I suggest to focus on more physical meaningful operators for the imaging processing. Sometimes traditional mathematical theory may not proper for a certain application, practical observation or experiment is always necessary.

3. In general I think the least square based method is a good approach for the near-range imaging problem. It can somehow compensate the artifacts caused by the waveform or the coarse sampling by minimizing the misfit function. Currently there are many advanced technique of solving the least square problem by adding more and more regularization terms, however, I think the main problem of least square based methods is not the performance but the ability of application. In order to solve these problem, many parameters are crucial for the final results such as the value of the regularization term. Although there are some existing technique to estimate the value of

regularization term, in most of the cases we still have to try different values to achieve a good imaging result. It is fine for research but it is not enough for the real applications and this is one of the main reason that I proposed the deblurring filter method as a practical estimation of the least square based methods.

4. The deblurring filter method works well with simulated data while the performance with the real data is still not good enough. The main problem is the simulated reference data. Since the reference model is built with only point scatterers, the deblurring is mainly working for the point target or the edge of the distributed target. When the deblurring window only include the distributed target or the imaging artifacts, the output is not predictable and may become new artifacts. I think a further weighting factor can be introduced for each deblurring window that is to enhance the window include the point response while suppress the output without the point response. On the other hand, more advanced methods of deconvolution should be also included in this approach because the main problem is still the suppression of the waveform.

5. After all the trials for the imaging problem, I have noticed a fact for the compress sensing based method. If we consider the output of the compress sensing based method, we may notice that the resolution can be greatly improved. While consider the imaging resolution from the view of SAR imaging, since the aperture size is constant, the only factor that can improve the resolution is just bandwidth, or compression of the waveform. In another word, compressed sensing based method improve the imaging resolution because it compressed the waveform into a pulse by the mathematical procedure. In this case, a problem arise: does the phase center of the signal can be recognized accurately with such mathematical approach which do not consider anything about the physics? If not, it means the compress sensing based method may not obtain a correct imaging result.

6. For the velocity estimation applications I concluded it is very similar to the imaging problem. In this case, a similar problem to above appears: we may not get the accurate velocity due to the effect of the waveform. Although we can get high resolution result by using least square based method, the compression of the waveform may not correct. And this is the main reason that I mentioned in Chapter 7 that it is better to detect the changes of the estimated velocity but not focus on the value of the estimated velocity. If we really need to estimate the accurate velocity value, the compensation on the phase center of the wavelet is necessary. It is similar to previous suggestion that we need to use more phase information in order to achieve the accurate velocity estimation value.

Publications and Awards

Journals Papers

[1] Li Yi, Kazunori Takahashi, and Motoyuki Sato, "A Fast Iterative Interpolation Method in f-k Domain for 3-D Irregularly Sampled GPR Data," IEEE Journal of Selected Topics in Applied Earth Observations and Remote Sensing, Vol.9, no.1, pp. 9-17,January 2016. (Chapter 2)

[2] Li Yi, Kazunori Takahashi, and Motoyuki Sato, "Large scale subsurface velocity estimation with array GPR system YAKUMO," accepted by the radio science bulletin. (Chapter 7)

[3] Li Yi, Kazunori Takahashi, and Motoyuki Sato, "High-resolution velocity analysis method with ℓ-1 norm regularized least square method for pavement inspection", submitted to IEEE Journal of Selected Topics in Applied Earth Observations and Remote Sensing. (Chapter 4 and Chapter 7)

Oral Presentations

[1] Li Yi, Kazunori Takahashi, and Motoyuki Sato, "Archaeological Survey of Dangoyama Kofun by 3DGPR", in Proc. the 11th SEGJ International Symposium, 19-21 November, Yokohama, Japan, 2013.

[2] Li Yi, Kazunori Takahashi, and Motoyuki Sato ," Optimization of data sampling and imaging reconstruction by GPR", in Proc. the 15th International Conference on Ground Penetrating Radar (GPR2014), 30 June- 4 July, Brussels, Belgium, 2014.

[3] Li Yi, Kazunori Takahashi, and Motoyuki Sato, "Estimation of vertical velocity profile by multistatic gpr Yakumo", in Proc. the International Geoscience and Remote Sensing Symposium 2015 (IGARSS 2015), 26 - 31 July, Milan, Italy, 2015.

[4] Li Yi, Kazunori Takahashi, and Motoyuki Sato, "Application of ℓ1 norm approach to data acquired by the array GPR Yakumo", in proc. the 10th European Conference on Antennas and Propagation (EUCAP2016), 10 - 15 April, Davos, Switzerland, 2016.

[5] Li Yi, Kazunori Takahashi, and Motoyuki Sato, "Enhancement of the migrated results with the deblurring filter", in proc. European Geosciences Union General Assembly 2016 (EGU2016), 17 - 22 April, Vienna, Austria, 2016.

[6] Li Yi, Kazunori Takahashi, and Motoyuki Sato, "Application of least square image reconstruction algorithm with ℓ1 norm constrains to sparsely acquired GPR data", in proc. 592th URSI-F conference, 18 March, Yokohama, Japan, 2015.

[7] Li Yi, Kazunori Takahashi, and Motoyuki Sato, "Large Scale Subsurface Velocity Estimation with Array GPR System YAKUMO," in proc. 2015 URSI – Japan radio science meeting, 3 - 4 September, Tokyo, Japan, 2015.

[8] Li Yi, Kazunori Takahashi, and Motoyuki Sato," Investigation on 3D migration of non-gridded GPR data", IEICE Technical Report, 2013, pp. 87-92.

[9] Li Yi, Kazunori Takahashi, and Motoyuki Sato," Simultaneous Estimation of Velocity and Thickness of Stratified Material with Array GPR System YAKUMO", IEICE Technical Report, 2015, pp. 19-24.

Award and Scholarship

- The 3rd prize of student paper competition of URSI Japan Radio Science Meeting 2015, 4 September 2015.
- Japanese Government Scholarship (Monbukagakusho: MEXT) Scholarship (10/2011–04/2017)

Acknowledgements

I would like to express my deep gratitude to my supervisor, Prof. Dr. Motoyuki Sato, for his various supports. His infinite enthusiasm on research and education inspired me during the past five years. “Something new?”, the core value of Sato laboratory on academic work, always motivates me to be more creative and pushes me with a moderate feeling of tension in daily life. On the other hand, I am very grateful for not only his instruction on research but also his concern on my life in Japan and he has taught me far more than the research. I also greatly appreciate for providing me many precious chances to participate in international conferences. All those experiences broadened my vision, and are irreplaceable and treasured memory in my life.

I wish to express my sincere thanks to Prof. Dr. Hiroyoshi Yamada with the Faculty of Engineering, Niigata University, Japan; Prof. Dr. Qiang Chen with the Department of Communications Engineering, Tohoku University, Japan and Prof. Dr. Takatoshi Ito with the Institute of Fluid Science, Tohoku University, Japan, for serving as my dissertation committee and provided me many constructive suggestions and comments.

I am also deeply indebted to Prof. Dr. Leo P. Ligthart with Delft University of Technology, Netherland, for his kind advices and instructive discussions during his stay at Tohoku University as a visiting professor in 2014 and attending of my master dissertation. And I am also appreciate for Dr. Zegang Ding with Beijing Institue of Technology, China. He has inspired and helped me a lot during his stay in Tohoku University in 2016 as a visiting professor. I am deeply grateful to him for his continuous encouragement and support of my research work. Best wishes for his future.

During my attendances and presentations at international conferences and workshops, I also got many encouragements and valuable suggestions. Here I should express my special thanks to Prof. Dr. Alexander Yarovoy with Delft University of Technology, Netherland and Dr. Sakamoto Takuya with the University of Hyogo, Japan that I have received so many appreciate suggestions at different conferences and had many personal discussions with them which greatly extended my knowledge on related topics. Also I have special thanks Prof. Dr. Hervé Chauris and Dr. Yubing LI with Institut de Physique du Globe de Paris for inviting me to visit there laboratory for the seminar on the imaging technique of seismic inversion which greatly inspired me on my own research work. At last, I would also thank for Dr. Raffaele Persico with Italian National Research Council for accepting my visit to his institute for the related topics on GPR technology. Many valuable opinions and ideas are gained during the one-day tour in his institute.

I am grateful for my previous and present colleagues and friends at Sato Laboratory of Tohoku University. I thank our previous Assistant Prof. Dr. Kazunori Takahashi for all his support on my work, we had many discussions which greatly improved my research work during the three-year doctoral

course and I have learnt a lot from all the drafts with his correction and revision. Also thanks to our current Assistant Prof. Dr. Lilong Zou who helped me a lot during the last few month for my graduation. I also wish to thank the visiting professor Prof. Dr. Zhining Chen from National university of Singapore, Singapore; Prof. Dr. Magaly Koch from Boston University, USA and the visiting Professor Dr. Li Liu from Taiyuan University, China, for sharing their knowledge and experience with us. Special thanks to our previous research fellow Christian Koyama that he has helped me so much with his research experience and also the fun time we have spent together as friends; Also thanks to Lilong Zou, Weike Feng and Iakov Chernyak for many interesting discussions on research work which also helped me a lot to improve my skills on academic. At last I need to extend my thanks to other colleagues who contributed to form a good environment for our daily study: Dr. Jun Sonoda, Dr. Hai Liu, Andrey Lyulyakin, Amila Thilanka Karunathilake, Masashi Nakaya, Yasunari Mori, Bo Yang, Yuanzhen Wang, Amarsaikhan Tsogtbaatar, Yu Tanaka, Yuka Asaya, Satoshi, Yamazaki, Shinpei Nakano… Further, I need to thank our secretary Ms. Naoko Nakai and Ms. Masako Kato who works hard to make our study more conveniently and smoothly.

In addition, I would like to thank for the Ministry of Education, Culture, Sports, Science, and Technology (*MEXT*) of Japan to award me a scholarship during my study in Tohoku University. It greatly benefit my daily life so I can focus on my research work in past few years.

It is impossible to list all your names here but you are really in my heart. It is lucky to know all of you and to receive all the helps from you. Thanks indeed and best wishes for all of you.

Finally, I would like to express my profound gratitude and deep thanks to my parents, Yunxia Su and Yuping Yi, for their hard working, uncounted supports and encouragements.

Li Yi

February 2017, in Sendai